(NASA-TM-X-2470) WIND-TUNNEL INVESTIGATION OF BASIC AERODYNAMIC CHARACTERISTICS OF A SUPERCRITICAL-WING RESEARCH AIRPLANE CONFIGURATION (NASA) 109 p HC A06/MF A01 CSCL 01A H1/02

N78-24078

Unclas
20751

AVAILABLE TO U.S. GOVERNMENT AGENCIES AND CONTRACTORS ONLY

PUBLIC RELEASE JUNE 13, 1978

~~CONFIDENTIAL~~

1. Report No.	2. Government Accession No.	3. Recipient's Catalog No.
NASA TM X-2470		

4. Title and Subtitle	5. Report Date
WIND-TUNNEL INVESTIGATION OF BASIC AERODYNAMIC CHARACTERISTICS OF A SUPERCRITICAL-WING RESEARCH AIRPLANE CONFIGURATION	February 1972
	6. Performing Organization Code
7. Author(s)	8. Performing Organization Report No.
Dennis W. Bartlett and Richard J. Re	L-7979
	10. Work Unit No.
9. Performing Organization Name and Address	742-73-01-14
NASA Langley Research Center Hampton, Va. 23365	11. Contract or Grant No.
	13. Type of Report and Period Covered
12. Sponsoring Agency Name and Address	Technical Memorandum
National Aeronautics and Space Administration Washington, D.C. 20546	14. Sponsoring Agency Code

15. Supplementary Notes

16. Abstract

An investigation has been conducted in the Langley 8-foot transonic pressure tunnel and the Langley 16-foot transonic tunnel to determine the aerodynamic characteristics of a 0.087-scale model of a supercritical-wing research airplane configuration at Mach numbers from 0.25 to 1.30. The investigation included tests to determine the basic longitudinal aerodynamic characteristics, the lateral-directional aerodynamic characteristics for sideslip angles of 0° and $\pm 2.5^{\circ}$, and the effects of Reynolds number and aeroelasticity.

CLASSIFICATION CHANGE

To UNCLASSIFIED

By authority of [illegible] Date [illegible]

Changed by [illegible] Control Station, NASA

Classified Document Master Scientific and Technical Information Facility

CLASSIFIED BY [illegible]

SUBJECT TO GENERAL DECLASSIFICATION

SCHEDULE OF EXECUTIVE ORDER [illegible]

AUTOMATICALLY [illegible]

TWO-YEAR [illegible]

DECLASSIFIED [illegible] 31 [illegible]

17. Key Words (Suggested by Author(s))	18. Distribution Statement
Transonic aerodynamics Supercritical airfoil application TF-8A supercritical wing research airplane	~~Available to U.S. Government Agencies and Their Contractors Only~~

19. Security Classif. (of this report)	20. Security Classif. (of this page)	21. No. of Pages	22. Price
~~Classified~~	Unclassified	107	

~~GROUP 4~~
~~Downgraded at 12 year intervals;~~
~~Declassified after 12 years~~

~~This material contains information affecting the national defense of the United States within the meaning of the espionage laws, Title 18, U.S.C., Secs. 793 and 794, the transmission or revelation of which in any manner to an unauthorized person is prohibited by law.~~

~~CONFIDENTIAL~~

[redacted]

WIND-TUNNEL INVESTIGATION OF BASIC AERODYNAMIC CHARACTERISTICS OF A SUPERCRITICAL-WING RESEARCH AIRPLANE CONFIGURATION*

By Dennis W. Bartlett and Richard J. Re
Langley Research Center

SUMMARY

An investigation has been conducted in the Langley 8-foot transonic pressure tunnel and the Langley 16-foot transonic tunnel to determine the aerodynamic characteristics of a 0.087-scale model of a supercritical-wing research airplane at Mach numbers from 0.25 to 1.30. The investigation included tests to determine the basic longitudinal aerodynamic characteristics, the lateral-directional aerodynamic characteristics for sideslip angles of 0° and $\pm 2.5^{\circ}$, and the effects of Reynolds number and aeroelasticity.

The results of this investigation indicated a drag-divergence Mach number of about 0.97 to 0.98 for the complete configuration; however, oil-flow photographs of the wing and wing pressure data indicated that the wing is still performing well at a Mach number of 0.99. The results also indicated improvements in the pitching-moment characteristics as the Reynolds number was increased for a Mach number of 0.25. The improved pitching-moment characteristics (improved in that pitch-up is also delayed to a higher lift coefficient) indicated at the higher subsonic Mach numbers (M = 0.50 to 1.00) for the higher dynamic pressures may be due primarily to increased aeroelasticity effects which tend to add "wash-out" at the wing tips as both the dynamic pressure and Reynolds number are increased.

Although pitch-up occurred at each Mach number tested, it was well beyond level-flight lift coefficients, and the pitching-moment curves became stable again at the higher angles of attack. The static margin increased with Mach number to about Mach 1.00, but an attendant increase in the pitching-moment coefficient at zero lift results in a powerful compensating effect so that little change in trim angle of attack occurs with increasing Mach number. The lift-curve slope also increased with Mach number up to Mach 1.00 and then decreased at supersonic speeds. Both directional stability and positive effective dihedral are indicated for the model at sideslip angles of 0° and $\pm 2.5^{\circ}$ for Mach numbers of 0.25, 0.95, and 0.99 and over an angle-of-attack range that varied from approximately -2° to 14°.

---

*[redacted]

[redacted]

INTRODUCTION

A unique airfoil, known as the NASA supercritical airfoil, has been under development over a period of years. This new airfoil is designed to delay shock-induced boundary-layer separation to Mach numbers and lift coefficients notably higher than those of conventional sections. These gains are achieved by limiting the upper surface shock strength through proper shaping of the airfoil section and, therefore, the pressure distribution. Wind-tunnel investigations of an early version of the supercritical airfoil which incorporated a slot located near the trailing edge indicated significant gains in performance. (See refs. 1 and 2.) Consideration of its application to aircraft and the structural problems associated with the slot, particularly the maintenance of close tolerances within the slot gap, led to the development of the integral (unslotted) supercritical airfoil. (See refs. 3 and 4.) The integral section in wind-tunnel investigations has also demonstrated the potential for obtaining significant increases in drag-divergence Mach number and in achieving high buffet-free maneuver load factors for configurations employing this new concept.

As with any new development, uncertainties exist in the areas of application of model results to the full-scale case and in the full-scale flying and handling qualities. Therefore, several full-scale "proof-of-concept" flight research programs have been initiated. One of these programs, which is being jointly conducted by the Flight and Langley Research Centers of the NASA, employs a U.S. Navy fighter aircraft (TF-8A) as a test-bed vehicle for a sweptback supercritical wing designed for possible future application to an advanced transport aircraft having a cruise Mach number very close to 1.0.

The purpose of this paper is to present results from wind-tunnel investigations of a near-final version of the TF-8A supercritical-wing research airplane at Mach numbers from 0.25 to 1.30, angles of attack from about -8° to 24°, and at Reynolds numbers varying from approximately 15.91×10^6 per meter (4.85×10^6 per foot) at a Mach number of 1.00 to a maximum of 19.95×10^6 per meter (6.08×10^6 per foot) at a Mach number of 0.80.

Included are results showing the basic longitudinal aerodynamic characteristics, the lateral-directional aerodynamic characteristics for sideslip angles of 0° and $\pm 2.5^{\circ}$, and Reynolds number effects. Also included for illustrative purposes are wing streamwise-chord pressure distributions at several semispan stations and the corresponding semispan-load distribution for a Mach number of 0.99 and lift coefficient of 0.443. Complete pressure data for the present investigation are contained in reference 5.

SYMBOLS

The results presented herein are referred to the stability-axis system for the longitudinal characteristics and the body-axis system for the lateral and directional characteristics. All coefficients are based on the geometry of the basic wing panel which does not include the leading-edge glove or the trailing-edge extension. (See fig. 1(a).) Moments are referenced, for consistency, to the quarter-chord point of the mean geometric chord of the basic wing panel. This point is located at model station 0.995 meter (39.155 inches) as shown in figure 1(a). Coefficients and symbols used herein are defined as follows:

A_e individual duct exit area

A_i total model inlet area

b wing span, 114.30 cm (45.000 inches)

C_D drag coefficient, $\frac{\text{Drag}}{qS}$, where drag is total measured drag minus base drag

$C_{D,i}$ internal-drag coefficient, $\frac{\text{Internal drag}}{qS}$

C_L lift coefficient, $\frac{\text{Lift}}{qS}$

C_{L_α} lift-curve slope per degree, $\frac{\partial C_L}{\partial \alpha}$

C_l rolling-moment coefficient, $\frac{\text{Rolling moment}}{qSb}$

C_{l_β} rate of change of rolling-moment coefficient with sideslip (effective-dihedral parameter) per degree, $\frac{\Delta C_l}{\Delta \beta}$

C_m pitching-moment coefficient, $\frac{\text{Pitching moment}}{qS\bar{c}}$

ORIGINAL PAGE IS
OF POOR QUALITY

$C_{m,o}$ pitching-moment coefficient at zero lift

$C_{m_{C_L}}$ longitudinal stability derivative, $\frac{\partial C_m}{\partial C_L}$

C_n yawing-moment coefficient, $\frac{\text{Yawing moment}}{qSb}$

C_{n_β} rate of change of yawing-moment coefficient with sideslip (directional-stability parameter) per degree, $\frac{\Delta C_n}{\Delta_\beta}$

C_p pressure coefficient, $\frac{p_l - p_\infty}{q}$, where p_l is local static pressure and p_∞ is free-stream static pressure

C_Y side-force coefficient, $\frac{\text{Side force}}{qS}$

C_{Y_β} rate of change of side-force coefficient with sideslip per degree, $\frac{\Delta C_Y}{\Delta_\beta}$

c streamwise chord of basic wing panel

$\bar{c}$ mean geometric chord of basic wing panel, 18.087 cm (7.121 inches), defined as $\frac{2}{S}\int_0^{1.0} c^2 d\left(\frac{y}{b/2}\right)$

c' streamwise chord of total wing planform which includes leading-edge glove and trailing-edge extension

c_{av} average chord of basic wing panel, S/b, 16.87 cm (6.64 inches)

c_n wing-section normal-force coefficient, $\int_{l.e.}^{t.e.} (C_{p,l} - C_{p,u}) d(x/c)$, where $C_{p,l}$ is lower surface pressure coefficient and $C_{p,u}$ is upper surface pressure coefficient

M Mach number of undisturbed stream

$p_{t,\infty}$ total pressure of undisturbed stream

q dynamic pressure of undisturbed stream

R Reynolds number

R/ft	Reynolds number per foot
R/m	Reynolds number per meter
S	wing area (basic panels) including fuselage intercept, 0.193 m^2 (2.075 sq ft)
V_e	velocity of flow in duct at the duct exit
V_∞	velocity of undisturbed stream
w	mass flow in duct, $\rho_e V_e A_e$
w/w_∞	mass-flow ratio of individual duct referenced to half the inlet area, $\dfrac{\rho_e V_e A_e}{\rho_\infty V_\infty A_i/2}$
$(w/w_\infty)_{av}$	average mass-flow ratio of the ducts, $\dfrac{\left[(w/w_\infty)_{duct\ 1} + (w/w_\infty)_{duct\ 2}\right]}{2}$
x	distance measured from leading edge of local streamwise chord of basic wing panel, positive toward wing trailing edge
x'	streamwise wing ordinate measured from leading edge of total streamwise chord of wing, c', positive toward wing trailing edge
y	distance measured spanwise from plane of symmetry, zero at fuselage center line
z'	vertical wing ordinate measured from model waterline 26.205 cm (10.371 inches)
α	angle of attack, referred to fuselage reference line, deg
β	angle of sideslip, referred to fuselage center line (positive when nose is left), deg
δ	vertical wing deflection under load

δ_h horizontal-tail deflection angle, referred to fuselage reference line (positive when trailing edge is down), deg

ρ_e mass density of flow in duct at duct exit

ρ_∞ mass density of undisturbed stream

Subscript:

t tip

Abbreviations:

l.e. leading edge

t.e. trailing edge

MODEL DESCRIPTION

Basic Model

Drawings of the 0.087-scale (1/11.5) model are presented in figure 1(a) and several model photographs are shown in figure 2. The wing semispan planform layout is shown in figure 1(b).

The model wing was mounted at a root incidence angle of 1.5° relative to the fuselage reference line and had a basic-panel (see fig. 1(a)) aspect ratio of 6.8, a basic-panel taper ratio of 0.36, and 42.24° sweepback at the basic-panel quarter-chord line. The area of the basic wing panels including the fuselage intercept is 0.193 m^2 (2.075 sq ft), and the basic-wing-panel mean geometric chord is 18.087 cm (7.121 inches) in length. The model wing also incorporates approximately 5° of twist between the root and tip chords (washout). The deflection of the model wing along the structural span due to aerodynamic load at a Mach number of 0.99 and a lift coefficient of 0.429 is presented in figure 3.

The supercritical-wing –fuselage juncture employs a leading-edge glove and a trailing-edge extension. (See fig. 1(a).) The present supercritical-wing model also employs an aft-fuselage area-rule fairing which is located on top of the fuselage and extends from approximately the wing trailing edge to the middle of the vertical tail as shown in the photographs of figure 2. This fuselage addition provides a fairing over the existing wing-hinge fittings and was designed to improve the cross-sectional area progression of the combined fuselage-tail region of the basic airplane. Previous tests for the

model without the aft-fuselage addition indicated an earlier drag divergence which was found to be associated with the cross-sectional area development for this region of the model.

The vertical and horizontal tails are scaled versions of those on the basic TF-8A aircraft. In fact, other than the addition of the supercritical wing (including the leading-edge glove and the trailing-edge extension) and the aft-fuselage fairing, the external contours of the basic TF-8A fuselage have not been altered. However, unlike the TF-8A aircraft which has a single-engine duct, the model was constructed with two ducts which are split toward the rear of the fuselage to allow room for the model support sting. The model has a total inlet capture area of 28.387 cm^2 (4.4 sq in.) and a combined duct exit area of 31.935 cm^2 (4.95 sq in.).

Model Configurations

A configuration schedule with associated test conditions is presented in table I. Data are presented in this report for configurations 136, 138, and 140; these designations were used during the development tests and are retained here because of their significance to the very extensive wind-tunnel research program conducted on the present supercritical-wing aircraft. The wind-tunnel design program culminated with the three configurations listed, and of these three, configuration 140 was used as the basis for establishing the wing and aft-fuselage fairing coordinates for the full-scale airplane. However, the completed flight vehicle differs from configuration 140 in several ways, and these differences are discussed in a subsequent section.

Configuration 138 included a modification to the model which provided additional cross-sectional area in the vicinity of the canopy and the glove-fuselage intersection. Although this additional cross-sectional area improved the area distribution of the model, it would have restricted the pilot's visibility; therefore, this modification to the model was removed, and the resulting configuration was designated 140. In determining configuration 140, the extension of the wing glove onto the canopy was further reduced from the original position as employed for configuration 136 which had preceded configuration 138 in the development program. The small part of the glove which extends onto the canopy is referred to as the "cape" and is shown in the schematic of figure 1(c). This diagram of the glove-cape arrangement is representative of configuration 140.

Although the exact contours for configurations 136 and 138 were not documented, the only significant difference in basic-model contours between the three configurations is the variation in glove cross-sectional area in the vicinity of the canopy which has been discussed. Although configuration 140 is closest to the flight vehicle, the results for configurations 136 and 138 were included since they contain the effects of variation in Reynolds

number and the higher angle-of-attack data which were obtained in this investigation for these configurations only.

For configuration 140, the longitudinal development of cross-sectional area taken normal to the fuselage reference line is presented in figure 4. This area distribution includes the total inlet capture area of 28.387 cm^2 (4.4 sq in.).

DISSIMILARITY BETWEEN MODEL AND FULL-SCALE AIRPLANE

The full-scale supercritical wing was constructed from the coordinates presented in table II. Each set of coordinates has been nondimensionalized by the total streamwise chord c' at each wing station. In order to compensate for the difference in the elastic properties between the model and full-scale wings, jig offsets were utilized so that under load, the full-scale wing would conform to the same twist distribution as the model wing for the design-load conditions $\left(\text{approximately } M = 0.99 \text{ and } C_L = 0.40\right)$.

Although the wing coordinates were originally taken from configuration 140, differences developed between the model and full-scale wings as a result of lofting and smoothing procedures and because of unexpected changes required during the construction of the wing and its adaptation to the TF-8A fuselage. Although the differences between the model and full-scale wing coordinates are felt to be small, other dissimilarities exist between the present model configurations and the full-scale airplane that would preclude a direct correlation between the present wind-tunnel results and flight data. These dissimilarities will be discussed in some detail in the following paragraphs.

The full-scale supercritical wing was lowered with respect to the fuselage by 0.137 cm (0.054 inch) model scale. Whereas the reference water line for the wing coordinates on the present model configurations is 26.343 cm (10.371 inches), the reference water line for the full-scale wing would correspond to 26.205 cm (10.317 inches) on the 0.087-scale model. As a result of lowering the wing, it was necessary to remove a small amount of area on the lower surface of the wing near the fuselage juncture. This modification is reflected in the full-scale wing coordinates of table II but was not included on the model wing for the present investigation since the wing was located in the higher position.

In the process of mating the rear-fuselage addition to the TF-8A aircraft, its length was reduced by 1.905 cm (0.75 inch) model scale and it was also slightly modified to cover completely the existing wing-hinge fittings which are located near the juncture of the wing trailing edge and the fuselage.

In addition to the basic contour modifications which have been noted, several major items have been employed on the full-scale airplane that were not incorporated on the present model configurations. These include underwing leading-edge vortex generators (developed in a more recent wind-tunnel investigation), aileron-hinge fairings, and a nose-

mounted airspeed probe. Smaller protuberances such as camera fairings and lights which exist on the flight vehicle were also not simulated on the present model configurations.

Although it was not the purpose of this paper to present a basis for a correlation of the wind-tunnel and full-scale results, it was felt that the differences which have been noted between the present model configurations and the full-scale aircraft should be documented. For more recent wind-tunnel investigations, the present 0.087-scale model has been modified in an effort to keep the disparity between the wind-tunnel model and the full-scale aircraft to a minimum.

TESTS AND CORRECTIONS

Tunnel Descriptions

Most of the investigation was conducted in the Langley 8-foot transonic pressure tunnel, but a limited amount of supersonic data were obtained in the Langley 16-foot transonic tunnel.

The Langley 8-foot transonic pressure tunnel is a continuous, single-return, rectangular, slotted-throat tunnel having controls that allow for the independent variation of Mach number, density, temperature, and dewpoint. The stagnation temperature and dewpoint temperature were maintained at values sufficient to avoid significant condensation effects. For the present investigation, because of the relatively large size of the model with respect to the tunnel, the normal tunnel slots (only the tunnel top and bottom walls are slotted) which give a tunnel-wall open ratio of 6 percent were replaced by special slots having an open ratio of 22 percent. These latter slots were designed on the basis of reference 6 to give theoretically zero three-dimensional blockage.

The Langley 16-foot transonic tunnel is a continuous, single-return, atmospheric tunnel with a slotted octagonal throat and test section which is 4.724 meters (15.5 feet) wide and 6.7056 meters (22 feet) long. A more complete description of these facilities is contained in reference 7.

Tunnel Test Conditions

Tests were conducted in the Langley 8-foot transonic pressure tunnel at a stagnation temperature of 322 K (120° F) and over a Mach number range that varied from 0.25 to 1.00, whereas in the Langley 16-foot transonic tunnel, tests were conducted at Mach numbers from 0.95 to 1.30. Although no attempts were made to correct the data from the Langley 16-foot facility for condensation effects, it is felt that they are small since the stagnation temperatures ranged from approximately 333 K (140° F) to 341 K (155° F). However, based on calibrations of the Langley 16-foot transonic tunnel, the test-section-wall divergence angle is adjusted as a function of airstream dewpoint in order to eliminate

longitudinal static-pressure gradients on the test-section center line that might occur because of condensation of atmospheric moisture at Mach numbers from 1.2 to 1.?.

Where possible, tests were conducted over the Mach number range at a constant dynamic pressure in the Langley 8-foot transonic pressure tunnel. This procedure in conjunction with unpublished results for a second supercritical wing, which is geometrically identical but more elastic, would permit aeroelasticity and Reynolds number effects to be isolated more easily. Furthermore, for a tunnel dynamic pressure of 44 193 N/m^2 (923 lb/sq ft), the present steel wing should have approximately the same relative deflection as the full-scale supercritical wing near a Mach number of 1 at 13.716 km (45 000 feet).

The tunnel-test conditions for the present investigation are summarized in table III.

Measurements

Six-component force and moment data were obtained by using an electrical strain-gage balance housed within the fuselage cavity. Measurements were taken over a Mach number range varying from 0.25 to 1.30 for angles of attack that generally varied from -8° to 15°. However, several runs were made to obtain higher angle-of-attack data, and this angle-of-attack range varied from approximately 9° to 24°. These higher angle-of-attack data were obtained by using an offset coupling which is shown in figure 1(d). Force and moment data were also obtained through the lower angle-of-attack range for sideslip angles of 2.5° and -2.5°.

For determination of the base drag, the static pressure in the balance chamber and in the plane of the model base were recorded by use of differential-pressure transducers referenced to the free-stream static pressure. In addition, the wing was instrumented with flush-surface static-pressure orifices distributed in streamwise rows over the upper right and lower left wing panels. The surface pressures were measured with the use of differential-pressure scanning-valve units mounted within the fuselage. A sample of these pressure data are included herein for a Mach number of 0.99 and a lift coefficient of 0.443. The semispan aerodynamic load distribution has also been included for the same Mach number and lift coefficient. Complete pressure data results for the present investigation are contained in reference 5.

To aid in the analysis of the boundary-layer flow patterns, photographs were taken at selected test conditions of the wing upper and lower surfaces employing the fluorescent oil film technique described in reference 8. Typical photographs for a Mach number of 0.99 are presented in figure 5.

ORIGINAL PAGE IS
OF POOR QUALITY

Corrections

Drag results presented herein have been adjusted to correspond to free-stream static pressure acting in the balance chamber and at the model base; however, no adjustments to drag have been made for the internal flow through the ducts. Results from more recent investigations of the internal-drag and mass-flow characteristics conducted in both the Langley 8-foot transonic pressure tunnel and the Langley 16-foot transonic tunnel with the same model are presented in figure 6. The results from the 8-foot transonic pressure tunnel are presented in figures 6(a) and 6(b) and a comparison of the results from the 8-foot transonic pressure tunnel and the 16-foot transonic tunnel are presented in figure 6(c).

The internal drag and mass-flow ratios were determined from measurements of the total-pressure distribution and the static pressure in the duct exit planes by use of a rake consisting of ten pitot-pressure tubes and one static-pressure tube per duct. The 16-foot transonic tunnel internal-drag coefficients and mass-flow ratios were determined for the Reynolds numbers shown in table III for that facility whereas the 8-foot transonic pressure tunnel internal-flow results were obtained only for the higher Reynolds numbers listed in table III for the 8-foot transonic pressure tunnel.

The model support sting (with the exception of the offset coupling) was designed on the basis of the results in reference 9 to minimize sting interference at near-sonic Mach numbers.

The large size of the present model relative to the tunnel size raises a question of absolute accuracy of the results at test Mach numbers approaching 1.00. Estimates have indicated that solid blockage effects for the present model in the 8-foot transonic pressure tunnel are theoretically zero based on the results of reference 6, but there is some question as to the accuracy of this theory at sonic speed. No corrections, however, have been applied to the data for either solid or wake blockage effects.

Corrections have been made to the measured angle of attack for model support sting and balance deflections occurring as a result of aerodynamic loads on the model and for tunnel airflow angularity. For the 8-foot transonic pressure tunnel data only, further corrections have been made to the measured angle of attack for the first-order boundary-induced effects as calculated from the theory of reference 10. This correction amounts to a reduction in the measured angle of attack by 0.24 multiplied by the normal-force coefficient.

Boundary-Layer Transition

The model boundary-layer transition arrangements (designated herein as types I, II, and III) that were used over the Mach number range for this investigation are described

ORIGINAL PAGE IS
OF POOR QUALITY

in table IV, and the type I and type II arrangements have been illustrated for the wing in figure 7.

For Mach numbers 0.95 to 1.30, boundary-layer trips were located on the wing and the tail surfaces by using the technique described in references 11 and 12 to simulate the full-scale Reynolds number boundary-layer characteristics at the wing trailing edge and the full-scale Reynolds number shock location. This particular transition arrangement has been designated herein as type I (see table IV) and is shown for the wing in figures 7(a) and 7(b). It might be noted that the boundary-layer trips used on the wing upper surface for the type I arrangement were located closer to the leading edge inboard of the 15.875 cm (6.25 inches) semispan station than the position which would be calculated from reference 12 for this section of the wing. This more forward location was determined experimentally by using the fluorescent oil film technique (ref. 8) and was used to prevent unnatural laminar separation from occurring ahead of the transition strip. It is important to note that this type of separation would not occur on the full-scale airplane since turbulent boundary-layer flow is usually established very close to the wing leading edge at the full-scale Reynolds numbers.

For Mach numbers of 0.50, 0.80, and 0.90, the boundary-layer transition arrangement which is designated type II was employed, and this pattern is shown in figure 7(c) for the wing upper surface. The wing lower surface and the remainder of the model boundary-layer trips were the same as those for the type I arrangement. The boundary-layer trips on the wing upper surface for the type II arrangement were located close to the leading edge to prevent laminar separation from occurring ahead of the transition strip. Again, such separation is unnatural in that it would not occur at full-scale Reynolds numbers.

At a Mach number of 0.25, the type III transition arrangement was employed. For this arrangement, all the model boundary-layer trips, except for the wing lower surface, were located at 5 percent of the local streamwise chords. The boundary-layer trips on the wing lower surface, however, were located at 45 percent of the local streamwise chords in an effort to simulate the full-scale Reynolds number boundary-layer thickness at the lower surface trailing-edge cusp.

For all test Mach numbers, boundary-layer trips of number 120 carborundum grains were applied around the fuselage 3.81 cm (1.50 inches) aft of the nose and 1.27 cm (0.50 inch) rearward of the inlet lip on both the inner and outer surfaces. All model transition strips were 0.127 cm (0.05 inch) wide and were located by measurements taken in the streamwise directions.

When employing the rearward transition locations as calculated from reference 12 to simulate the full-scale Reynolds number boundary-layer characteristics at the wing trailing edge, transition must only occur at the prescribed trip locations. As a result, it

is important to maintain the model region ahead of the boundary-layer trips in an extremely smooth condition to prevent premature transition to turbulent flow. Furthermore, any appreciable separation of the laminar boundary layer ahead of the rearward transition strips could cause erroneous results and would therefore compromise the original intent of simulating the full-scale Reynolds number boundary-layer characteristics at the trailing edge. For the present investigation, when laminar separation did occur at the relatively low test Reynolds numbers, the boundary-layer trips were moved to a more conventional location near the wing leading edge. (Note wing upper surface for the type II arrangement and the wing upper surface inboard of the 15.875 cm (6.25 inches) semispan station for the type I arrangement.)

The more forward boundary-layer trips (at 0.05c') were located and sized by the procedures described in reference 13. Although located as prescribed in reference 12, the rearward boundary-layer trips were also sized by the procedures discussed in reference 13.

PRESENTATION OF RESULTS

The results of this investigation are presented in the following figures:

	Figure
Longitudinal aerodynamic characteristics:	
Effect of Reynolds number on the longitudinal aerodynamic characteristics. $\beta = 0^{\circ}$; $\delta_h = -2.5^{\circ}$	8
Longitudinal aerodynamic characteristics for an extended angle-of-attack range. $\beta = 0^{\circ}$; $\delta_h = -2.5^{\circ}$	9
Longitudinal aerodynamic characteristics for configuration 140 with the horizontal tail off. $\beta = 0^{\circ}$	10
Longitudinal aerodynamic characteristics for configuration 140 obtained in the Langley 8-foot transonic pressure tunnel and the Langley 16-foot transonic tunnel. $\beta = 0^{\circ}$; $\delta_h = -2.5^{\circ}$	11
Variation with Mach number of the longitudinal aerodynamic characteristics. $\beta = 0^{\circ}$	12
Variation with Mach number of the drag coefficient at a lift coefficient of 0.44. $\beta = 0^{\circ}$; $\delta_h = -2.5^{\circ}$	13
Effect of sideslip on the longitudinal aerodynamic characteristics. $\delta_h = -2.5^{\circ}$	14
Lateral-directional aerodynamic characteristics:	
Effect of sideslip on the lateral-directional aerodynamic coefficients. $\delta_h = -2.5^{\circ}$	15

ORIGINAL PAGE IS
OF POOR QUALITY

Figure

Variation with Mach number of the lateral-directional aerodynamic stability derivatives. $\delta_h = -2.5^{\circ}$ 16

Aerodynamic load results:

Streamwise-chord pressure distributions at a Mach number of 0.99 and a lift coefficient of 0.443 17

Semispan aerodynamic load distribution for a Mach number of 0.99 and a lift coefficient of 0.443 18

DISCUSSION OF RESULTS

Effects of Reynolds Number and Aeroelasticity on the Pitching-Moment Characteristics

At any Mach number, increasing the tunnel total pressure results in an increase of both Reynolds number and dynamic pressure. For this reason, it is very difficult to study their effects independently. The combined effects of increased Reynolds number and wing aeroelastic deflection on pitch-up are more pronounced than their effects on the lift characteristics as shown in figure 8.

For example, figure 8(a) indicates that the lift coefficient at which pitch-up occurs for a Mach number of 0.25 is extended by approximately 0.09 when the Reynolds number is increased from 6.6×10^6/m (2.0×10^6/ft) to 10.2×10^6/m (3.1×10^6/ft). Unpublished results for tests up to a Reynolds number of 30.6×10^6/m (9.3×10^6/ft) at a Mach number of 0.25 also indicate that the lift coefficient at pitch-up is further increased by similar increments as the Reynolds number is increased.

As noted earlier, the effects described occur as a result of increases in both Reynolds number and wing aeroelastic deflection. In an effort to distinguish between the effects of Reynolds number and aeroelasticity, a second wing, constructed of aluminum and therefore more elastic, was tested at tunnel pressures so that the aeroelastic deflections for both the steel and aluminum wings were approximately the same. Based upon these results (unpublished), it appears that at the higher subsonic Mach numbers, Reynolds number effects on pitch-up may be less predominant than the effects of aeroelasticity for the relatively high swept wing, although both tend to delay pitch-up as they increase. Increased dynamic pressure results in increased wing loading and in greater wing twist. This twist increment tends to unload or "wash-out" the wing tips and delays stall on the region of the wing. Improved pitching-moment characteristics which are associated with the effects noted are evident (see fig. 8) at all the higher subsonic Mach numbers.

Longitudinal Aerodynamic Characteristics

Lift characteristics.- As shown in figure 9, although the lift-curve slopes decrease at the higher angles of attack, a point of maximum lift is not reached over the range of these tests. The variation of lift-curve slope with Mach number is presented in figure 12(a). These slopes were taken at angles of attack between 0° and 4°, and it might be noted that the curves are practically linear over this angle-of-attack range. Figure 12(a) indicates that the lift-curve slopes increase up to Mach 1.0 and then decrease as the Mach number is increased above 1.0.

Pitching-moment characteristics.- The variations with Mach number of the longitudinal stability derivatives, which were measured at angles of attack between 0° and 4° and the pitching-moment coefficient at zero lift are presented in figures 12(b) and 12(c), respectively. Although at the high Mach numbers the static margin increases considerably as indicated by the more negative trend of $C_{m_{C_L}}$, trim-drag penalties near the cruise-lift coefficient are minimized to a large extent by the positive trend of $C_{m,o}$ with Mach number. Another important factor relating to the level of stability of the aircraft is that the present data were computed about a center-of-gravity location of $0.25\bar{c}$ whereas it is anticipated that the aircraft will fly with the center of gravity at $0.35\bar{c}$.

As a matter of interest, the curve of $C_{m,o}$ plotted against Mach number (fig. 12(c)) is for a configuration having a horizontal-tail angle of -2.5°. This configuration was chosen because estimates have indicated that this tail angle would be required for trim at the cruise Mach number and lift coefficient with the aircraft center of gravity located at $0.35\bar{c}$.

With regard to the variation of pitching-moment coefficient with angle of attack, the results for the extended angle-of-attack range are presented in figure 9. Although pitch-up does occur at each Mach number, it is well beyond level-flight lift coefficients and all the pitching-moment curves become stable again as the angle of attack is increased beyond the point of pitch-up. Unpublished results from more recent wind-tunnel tests employing the same model show that with the addition of underwing leading-edge vortex generators, pitch-up is either eliminated or significantly reduced over the same angle of attack and Mach number range for which data are presented herein. The higher angle-of-attack data were obtained with an offset-sting arrangement shown in figure 1(c) and the interference effects associated with this support account for the slight misalinement with the lower angle-of-attack results. Nevertheless, the agreement for these two sets of data obtained with considerably different sting arrangements is considered to be good.

Drag characteristics.- The variation of drag coefficient with Mach number at a lift coefficient of 0.44 (approximately the cruise lift coefficient) is shown in figure 13. It should be noted that the drag coefficients have not been corrected for internal drag; how-

ORIGINAL PAGE IS
OF POOR QUALITY

ever, the internal drag coefficients and mass-flow ratios for the model are presented in figure 6. Figure 13 indicates a drag-divergence Mach number of about 0.97 to 0.98 for configurations 136 and 140 (drag-divergence Mach number is defined as the Mach number where $\left(\partial C_D/\partial M\right) = 0.1$). All drag values in figure 13 were selected from the higher Reynolds number data for the results from the Langley 8-foot transonic pressure tunnel, and the drag points at Mach numbers of 0.98 and 1.00 were obtained from limited-range drag polars which have not been included in this report.

In regard to the determination of drag-divergence Mach number, it should be pointed out that although the drag divergence for the complete configuration occurs at a Mach number of about 0.97 to 0.98, the oil-flow photographs of figure 5 and the pressure distributions given in figure 17 for a Mach number of 0.99 indicate that the flow over the wing is still good, only a small degree of trailing-edge separation being evident. It was conjectured that the drag divergence noted is associated with the overall configuration area distribution. Unpublished results verify this result in that improvement in the overall area distribution through the use of area-rule, fuselage-side fairings resulted in increases in drag divergence Mach number and clean wing flow characteristics at a Mach number of 1.00 for lift coefficients of approximately 0.44. Figure 12(a) also substantiates this result in that the lift-curve slope reaches a maximum near Mach 1.00.

The drag values for the horizontal-tail-off configuration shown in figure 13 were taken at the angle of attack which corresponds to a lift coefficient of 0.44 for the same horizontal-tail-on configuration. (See fig. 10.) For the corresponding angles of attack, the lift coefficients for the horizontal-tail-off configuration were only slightly different from 0.44 between Mach numbers of 0.80 and 1.00 (that is, $C_L = 0.42$ at $M = 0.80$ and $C_L = 0.44$ at $M = 1.00$).

Based on unpublished data for several similar configurations, the drag results for configuration 136 at a Mach number of 0.80 (see fig. 13) appear to be in error. Therefore, the drag point at a Mach number of 0.80 in figure 13 was faired on the basis of the unpublished data and the drag polar at a Mach number of 0.80 for configuration 136 in figure 8 has been omitted.

A review of the summary results presented in figures 12 and 13 indicates measurable differences between the results obtained in the Langley 8-foot transonic pressure tunnel and the Langley 16-foot transonic tunnel, particularly in the $M = 0.99$ data. The agreement between the data at $M = 0.95$ is thought to be reasonably good (see fig. 11); however, the reasons for the differences in the results at a Mach number of 0.99 remain uncertain. Although tests were conducted in the two facilities at different Reynolds numbers, the differences noted in figure 11 do not correspond with the effects of variation in Reynolds number as shown in figure 8, especially for the pitching-moment and lift characteristics.

Lateral-Directional Aerodynamic Characteristics

Figure 14 presents the effect of sideslip angle on the longitudinal aerodynamic characteristics for Mach numbers of 0.25, 0.95, and 0.99. Although some changes are noted in the pitching-moment curves for the sideslip angles at which data were obtained, the effect of variation in sideslip angle on the lift and drag characteristics is small.

The lateral-directional aerodynamic coefficients at sideslip angles of 0° and $\pm 2.5^{\circ}$ and for an angle-of-attack range that varied from -2° to 14° are presented in figure 15 for Mach numbers of 0.25, 0.95, and 0.99. The lateral-directional aerodynamic stability derivatives $\left(C_{l_\beta}, C_{n_\beta}, \text{and } C_{Y_\beta}\right)$ have been computed for angles of attack of 0°, 4°, and 8° and are presented in figure 16 for Mach numbers of 0.25, 0.95, and 0.99. Directional stability and positive effective dihedral are indicated throughout the angle-of-attack and sideslip-angle range for the three Mach numbers at which data are presented in figure 15.

Aerodynamic Load Results

As a matter of interest, the streamwise-chord pressure distributions at a Mach number of 0.99 and a lift coefficient of 0.443 are given in figure 17, and the semispan aerodynamic load distribution for the same Mach number and lift coefficient is presented in figure 18. It might be noted that in figure 17, the 4.4-percent-semispan station is along the fuselage and thereby accounts for the abrupt pressure changes, and the first 12 points, which are unfaired, are located on the canopy. No appreciable separation on the wing is indicated by these pressure data at this Mach number and lift coefficient. Complete-wing pressure data results and analysis for this investigation are contained in reference 5.

CONCLUSIONS

The present wind-tunnel investigation of the basic aerodynamic characteristics of a supercritical-wing research airplane configuration has shown the following results:

1. A drag-divergence Mach number of approximately 0.97 to 0.98 at a lift coefficient of 0.44 is indicated for the complete configuration; however, oil-flow photographs of the wing and wing pressure data indicate that the wing is still performing well at a Mach number of 0.99.

2. The combined effects of increased Reynolds number and increased wing twist due to aerodynamic load result in significant improvements in the pitch-up characteristics, particularly at a Mach number of 0.25.

3. Notable increases in longitudinal stability occur as the Mach number is increased above 0.90. However, an attendant increase in the positive values of pitching-moment

ORIGINAL PAGE IS
OF POOR QUALITY

coefficients at zero lift $\left(C_{m,o}\right)$ results in a powerful compensating effect so that little change in trim angle of attack occurs with increasing Mach number.

4. Both directional stability and positive effective dihedral are indicated throughout the Mach number, angle-of-attack, and sideslip-angle range for which data were obtained ($M = 0.25, 0.95, 0.99$; $\beta = 0^{\circ}, \pm 2.5^{\circ}$; and $\alpha = -2^{\circ}$ to 14°).

Langley Research Center,
National Aeronautics and Space Administration,
Hampton, Va., November 29, 1971.

REFERENCES

1. Whitcomb, Richard T.; and Clark, Larry R.: An Airfoil Shape for Efficient Flight at Supercritical Mach Numbers. NASA TM X-1109, 1965.
2. Whitcomb, Richard T.; and Blackwell, James A., Jr.: Status of Research on a Supercritical Wing. Conference on Aircraft Aerodynamics, NASA SP-124, 1966, pp. 367-381.
3. Harris, Charles D.: Wind-Tunnel Investigation of Effects of Trailing-Edge Geometry on a NASA Supercritical Airfoil Section. NASA TM X-2336, 1971.
4. Harris, Charles D.; and Blackwell, James A., Jr.: Wind-Tunnel Investigation of Effects of Rear Upper Surface Modification on an NASA Supercritical Airfoil. NASA TM X-2454, 1972.
5. Harris, Charles D.: Wind-Tunnel Measurements of Aerodynamic Load Distribution on an NASA Supercritical-Wing Research Airplane Configuration. NASA TM X-2469, 1971.
6. Davis, Don D., Jr.; and Moore, Dewey: Analytical Study of Blockage- and Lift-Interference Corrections for Slotted Tunnels Obtained by the Substitution of an Equivalent Homogeneous Boundary for the Discrete Slots. NACA RM L53E07b, 1953.
7. Schaefer, William T., Jr.: Characteristics of Major Active Wind Tunnels at the Langley Research Center. NASA TM X-1130, 1965.
8. Loving, Donald L.; and Katzoff, Samuel: The Fluorescent Oil Film Method and Other Techniques for Boundary-Layer Flow Visualization. NASA MEMO 3-17-59L, 1959.
9. Lee, George; and Summers, James L.: Effects of Sting-Support Interference on the Drag of an Ogive-Cylinder Body With and Without a Boattail at 0.6 to 1.4 Mach Number. NACA RM A57I09, 1957.
10. Wright, Ray H.; and Barger, Raymond L.: Wind-Tunnel Lift Interference on Swept-back Wings in Rectangular Test Sections With Slotted Top and Bottom Walls. NASA TR R-241, 1966.
11. Loving, Donald L.: Wind-Tunnel—Flight Correlation of Shock-Induced Separated Flow. NASA TN D-3580, 1966.
12. Blackwell, James A., Jr.: Preliminary Study of Effects of Reynolds Number and Boundary-Layer Transition on Shock-Induced Separation. NASA TN D-5003, 1969.
13. Braslow, Albert L.; and Knox, Eugene C.: Simplified Method for Determination of Critical Height of Distributed Roughness Particles for Boundary-Layer Transition at Mach Numbers From 0 to 5. NACA TN 4363, 1958.

TABLE I.- CONFIGURATION SCHEDULE

Configuration	δ_h, deg	β, deg	Transition type	Mach number range	Wind tunnel
136	-2.5	0	I	0.95, 0.98, 0.99, 1.00	8-ft TPT
136		0	II	0.50, 0.80, 0.90	
136		±2.5	I	0.95, 0.99	
136		0, ±2.5	III	0.25	
138		0	I	0.95, 0.98, 0.99, 1.00	
138			II	0.50, 0.80, 0.90	
138			III	0.25	
140			I	0.95, 0.99	
140			I	0.95, 0.99, 1.02, 1.20, 1.30	16-ft TT
140	Horizontal tail off		I	0.95, 0.98, 0.99, 1.00	8-ft TPT
140	Horizontal tail off		II	0.50, 0.80, 0.90	8-ft TPT

ORIGINAL PAGE IS
OF POOR QUALITY

TABLE II. WING COORDINATES ALONG STREAMWISE CHORDS

(a) Wing planform coordinate layout

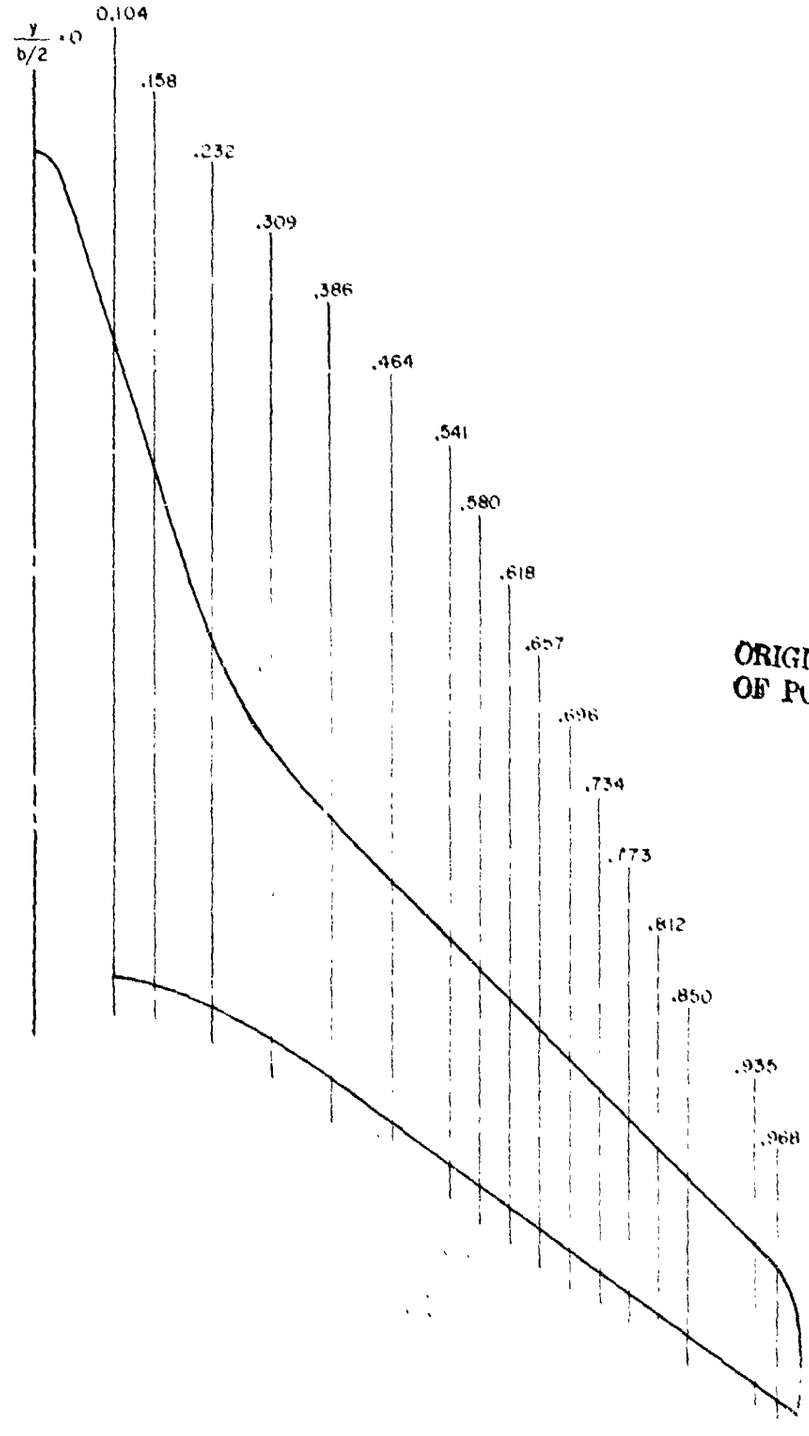

ORIGINAL PAGE IS
OF POOR QUALITY

TABLE II.- WING COORDINATES ALONG STREAMWISE CHORDS – Continued

(b) $\frac{y}{b/2} = 0.104$; c' = 45.639 cm (18.047 in.)

x'/c'	z'/c'		x'/c'	z'/c'		x'/c'	z'/c'	
	Upper surface	Lower surface		Upper surface	Lower surface		Upper surface	Lower surface
0	0.0379	0.0379	0.0240	0.0608	0.0133	0.0958	0.0777	-0.0057
.00001	.0384	.0373	.0250	.0613	.0128	.0979	.0781	-.0061
.00004	.0389	.0368	.0261	.0617	.0123	.1000	.0784	-.0064
.00010	.0395	.0362	.0272	.0621	.0118	.1022	.0787	-.0068
.0002	.0400	.0357	.0283	.0625	.0114	.1043	.0790	-.0071
.0003	.0406	.0351	.0294	.0629	.0109	.1065	.0793	-.0075
.0004	.0411	.0345	.0306	.0633	.0104	.1087	.0797	-.0078
.0006	.0417	.0340	.0318	.0637	.0100	.1110	.0800	-.0081
.0007	.0422	.0334	.0330	.0641	.0095	.1132	.0803	-.0085
.0009	.0428	.0329	.0342	.0645	.0091	.1155	.0806	-.0088
.0011	.0433	.0323	.0355	.0649	.0086	.1178	.0809	-.0091
.0014	.0438	.0318	.0368	.0653	.0082	.1201	.0812	-.0094
.0016	.0444	.0312	.0381	.0657	.0078	.1224	.0815	-.0097
.0019	.0449	.0307	.0394	.0661	.0073	.1248	.0818	-.0100
.0022	.0454	.0301	.0408	.0665	.0069	.1272	.0821	-.0103
.0025	.0460	.0296	.0421	.0669	.0065	.1296	.0824	-.0107
.0029	.0465	.0290	.0435	.0673	.0061	.1321	.0827	-.0110
.0033	.0470	.0285	.0449	.0677	.0056	.1345	.0829	-.0113
.0037	.0475	.0279	.0464	.0681	.0052	.1370	.0832	-.0116
.0041	.0481	.0274	.0478	.0685	.0048	.1395	.0835	-.0119
.0045	.0486	.0268	.0493	.0688	.0044	.1420	.0838	-.0122
.0050	.0491	.0263	.0508	.0692	.0040	.1446	.0840	-.0125
.0055	.0496	.0257	.0523	.0696	.0036	.1471	.0843	-.0128
.0060	.0501	.0252	.0539	.0700	.0032	.1497	.0845	-.0131
.0065	.0506	.0246	.0555	.0703	.0027	.1523	.0848	-.0134
.0071	.0511	.0241	.0571	.0707	.0024	.1550	.0851	-.0136
.0077	.0516	.0236	.0587	.0710	.0020	.1576	.0853	-.0139
.0083	.0521	.0230	.0603	.0713	.0016	.1603	.0855	-.0142
.0089	.0526	.0225	.0620	.0717	.0012	.1630	.0858	-.0145
.0095	.0531	.0220	.0637	.0720	.0008	.1658	.0860	-.0148
.0102	.0536	.0214	.0654	.0723	.0004	.1685	.0863	-.0150
.0109	.0541	.0209	.0671	.0727	0	.1713	.0865	-.0153
.0116	.0546	.0204	.0689	.0730	-.0004	.1741	.0868	-.0156
.0123	.0550	.0198	.0707	.0733	-.0007	.1769	.0870	-.0158
.0131	.0555	.0193	.0725	.0736	-.0011	.1797	.0872	-.0161
.0139	.0560	.0188	.0743	.0740	-.0015	.1826	.0874	-.0163
.0147	.0565	.0183	.0761	.0743	-.0019	.1855	.0877	-.0166
.0155	.0569	.0178	.0780	.0747	-.0023	.1884	.0879	-.0168
.0163	.0574	.0172	.0799	.0750	-.0026	.1913	.0881	-.0171
.0172	.0578	.0167	.0818	.0754	-.0030	.1943	.0883	-.0173
.0181	.0583	.0162	.0837	.0757	-.0034	.1973	.0885	-.0175
.0190	.0587	.0157	.0857	.0760	-.0038	.2003	.0887	-.0178
.0200	.0591	.0152	.0877	.0764	-.0042	.2033	.0889	-.0180
.0209	.0596	.0147	.0897	.0767	-.0046	.2063	.0891	-.0182
.0219	.0600	.0142	.0917	.0771	-.0050	.2094	.0892	-.0184
.0229	.0604	.0137	.0938	.0779	-.0053	.2125	.0894	-.0187

[redacted]

TABLE II.- WING COORDINATES ALONG STREAMWISE CHORDS – Continued

(b) $\frac{y}{b/2} = 0.104$; c' = 45.839 cm (18.047 in.) – Concluded

x'/c'	z'/c' Upper surface	z'/c' Lower surface	x'/c	z'/c' Upper surface	z'/c' Lower surface
0.2156	0.0896	-0.0189	0.3833	0.0876	-0.0238
.2187	.0897	-.0191	.3875	.0873	-.0238
.2219	.0899	-.0193	.3917	.0871	-.0238
.2251	.0900	-.0195	.3959	.0868	-.0237
.2283	.0902	-.0197	.4001	.0865	-.0237
.2315	.0903	-.0200	.4044	.0861	-.0236
.2348	.0905	-.0201	.4087	.0858	-.0235
.2380	.0906	-.0203	.4130	.0855	-.0234
.2413	.0907	-.0205	.4173	.0851	-.0233
.2446	.0908	-.0206	.4217	.0848	-.0232
.2480	.0909	-.0208	.4261	.0844	-.0230
.2513	.0910	-.0210	.4305	.0841	-.0230
.2547	.0911	-.0212	.4817	.0793	-.0209
.2581	.0911	-.0213	.5515	.0726	-.0155
.2616	.0912	-.0215	.6095	.0669	-.0095
.2650	.0912	-.0216	.6591	.0617	-.0035
.2685	.0913	-.0218	.7023	.0571	.0018
.2720	.0913	-.0219	.7406	.0530	.0065
.2755	.0913	-.0220	.7748	.0493	.0105
.2791	.0913	-.0222	.8057	.0454	.0135
.2826	.0913	-.0223	.8341	.0414	.0157
.2862	.0913	-.0224	.8602	.0374	.0168
.2898	.0913	-.0225	.8843	.0336	.0170
.2935	.0912	-.0226	.9068	.0299	.0163
.2971	.0912	-.0227	.9277	.0265	.0153
.3008	.0912	-.0228	.9474	.0232	.0140
.3045	.0911	-.0229	.9659	.0196	.0124
.3082	.0910	-.0230	.9747	.0178	.0115
.3120	.0909	-.0231	.9833	.0159	.0103
.3157	.0908	-.0232	.9943	.0132	.0088
.3195	.0907	-.0232	.9966	.0126	.0085
.3233	.0906		1.0000		.0080
.3272	.0904				
.3310	.0903				
.3349	.0901				
.3388	.0900				
.3428	.0898				
.3467	.0897				
.3507	.0895				
.3547	.0893	-.0238			
.3587	.0891	-.0238			
.3627	.0888	-.0239			
.3668	.0886	-.0239			
.3709	.0884	-.0239			
.3750	.0881	-.0239			
.3791	.0879	-.0239			

[redacted]

ORIGINAL PAGE IS OF POOR QUALITY

TABLE II.- WING COORDINATES ALONG STREAMWISE CHORDS – Continued

(c) $\frac{y}{b/2} = 0.158$; c' = 36.873 cm (14.517 in.)

x'/c'	z'/c' Upper surface	z'/c' Lower surface	x'/c'	z'/c' Upper surface	z'/c' Lower surface	x'/c'	z'/c' Upper surface	z'/c' Lower surface
0	0.0384	0.0384	0.1373	0.0834	-0.0104	0.2747	0.0881	-0.0191
.0030	.0472	.0294	.1403	.0837	-.0107	.2776	.0881	-.0191
.0060	.0507	.0257	.1433	.0839	-.0110	.2806	.0880	-.0192
.0090	.0533	.0229	.1463	.0842	-.0113	.2836	.0880	-.0193
.0119	.0554	.0206	.1493	.0844	-.0116	.2866	.0879	-.0194
.0149	.0572	.0186	.1523	.0846	-.0118	.2896	.0879	-.0194
.0179	.0588	.0168	.1552	.0848	-.0121	.2926	.0878	-.0195
.0209	.0602	.0152	.1582	.0851	-.0124	.2956	.0878	-.0196
.0239	.0615	.0137	.1612	.0853	-.0127	.2985	.0877	-.0196
.0269	.0626	.0124	.1642	.0855	-.0129	.3015	.0876	-.0197
.0299	.0636	.0112	.1672	.0857	-.0132	.3045	.0876	-.0197
.0328	.0646	.0100	.1702	.0859	-.0135	.3075	.0875	-.0198
.0358	.0656	.0090	.1732	.0860	-.0137	.3105	.0874	-.0198
.0388	.0665	.0079	.1761	.0862	-.0139	.3828	.0845	-.0192
.0418	.0674	.0070	.1791	.0864	-.0142	.4600	.0802	-.0158
.0448	.0683	.0061	.1821	.0865	-.0144	.5245	.0761	-.0115
.0478	.0691	.0053	.1851	.0867	-.0146	.5797	.0721	-.0068
.0508	.0698	.0045	.1881	.0868	-.0148	.6279	.0681	-.0021
.0537	.0706	.0037	.1911	.0869	-.0151	.6707	.0642	.0027
.0567	.0713	.0029	.1941	.0871	-.0153	.7095	.0605	.0071
.0597	.0719	.0022	.1970	.0872	-.0155	.7447	.0568	.0114
.0627	.0726	.0015	.2000	.0873	-.0157	.7769	.0533	.0153
.0657	.0732	.0008	.2030	.0874	-.0159	.8066	.0501	.0183
.0687	.0738	.0002	.2060	.0874	-.0161	.8341	.0470	.0205
.0717	.0744	-.0005	.2090	.0875	-.0162	.8596	.0438	.0219
.0746	.0750	-.0011	.2120	.0876	-.0164	.8836	.0402	.0225
.0776	.0756	-.0017	.2149	.0877	-.0166	.9075	.0368	.0225
.0806	.0761	-.0022	.2179	.0877	-.0167	.9313	.0333	.0220
.0836	.0766	-.0028	.2209	.0878	-.0169	.9548	.0295	.0207
.0866	.0771	-.0033	.2239	.0878	-.0170	.9663	.0276	.0199
.0896	.0775	-.0038	.2269	.0879	-.0172	.9776	.0255	.0190
.0925	.0780	-.0043	.2299	.0879	-.0174	.9924	.0226	.0174
.0955	.0784	-.0048	.2329	.0880	-.0175	.9956	.0220	.0170
.0985	.0789	-.0052	.2358	.0880	-.0176	1.0000		.0164
.1015	.0793	-.0057	.2388	.0881	-.0178			
.1045	.0797	-.0061	.2418	.0881	-.0179			
.1075	.0801	-.0066	.2448	.0882	-.0180			
.1105	.0804	-.0070	.2478	.0882	-.0182			
.1134	.0808	-.0074	.2508	.0882	-.0183			
.1164	.0811	-.0078	.2538	.0882	-.0184			
.1194	.0815	-.0082	.2567	.0882	-.0185			
.1224	.0818	-.0086	.2597	.0882	-.0186			
.1254	.0821	-.0090	.2627	.0882	-.0187			
.1284	.0825	-.0093	.2657	.0882	-.0188			
.1314	.0828	-.0097	.2687	.0882	-.0189			
.1343	.0831	-.0101	.2717	.0881	-.0190			

[redacted]

TABLE II.- WING COORDINATES ALONG STREAMWISE CHORDS – Continued

(d) $\frac{y}{b/2} = 0.232$; c' = 26.355 cm (10.376 in.)

x'/c'	z'/c' Upper surface	z'/c' Lower surface
0	0.0378	0.0378
.0006	.0420	.0336
.0028	.0471	.0284
.0055	.0507	.0246
.0096	.0545	.0206
.0150	.0581	.0167
.0204	.0607	.0136
.0335	.0654	.0080
.0648	.0723	0
.0942	.0764	-.0045
.1218	.0792	-.0073
.1727	.0826	-.0109
.2184	.0843	-.0130
.2987	.0860	-.0140
.3683	.0859	-.0128
.4293	.0847	-.0105
.4835	.0827	-.0077
.5322	.0805	-.0044
.5764	.0780	-.0007
.6174	.0751	.0033
.6575	.0725	.0081
.6962	.0699	.0129
.7335	.0669	.0178
.7694	.0641	.0228
.8043	.0611	.0273
.8382	.0579	.0310
.8713	.0544	.0334
.9038	.0506	.0347
.9361	.0461	.0346
.9522	.0438	.0336
.9683	.0414	.0329
.9893	.0381	.0308
.9937	.0374	.0302
1.0000		.0293

(e) $\frac{y}{b/2} = 0.309$; c' = 20.808 cm (8.192 in.)

x'/c'	z'/c' Upper surface	z'/c' Lower surface
0	0.0318	0.0318
.0004	.0349	.0288
.0018	.0385	.0251
.0035	.0411	.0224
.0062	.0439	.0196
.0097	.0465	.0169
.0131	.0486	.0147
.0217	.0529	.0107
.0426	.0597	.0046
.0626	.0642	.0007
.0819	.0677	-.0020
.1186	.0725	-.0063
.1530	.0758	-.0091
.2174	.0804	-.0117
.2770	.0828	-.0122
.3329	.0837	-.0117
.3857	.0838	-.0102
.4362	.0833	-.0081
.4846	.0822	-.0054
.5318	.0807	-.0020
.5781	.0794	.0023
.6236	.0780	.0076
.6682	.0763	.0139
.7120	.0745	.0209
.7549	.0722	.0283
.7972	.0696	.0353
.8388	.0665	.0408
.8799	.0628	.0441
.9204	.0582	.0449
.9404	.0554	.0441
.9604	.0523	.0424
.9866	.0475	.0385
.9921	.0464	.0374
1.0000		.0358

(f) $\frac{y}{b/2} = 0.386$; c' = 18.654 cm (7.344 in.)

x'/c'	z'/c' Upper surface	z'/c' Lower surface
0	0.0255	0.0255
.0002	.0282	.0229
.0013	.0314	.0196
.0025	.0337	.0173
.0044	.0361	.0148
.0069	.0384	.0124
.0094	.0402	.0106
.0156	.0435	.0074
.0310	.0492	.0024
.0462	.0532	-.0010
.0613	.0563	-.0037
.0911	.0610	-.0076
.1204	.0646	-.0103
.1777	.0697	-.0129
.2334	.0728	-.0141
.2876	.0750	-.0139
.3405	.0765	-.0129
.3922	.0773	-.0111
.4430	.0775	-.0088
.4927	.0775	-.0057
.5417	.0773	-.0017
.5898	.0768	.0034
.6373	.0760	.0099
.6842	.0749	.0179
.7306	.0733	.0266
.7765	.0712	.0355
.8220	.0688	.0427
.8671	.0655	.0471
.9118	.0610	.0481
.9[illegible]41	.0582	.0471
.9562	.0549	.0448
.9852	.0495	.0397
.9913	.0462	.0383
1.0000		.0364

ORIGINAL PAGE IS
OF POOR QUALITY

[redacted]

TABLE II.- WING COORDINATES ALONG STREAMWISE CHORDS – Continued

(g) $\frac{y}{b/2} = 0.464$;
c' = 12.537 cm (4.936 in.)

x'/c'	z'/c' Upper surface	z'/c' Lower surface
0	0.0193	0.0193
.0002	.0218	.0168
.0012	.0249	.0137
.0023	.0270	.0115
.0041	.0294	.0091
.0064	.0316	.0068
.0088	.0332	.0051
.0146	.0367	.0020
.0291	.0420	-.0029
.0435	.0459	-.0062
.0578	.0488	-.0087
.0862	.0530	-.0122
.1143	.0561	-.0145
.1697	.0610	-.0170
.2241	.0646	-.0177
.2776	.0673	-.0173
.3304	.0694	-.0161
.3824	.0707	-.0144
.4338	.0720	-.0119
.4846	.0729	-.0085
.5347	.0734	-.0045
.5841	.0735	.0008
.6329	.0732	.0075
.6810	.0725	.0156
.7284	.0714	.0250
.7752	.0700	.0341
.8213	.0677	.0416
.8669	.0646	.0464
.9118	.0603	.0476
.9341	.0576	.0464
.9562	.0542	.0438
.9852	.0487	.0388
.9913	.0474	.0374
1.0000		.0352

(h) $\frac{y}{b/2} = 0.541$;
c' = 16.231 cm (6.390 in.)

x'/c'	z'/c' Upper surface	z'/c' Lower surface
0	0.0122	0.0122
.0002	.0146	.0097
.0011	.0175	.0068
.0023	.0197	.0046
.0040	.0219	.0023
.0063	.0240	.0001
.0086	.0257	-.0015
.0143	.0289	-.0046
.0286	.0343	-.0093
.0429	.0380	-.0123
.0570	.0410	-.0145
.0852	.0454	-.0177
.1132	.0488	-.0198
.1686	.0540	-.0215
.2232	.0578	-.0218
.2770	.0608	-.0211
.3300	.0633	-.0195
.3823	.0654	-.0173
.4338	.0672	-.0147
.4846	.0686	-.0112
.5347	.0694	-.0069
.5841	.0700	-.0013
.6329	.0704	.0055
.6810	.0702	.0141
.7284	.0696	.0235
.7752	.0683	.0326
.8213	.0663	.0402
.8669	.0635	.0452
.9118	.0592	.0463
.9341	.0565	.0452
.9562	.0531	.0427
.9852	.0475	.0376
.9913	.0462	.0362
1.0000		.0339

(i) $\frac{y}{b/2} = 0.580$;
c' = 15.624 cm (6.151 in.)

x'/c'	z'/c' Upper surface	z'/c' Lower surface
0	0.0082	0.0082
.0002	.0106	.0058
.0011	.0135	.0029
.0023	.0156	.0008
.0040	.0178	-.0015
.0063	.0199	-.0037
.0086	.0216	-.0053
.0143	.0248	-.0082
.0286	.0301	-.0127
.0429	.0340	-.0157
.0570	.0369	-.0178
.0852	.0414	-.0207
.1132	.0450	-.0226
.1686	.0504	-.0241
.2232	.0545	-.0241
.2770	.0577	-.0230
.3300	.0603	-.0214
.3823	.0626	-.0191
.4338	.0646	-.0163
.4846	.0662	-.0126
.5347	.0673	-.0082
.5841	.0681	-.0025
.6329	.0687	.0045
.6810	.0688	.0129
.7284	.0686	.0225
.7752	.0676	.0318
.8213	.0656	.0395
.8669	.0628	.0444
.9118	.0586	.0455
.9341	.0559	.0445
.9562	.0525	.0421
.9782	.0484	.0385
.9913	.0454	.0354
1.0000		.0331

TABLE II.- WING COORDINATES ALONG STREAMWISE CHORDS – Continued

(j) $\frac{y}{b/2} = 0.618$; c' = 15.019 cm (5.913 in.)

x'/c'	z'/c' Upper surface	z'/c' Lower surface
0	0.0043	0.0043
.0002	.0066	.0019
.0012	.0095	-.0010
.0023	.0116	-.0031
.0040	.0138	-.0053
.0063	.0158	-.0075
.0086	.0174	-.0091
.0143	.0205	-.0119
.0286	.0259	-.0164
.0429	.0298	-.0194
.0570	.0328	-.0213
.0852	.0374	-.0239
.1132	.0411	-.0255
.1686	.0467	-.0268
.2232	.0509	-.0265
.2770	.0543	-.0251
.3300	.0571	-.0233
.3823	.0597	-.0209
.4338	.0618	-.0180
.4846	.0637	-.0142
.5347	.0650	-.0097
.5841	.0661	-.0039
.6329	.0669	.0033
.6810	.0673	.0117
.7284	.0672	.0216
.7752	.0664	.0308
.8213	.0647	.0385
.8669	.0620	.0437
.9118	.0579	.0446
.9341	.0551	.0436
.9562	.0518	.0414
.9782	.0476	.0376
.9913	.0445	.0346
1.0000		.0322

(k) $\frac{y}{b/2} = 0.657$; c' = 14.412 cm (5.674 in.)

x'/c'	z'/c' Upper surface	z'/c' Lower surface
0	0.0002	0.0002
.0002	.0025	-.0022
.0011	.0054	-.0050
.0023	.0074	-.0071
.0040	.0096	-.0093
.0063	.0116	-.0114
.0086	.0131	-.0129
.0143	.0162	-.0160
.0286	.0218	-.0201
.0429	.0256	-.0230
.0570	.0287	-.0250
.0852	.0333	-.0273
.1132	.0370	-.0286
.1686	.0428	-.0294
.2232	.0472	-.0289
.2770	.0507	-.0274
.3300	.0538	-.0253
.3823	.0564	-.0229
.4338	.0588	-.0199
.4846	.0608	-.0159
.5347	.0626	-.0112
.5841	.0639	-.0053
.6329	.0650	.0018
.6810	.0656	.0106
.7284	.0657	.0205
.7752	.0650	.0297
.8213	.0636	.0374
.8669	.0610	.0425
.9118	.0570	.0436
.9341	.0543	.0426
.9562	[illegible]	.0404
.9782	.0467	.0367
.9913	.0436	.0336
1.0000		.0312

(l) $\frac{y}{b/2} = 0.696$; c' = 13.807 cm (5.436 in.)

x'/c'	z'/c' Upper surface	z'/c' Lower surface
0	-0.0041	-0.0041
.0002	-.0018	-.0064
.0011	[illegible]	-.0092
.0023	.0031	-.0112
.0040	.0052	-.0134
.0063	.0072	-.0155
.0086	.0087	-.0170
.0143	.0119	-.0201
.0286	.0175	-.0241
.0429	.0214	-.0266
.0570	.0244	-.0285
.0852	.0291	-.0306
.1132	.0328	-.0318
.1686	.0388	-.0325
.2232	.0434	-.0317
.2770	.0469	-.0299
.3300	.0503	-.0277
.3823	.0530	-.0251
.4338	.0557	-.0219
.4846	.0579	-.0178
.5347	.0600	-.0129
.5841	.0616	-.0069
.6329	.0627	.0004
.6810	.0636	.0093
.7284	.0640	.0191
.7752	.0636	.0284
.8213	.0623	.0360
.8669	.0599	.0411
.9118	.0559	.0424
.9341	.0532	.0414
.9562	.0498	.0393
.9782	.0457	.0357
.9913	.0426	.0326
1.0000		.0302

[redacted]

TABLE II.- WING COORDINATES ALONG STREAMWISE CHORDS – Continued

(m) $\frac{y}{b/2} = 0.734$;

c' = 13.200 cm (5.197 in.)

x'/c'	z'/c' Upper surface	z'/c' Lower surface
0	-0.0085	-0.0085
.0002	-.0063	-.0108
.0011	-.0035	-.0136
.0023	-.0015	-.0156
.0040	.0006	-.0177
.0063	.0025	-.0197
.0086	.0041	-.0212
.0143	.0074	-.0239
.0286	.0130	-.0282
.0429	.0170	-.0305
.0570	.0199	-.0321
.0852	.0246	-.0340
.1132	.0285	-.0352
.1686	.0347	-.0357
.2232	.0394	-.0347
.2770	.0432	-.0327
.3300	.0467	-.0304
.3823	.0497	-.0274
.4338	.0525	-.0240
.4846	.0550	-.0198
.5347	.0572	-.0148
.5841	.0590	-.0086
.6329	.0603	-.0012
.6810	.0614	.0077
.7284	.0620	.0174
.7752	.0619	.0268
.8213	.0608	.0345
.8669	.0587	.0396
.9118	.0546	.0409
.9341	.0520	.0400
.9562	.0485	.0379
.9782	.0445	.0344
.9913	.0414	.0314
1.0000		.0290

(n) $\frac{y}{b/2} = 0.773$;

c' = 12.596 cm (4.959 in.)

x'/c'	z'/c' Upper surface	z'/c' Lower surface
0	-0.0128	-0.0128
.0002	-.0106	-.0151
.0011	-.0078	-.0178
.0023	-.0059	-.0198
.0040	-.0038	-.0219
.0063	-.0019	-.0239
.0086	-.0002	-.0253
.0143	.0029	-.0282
.0286	.0083	-.0322
.0429	.0121	-.0344
.0570	.0151	-.0361
.0852	.0199	-.0377
.1132	.0241	-.0387
.1686	.0305	-.0389
.2232	.0353	-.0377
.2770	.0393	-.0356
.3306	.0430	-.0332
.3823	.0461	-.0300
.4338	.0491	-.0263
.4846	.0518	-.0220
.5347	.0541	-.0169
.5841	.0561	-.0105
.6329	.0578	-.0031
.6810	.0590	.0058
.7284	.0596	.0154
.7752	.0598	.0249
.8213	.0590	.0328
.8669	.0569	.0378
.9118	.0531	.0393
.9341	.0505	.0384
.9562	.0471	.0364
.9782	.0431	.0330
.9913	.0398	.0301
1.0000		.0276

(o) $\frac{y}{b/2} = 0.812$;

c' = 11.989 cm (4.720 in.)

x'/c'	z'/c' Upper surface	z'/c' Lower surface
0	-0.0173	-0.0173
.0002	-.0151	-.0196
.0011	-.0124	-.0223
.0023	-.0105	-.0242
.0040	-.0085	-.0263
.0063	-.0066	-.0282
.0086	-.0049	-.0296
.0143	-.0013	-.0325
.0286	.0035	-.0363
.0429	.0073	-.0384
.0570	.0104	-.0400
.0852	.0153	-.0416
.1132	.0194	-.0425
.1686	.0258	-.0425
.2232	.0309	-.0411
.2770	.0352	-.0388
.3300	.0389	-.0362
.3823	.0422	-.0329
.4338	.0454	-.0288
.4846	.0482	-.0244
.5347	.0506	-.0191
.5841	.0528	-.0127
.6329	.0548	-.0052
.6810	.0561	.0037
.7284	.0570	.0133
.7752	.0574	.0227
.8213	.0568	.0306
.8669	.0548	.0357
.9118	.0514	.0374
.9341	.0489	.0366
.9562	.0455	.0347
.9782	.0414	.0314
.9913	.0382	.0286
1.0000		.0261

[redacted]

TABLE II.- WING COORDINATES ALONG STREAMWISE CHORDS – Concluded

(p) $\frac{y}{b/2} = 0.850$;

c' = 11.382 cm (4.481 in.)

x'/c'	z'/c' Upper surface	z'/c' Lower surface
0	-0.0221	-0.0221
.0002	-.0199	-.0243
.0011	-.0172	-.0270
.0023	-.0153	-.0289
.0040	-.0133	-.0309
.0063	-.0115	-.0328
.0086	-.0099	-.0342
.0143	-.0068	-.0368
.0286	-.0014	-.0405
.0429	.0025	-.0425
.0570	.0057	-.0440
.0852	.0105	-.0458
.1132	.0144	-.0467
.1686	.0208	-.0465
.2232	.0261	-.0448
.2770	.0304	-.0424
.3300	.0344	-.0394
.3823	.0379	-.0361
.4338	.0411	-.0318
.4846	.0440	-.0271
.5347	.0466	-.0217
.5841	.0493	-.0153
.6329	.0513	-.0077
.6810	.0529	.0014
.7284	.0541	.0109
.7752	.0547	.0202
.8213	.0542	.0282
.8669	.0526	.0334
.9118	.0494	.0353
.9341	.0469	.0347
.9562	.0438	.0329
.9782	.0397	.0296
.9913	.0367	.0269
1.0000		.0246

(q) $\frac{y}{b/2} = 0.935$;

c' = 10.051 cm (3.957 in.)

x'/c'	z'/c' Upper surface	z'/c' Lower surface
0	-0.0330	-0.0330
.0002	-.0309	-.0352
.0011	-.0283	-.[illegible]8
.0023	-.0264	-.0397
.0040	-.0245	-.0418
.0063	-.0227	-.0434
.0086	-.0213	-.0448
.0143	-.0185	-.0473
.0286	-.0133	-.0509
.0429	-.0094	-.0532
.0570	-.0064	-.0549
.0852	-.0014	-.0568
.1132	.0026	-.0574
.1686	.0090	-.0568
.2232	.0143	-.0546
.2770	.0189	-.0519
.3300	.0231	-.0481
.3823	.0271	-.0441
.4338	.0307	-.0395
.4846	.0340	-.0343
.5347	.0371	-.0287
.5841	.0401	-.0221
.6329	.0426	-.0141
.6810	.0447	-.0050
.7284	.0465	.0043
.7752	.0477	.0135
.8213	.0477	.0215
.8669	.0468	.0274
.9118	.0441	.0299
.9341	.0419	.0295
.9562	.0393	.0277
.9852	.0342	.0233
.9913	.0330	.0221
1.0000		.0202

(r) $\frac{y}{b/2} = 0.968$;

c' = 9.467 cm (3.727 in.)

x'/c'	z'/c' Upper surface	z'/c' Lower surface
0	-0.0382	-0.0382
.0002	-.0362	-.0405
.0011	-.0339	-.0432
.0023	-.0321	-.0450
.0040	-.0301	-.0467
.0063	-.0282	-.0484
.0086	-.0266	-.0497
.0143	-.0235	-.0522
.0286	-.0180	-.0558
.0429	-.0410	-.0580
.0570	-.0108	-.0598
.0852	-.0057	-.0618
.1132	-.0014	-.0622
.1686	.0052	-.0611
.2232	.0102	-.0590
.2770	.0147	-.0560
.3330	.0188	-.0521
.3823	.0230	-.0478
.4338	.0268	-.0428
.4846	.0303	-.0373
.5347	.0338	-.0314
.5841	.0368	-.0247
.6329	.0395	-.0166
.6810	.0417	-.0075
.7284	.0434	.0015
.7752	.0446	.0101
.8213	.0453	.0185
.8669	.0448	.0248
.9118	.0425	.0278
.9341	.0403	.0274
.9562	.0374	.0258
.9852	.0322	.0215
.9913	.0310	.0203
1.0000		.0184

[redacted]

TABLE III.- TUNNEL-TEST CONDITIONS

(a) SI Units

Mach number	$p_{t,\infty}$, N/m^2		q, N/m^2		R/m	
	8-ft TPT	16-ft TT	8-ft TPT	16-ft TT	8-ft TPT	16-ft TT
0.25	131 958		5 506		6.6×10^6	
.25	203 012		8 523		10.2	
.50	105 528		15 561		9.5	
.50	162 314		23 940		14.4	
.80	105 911		31 122		13.1	
.80	162 984		47 880		20.0	
.90	92 840		31 122		12.1	
.90	142 827		47 880		18.4	
.95	81 301	101 506	28 728	35 384	10.8	13.1×10^6
.95	125 063		44 193		16.4	
.98	79 050		28 728		10.5	
.98	121 568		44 193		16.1	
.99	78 332	101 506	28 728	36 676	10.5	12.8
.99	120 515		44 193		16.1	
1.00	77 662		28 728		10.5	
1.00	119 509		44 193		16.1	
1.02		101 506		37 586		12.8
1.20		101 506		41 560		12.8
1.30		101 506		42 661		12.5

ORIGINAL PAGE IS
OF POOR QUALITY

[redacted]

TABLE III.- TUNNEL-TEST CONDITIONS – Concluded

(b) U.S. Customary Units

Mach number	$p_{t,\infty}$, lb/sq ft		q, lb/sq ft		R/ft	
	8-ft TPT	16-ft TT	8-ft TPT	16-ft TT	8-ft TPT	16-ft TT
0.25	2756		115		2.0×10^6	
.25	4240		178		3.1	
.50	2204		325		2.9	
.50	3390		500		4.4	
.80	2212		650		4.0	
.80	3404		1000		6.1	
.90	1939		650		3.7	
.90	2983		1000		5.6	
.95	1698	2120	600	739	3.3	4.0×10^6
.95	2612		923		5.0	
.98	1651		600		3.2	
.98	2539		923		4.9	
.99	1636	2120	600	766	3.2	3.9
.99	2517		923		4.9	
1.00	1622		600		3.2	
1.00	2496		923		4.9	
1.02		2120		785		3.9
1.20		2120		868		3.9
1.30		2120		891		3.8

TABLE IV.- BOUNDARY-LAYER TRANSITION LOCATIONS AND CARBORUNDUM GRAIN SIZES FOR THE WING AND TAIL SURFACES

Model component	Location (percent of streamwise chords, c')	Carborundum grain size
Type I		
Mach numbers: 0.95, 0.98, 0.99, 1.00, 1.02, 1.20, 1.30		
Wing upper surface	See fig. 7(a)	See fig. 7(a)
Wing lower surface	See fig. 7(b)	See fig. 7(b)
Horizontal tail	31	120
Vertical tail	31	120
Type II		
Mach numbers: 0.50, 0.80, 0.90		
Wing upper surface	See fig. 7(c)	See fig. 7(a)
Wing lower surface	See fig. 7(b)	See fig. 7(b)
Horizontal tail	31	120
Vertical tail	31	120
Type III		
Mach number: 0.25		
Wing upper surface	5	120
Wing lower surface	45	80
Horizontal tail	5	120
Vertical tail	5	120

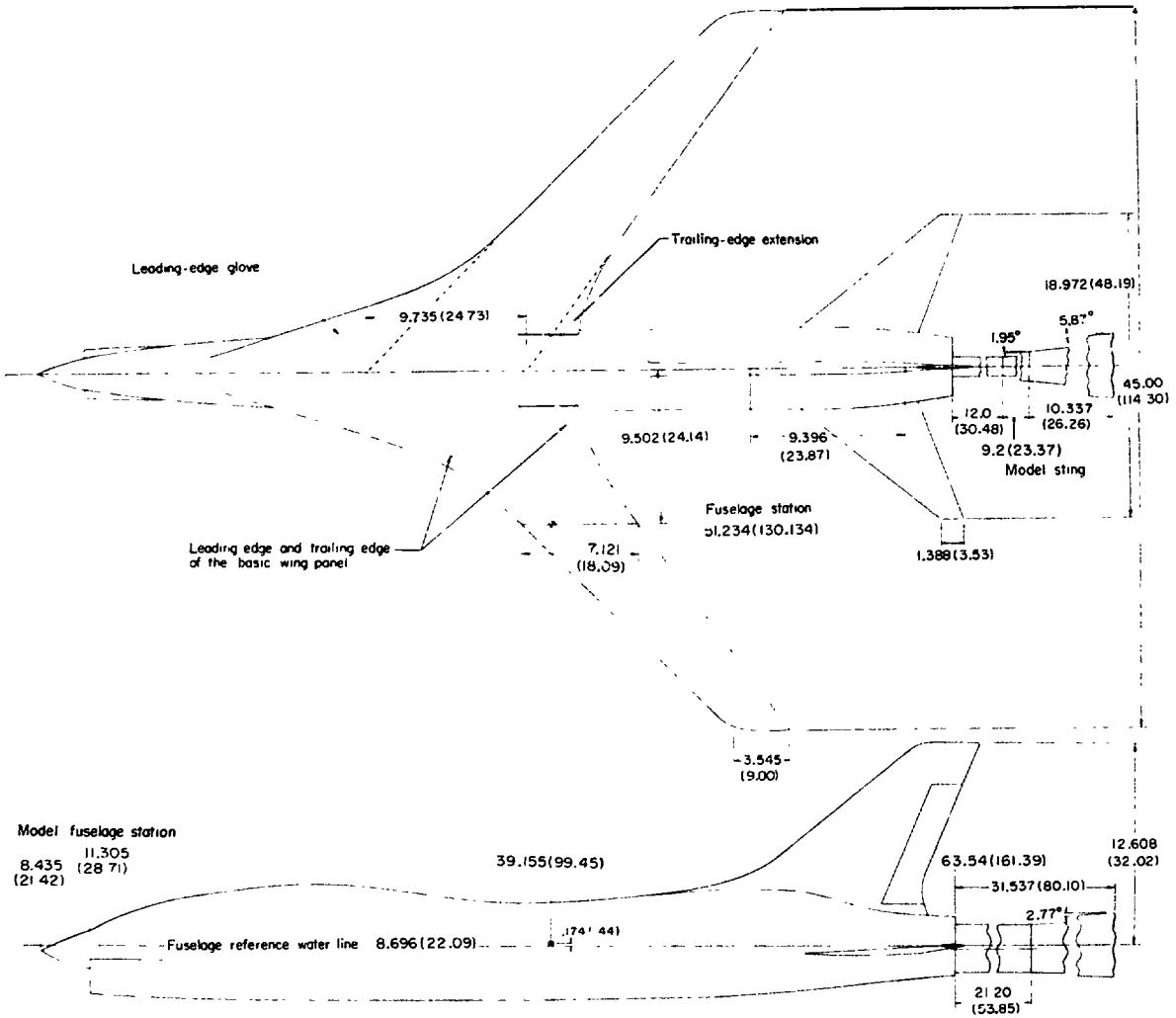

(a) General arrangement of the 0.087-scale model.

Figure 1.- Model and support sting details. All linear dimensions are in inches (centimeters in parentheses) unless otherwise noted.

ORIGINAL PAGE IS
OF POOR QUALITY

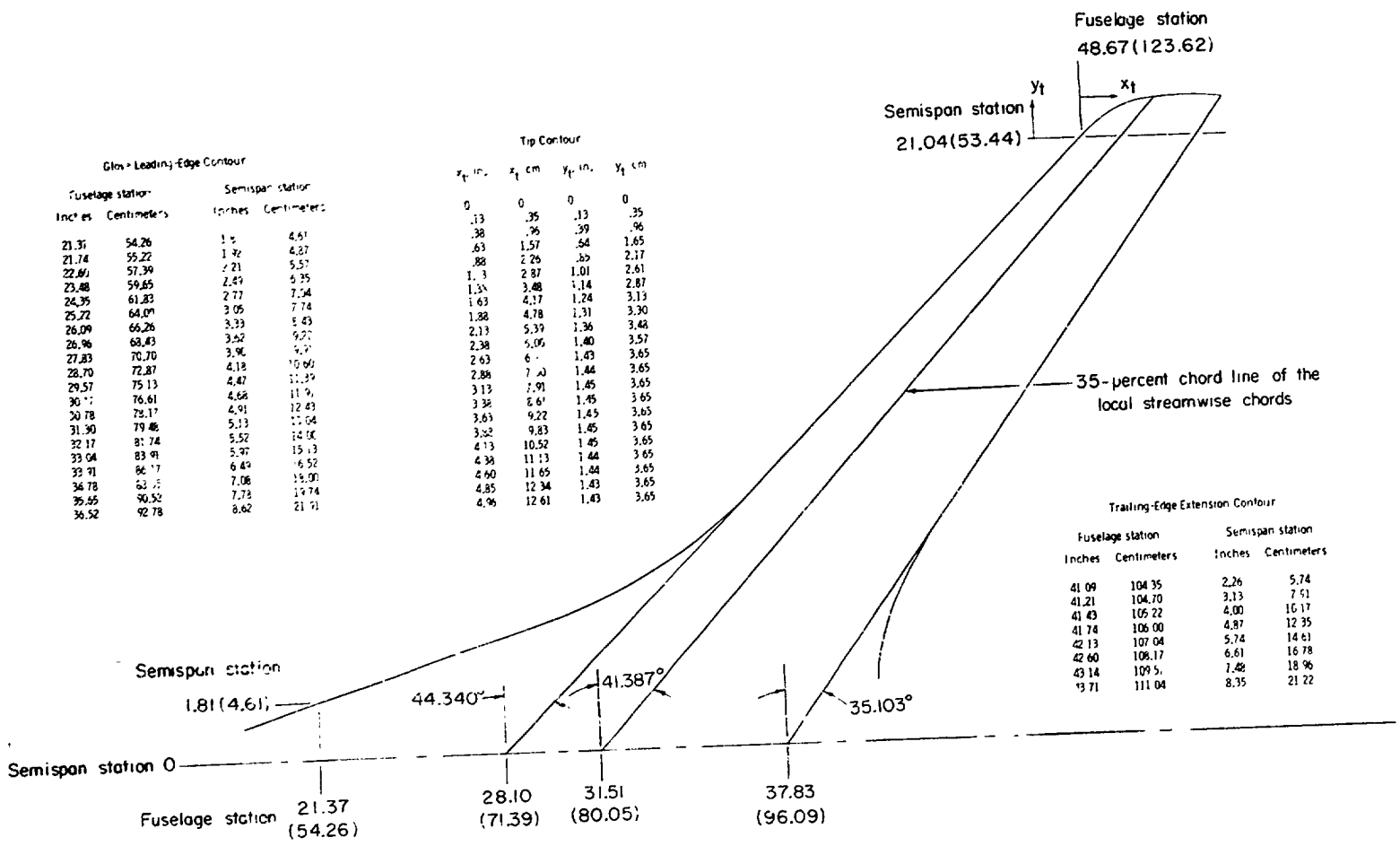

Glove Leading-Edge Contour

Fuselage station, Inches	Fuselage station, Centimeters	Semispan station, Inches	Semispan station, Centimeters
21.36	54.26	1.81	4.61
21.74	55.22	1.92	4.87
22.60	57.39	2.21	5.57
23.48	59.65	2.49	6.35
24.35	61.83	2.77	7.04
25.22	64.09	3.05	7.74
26.09	66.26	3.33	8.43
26.96	68.43	3.62	9.20
27.83	70.70	3.90	9.91
28.70	72.87	4.18	10.60
29.57	75.13	4.47	11.39
30.44	76.61	4.68	11.90
30.78	78.17	4.91	12.43
31.30	79.46	5.13	13.04
32.17	81.74	5.52	14.02
33.04	83.91	5.97	15.13
33.91	86.17	6.49	16.52
34.78	88.35	7.08	18.00
35.65	90.52	7.78	19.74
36.52	92.78	8.62	21.91

Tip Contour

x_t, in.	x_t, cm	y_t, in.	y_t, cm
0	0	0	0
.13	.35	.13	.35
.38	.96	.39	.96
.63	1.57	.64	1.65
.88	2.26	.85	2.17
1.13	2.87	1.01	2.61
1.38	3.48	1.14	2.87
1.63	4.17	1.24	3.13
1.88	4.78	1.31	3.30
2.13	5.39	1.36	3.48
2.38	6.05	1.40	3.57
2.63	6.[illegible]	1.43	3.65
2.88	7.[illegible]	1.44	3.65
3.13	7.91	1.45	3.65
3.38	8.61	1.45	3.65
3.63	9.22	1.45	3.65
3.88	9.83	1.45	3.65
4.13	10.52	1.45	3.65
4.38	11.13	1.44	3.65
4.60	11.65	1.44	3.65
4.85	12.34	1.43	3.65
4.96	12.61	1.43	3.65

Trailing-Edge Extension Contour

Fuselage station, Inches	Fuselage station, Centimeters	Semispan station, Inches	Semispan station, Centimeters
41.09	104.35	2.26	5.74
41.21	104.70	3.13	7.91
41.43	105.22	4.00	10.17
41.74	106.00	4.87	12.35
42.13	107.04	5.74	14.61
42.60	108.17	6.61	16.78
43.14	109.5[illegible]	7.48	18.96
43.71	111.04	8.35	21.22

(b) Wing semispan planform layout.

Figure 1.- Continued.

ORIGINAL PAGE IS
OF POOR QUALITY

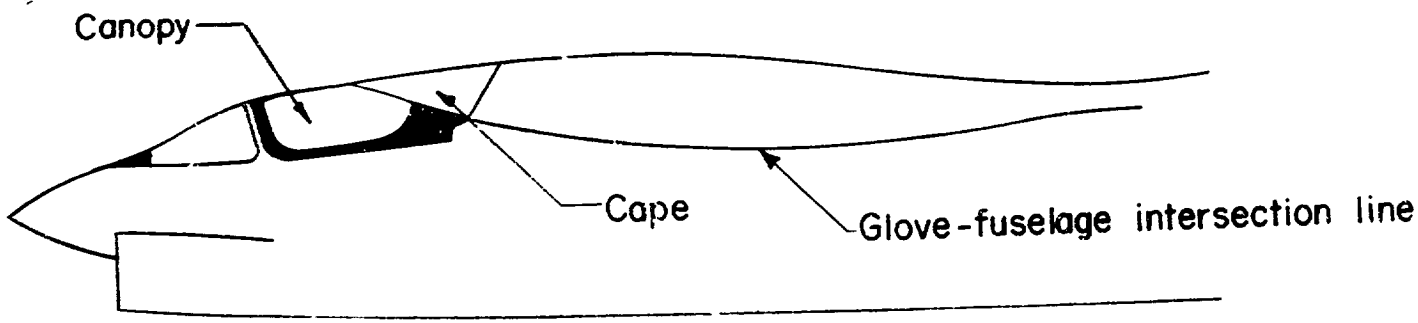

(c) Schematic of glove and cape arrangement.

Figure 1.- Continued.

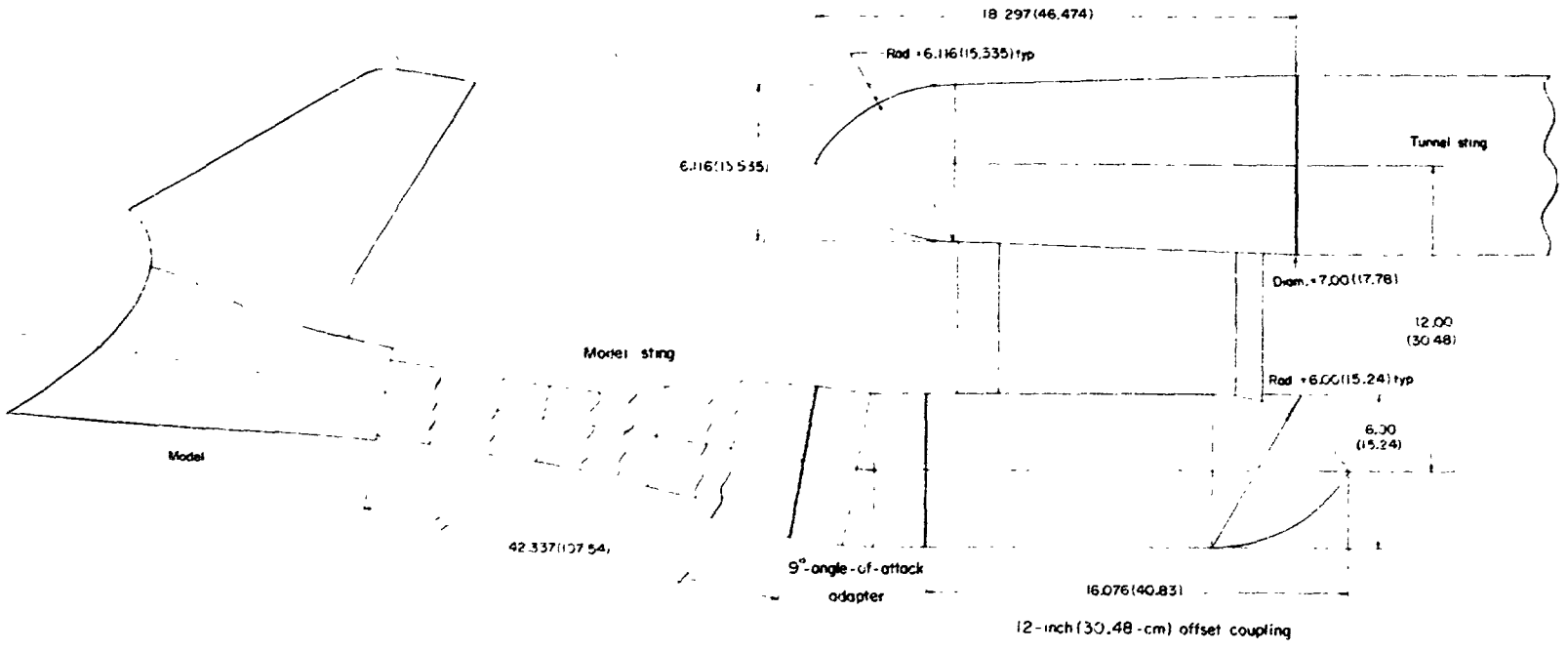

(d) Offset sting arrangement.

Figure 1.- Concluded.

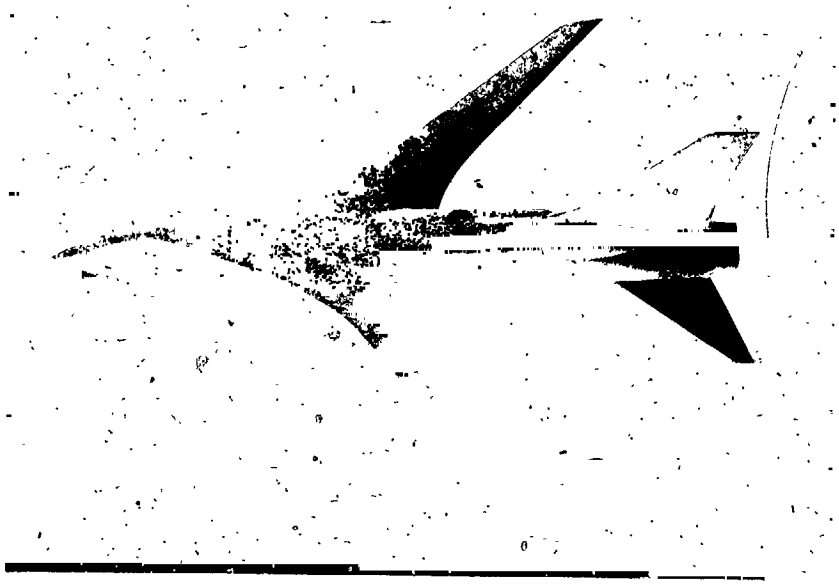

L-69-6086

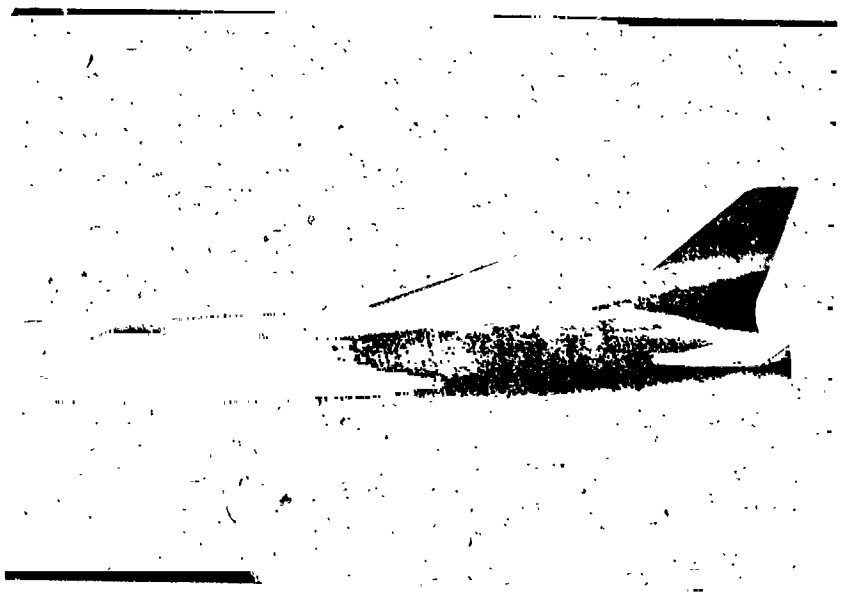

L-69-6085

Figure 2.- Photographs of 0.087-scale wind-tunnel model.

ORIGINAL PAGE IS
OF POOR QUALITY

L-69-6079

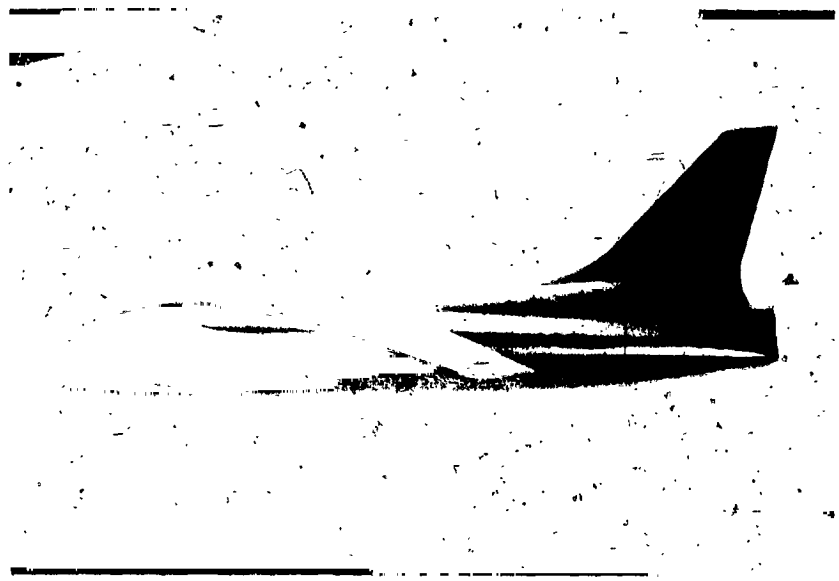

L-69-6083

Figure 2.- Concluded.

ORIGINAL PAGE IS
OF POOR QUALITY

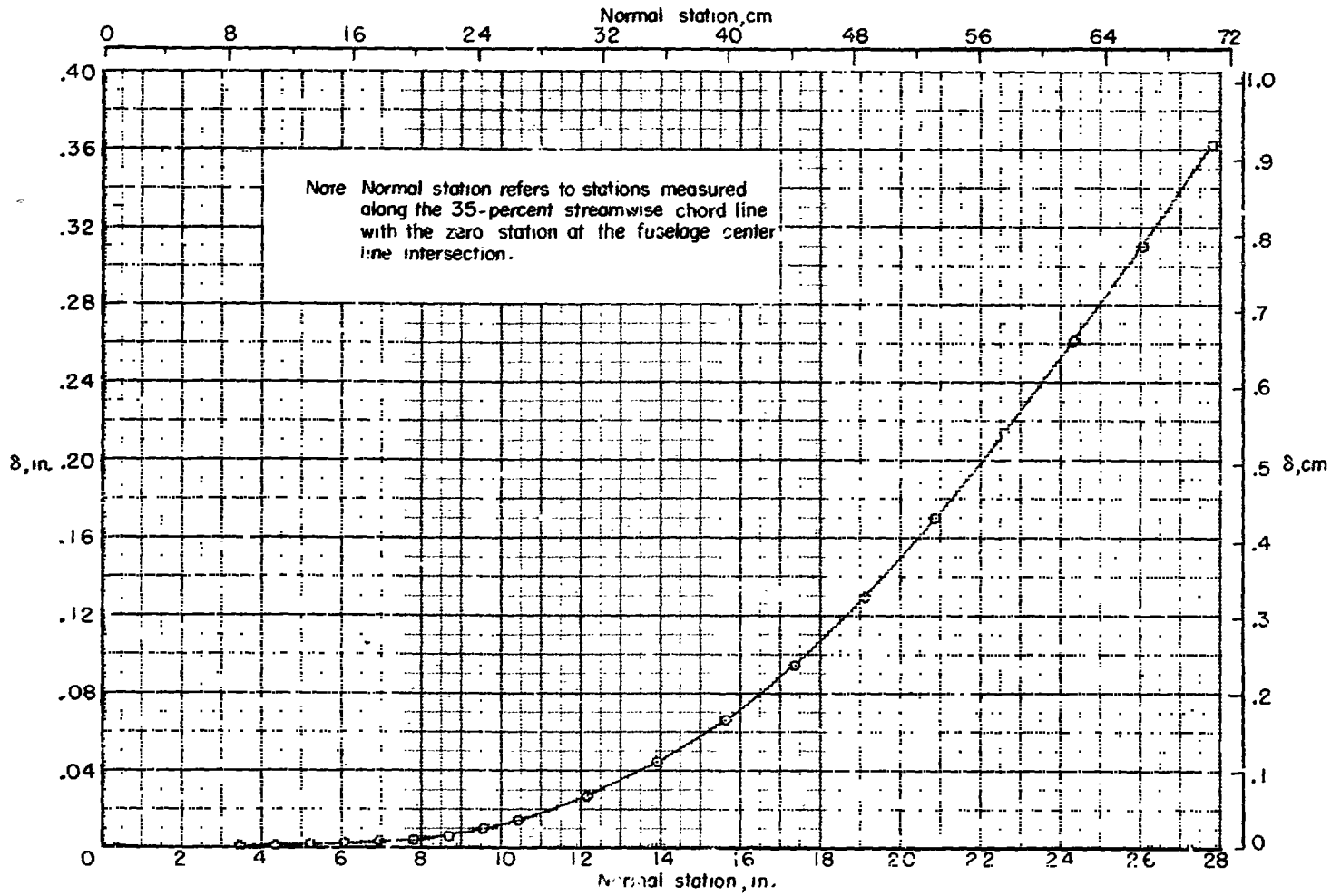

Figure 3.- Vertical deflection of model wing due to aerodynamic loading. $M = 0.99$; $C_L = 0.429$; $q = 44\ 193\ N/m^2$ (923 lb/sq ft); and $R/m = 16.1 \times 10^6$ ($R/ft = 4.9 \times 10^6$).

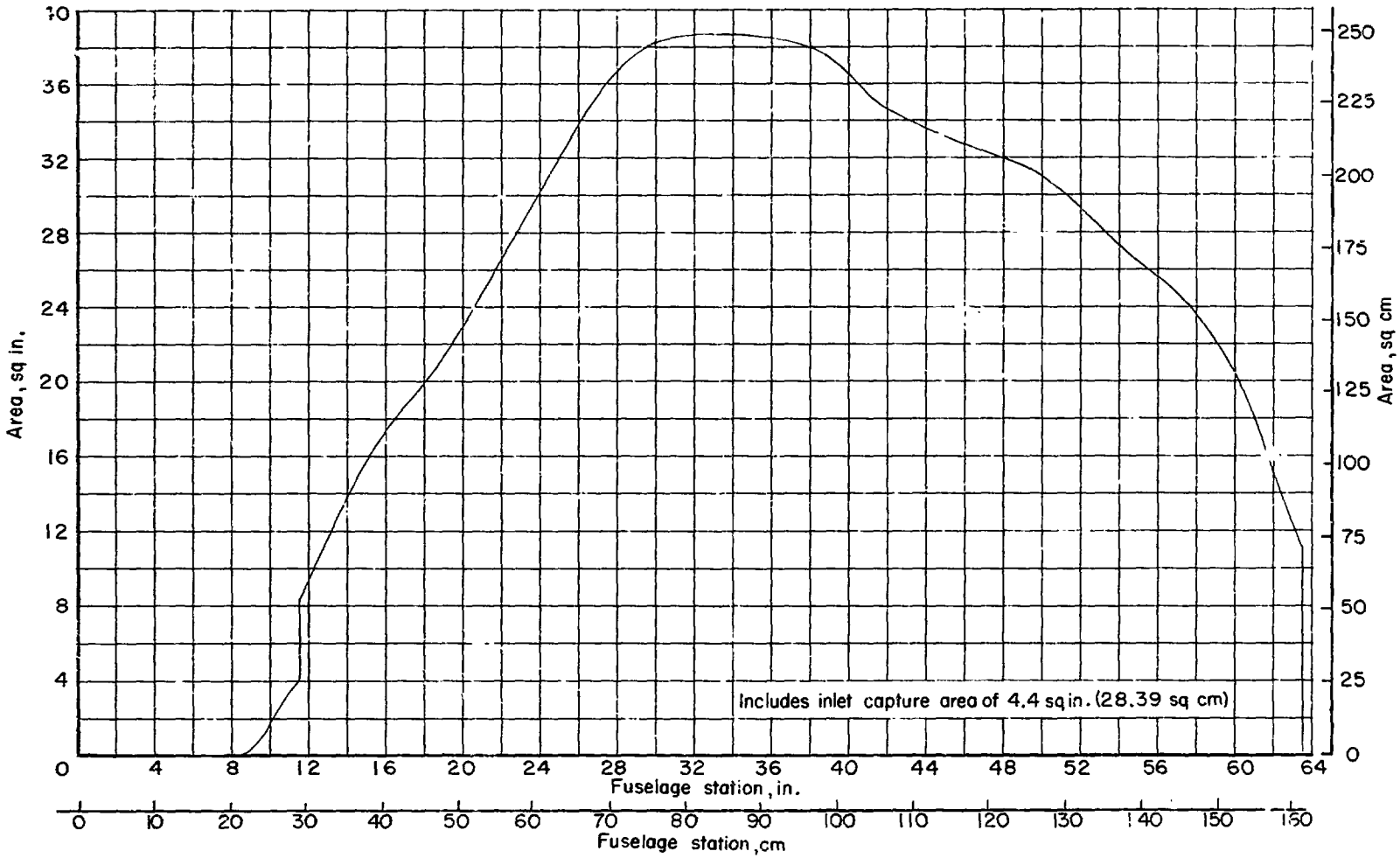

Figure 4.- Longitudinal progression of cross-sectional area taken normal to fuselage reference line for configuration 140.

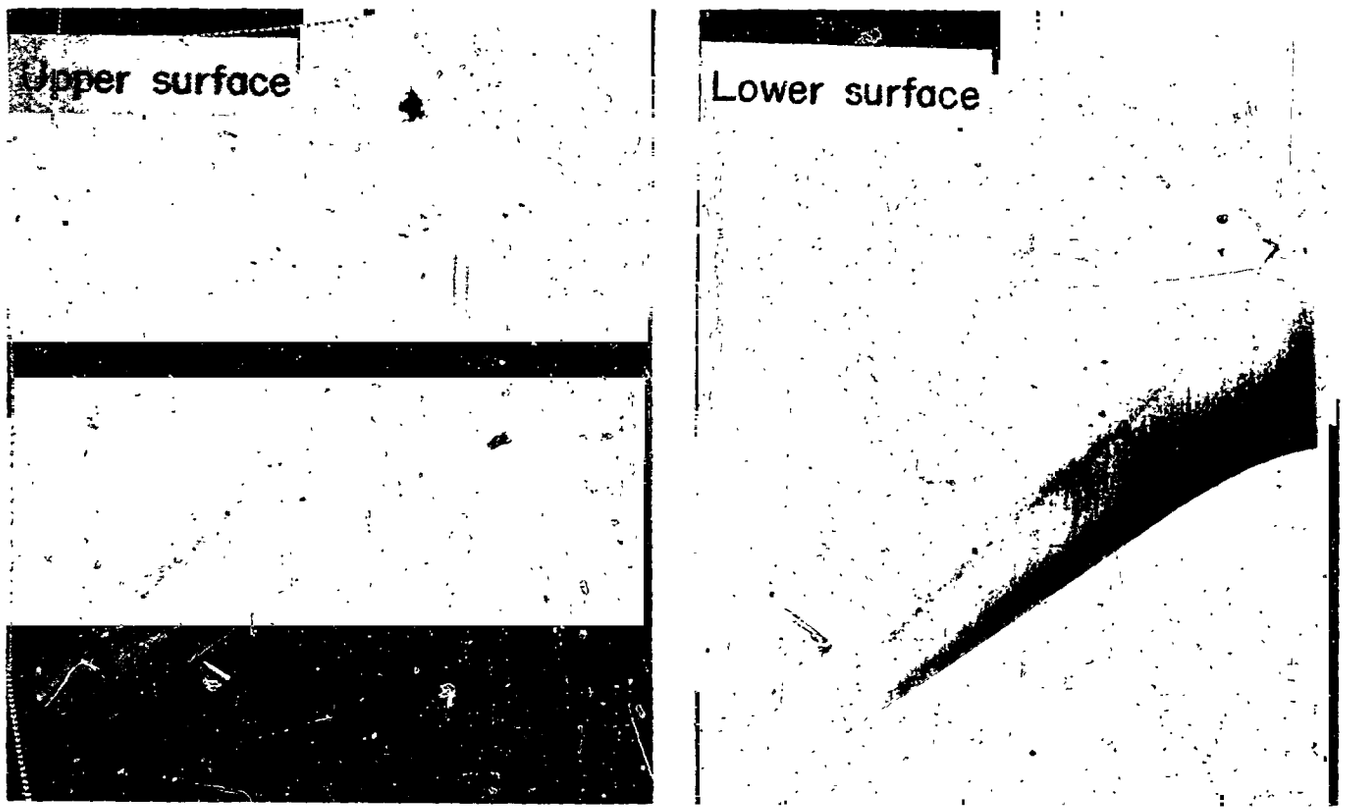

L-71-7129

(a) $C_L = 0.40$ and $\alpha = 2.9^{\circ}$.

Figure 5.- Oil-flow photographs of wing upper and lower surfaces. M = 0.99.

ORIGINAL PAGE IS
OF POOR QUALITY

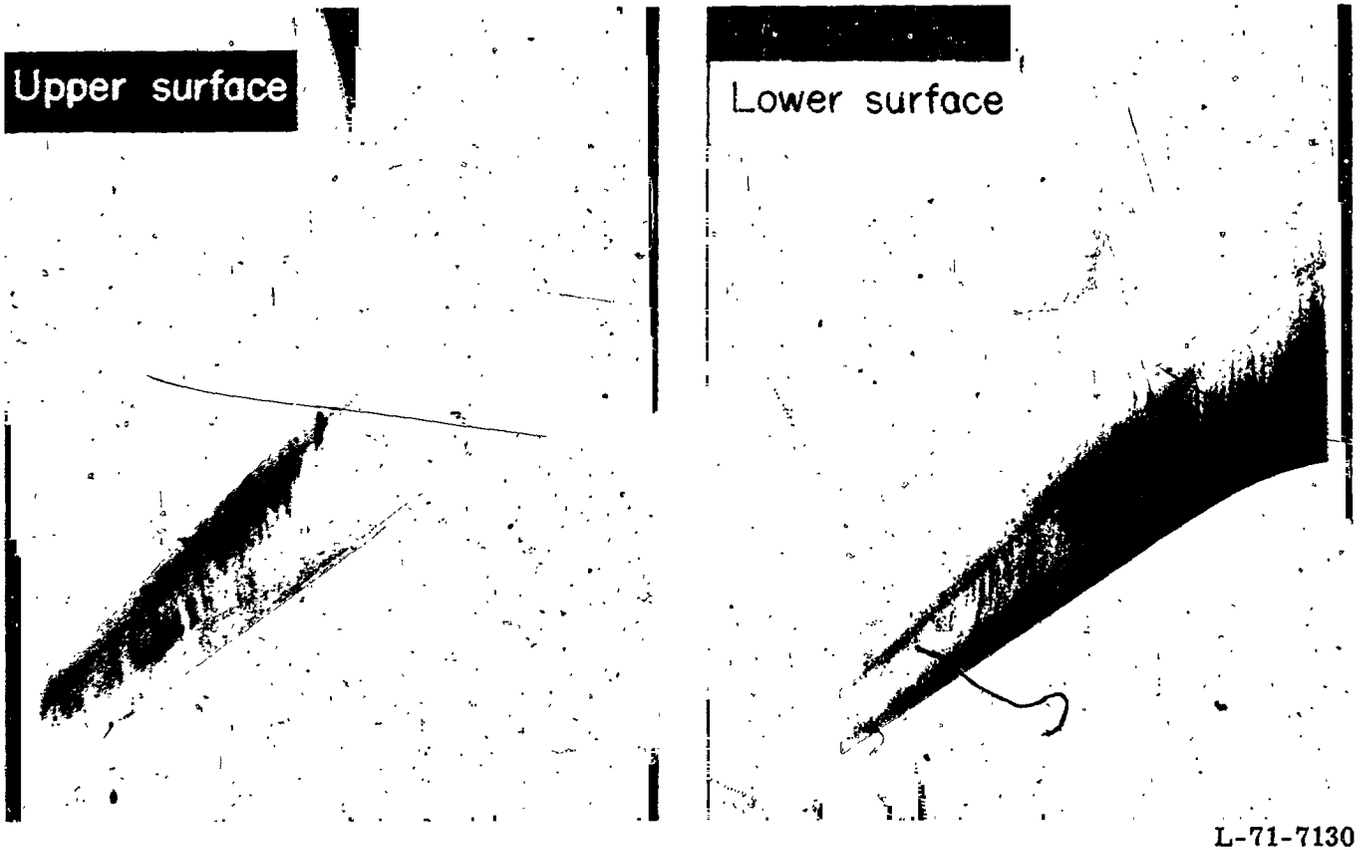

L-71-7130

(b) $C_L = 0.45$ and $\alpha = 3.2^{\circ}$.

Figure 5.- Continued.

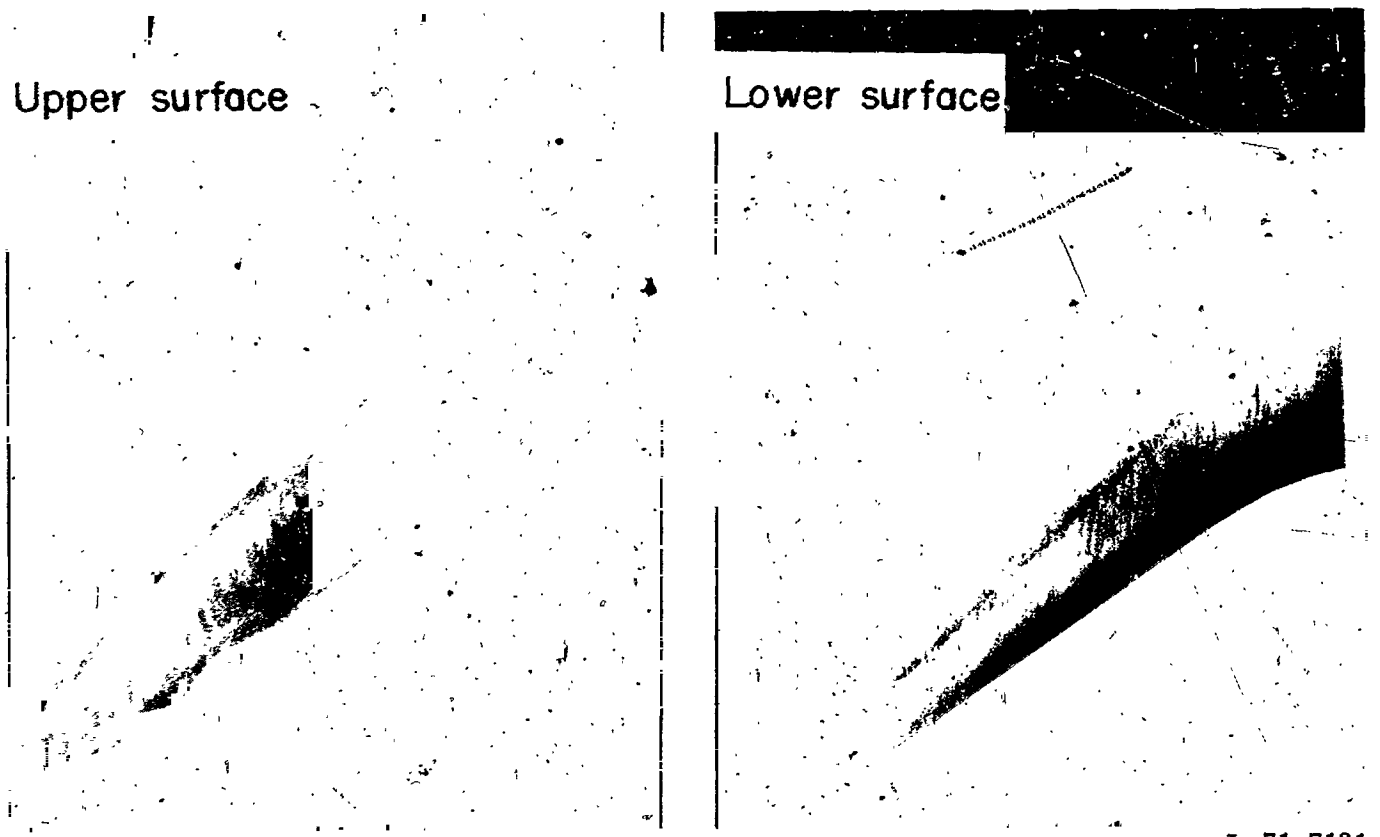

L-71-7131

(c) $C_L = 0.49$ and $\alpha = 3.5^{\circ}$.

Figure 5.- Concluded.

ORIGINAL PAGE IS
OF POOR QUALITY

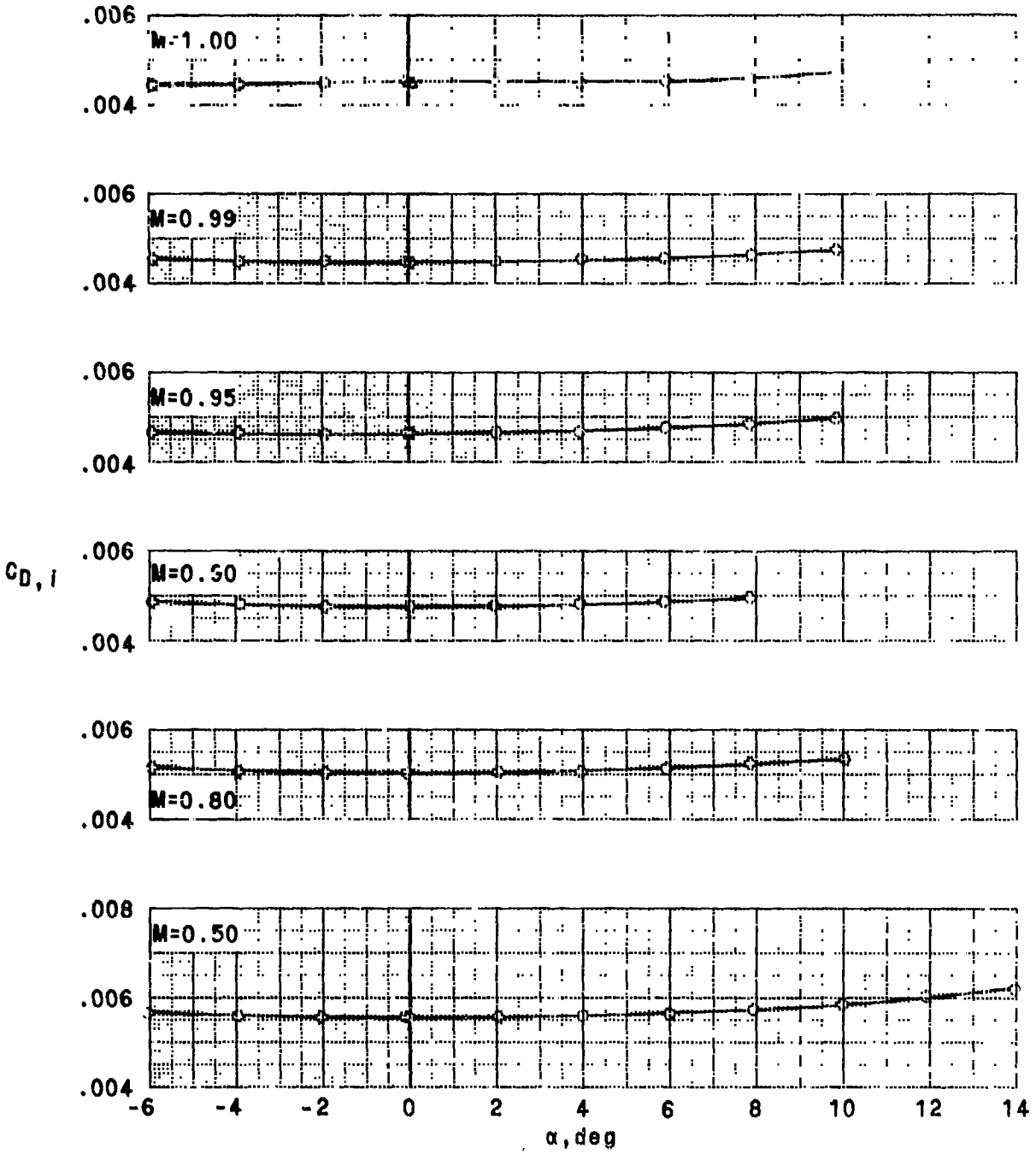

(a) Variation with angle of attack of internal-drag coefficient as measured in Langley 8-foot transonic pressure tunnel.

Figure 6.- Model internal drag and mass-flow characteristics.

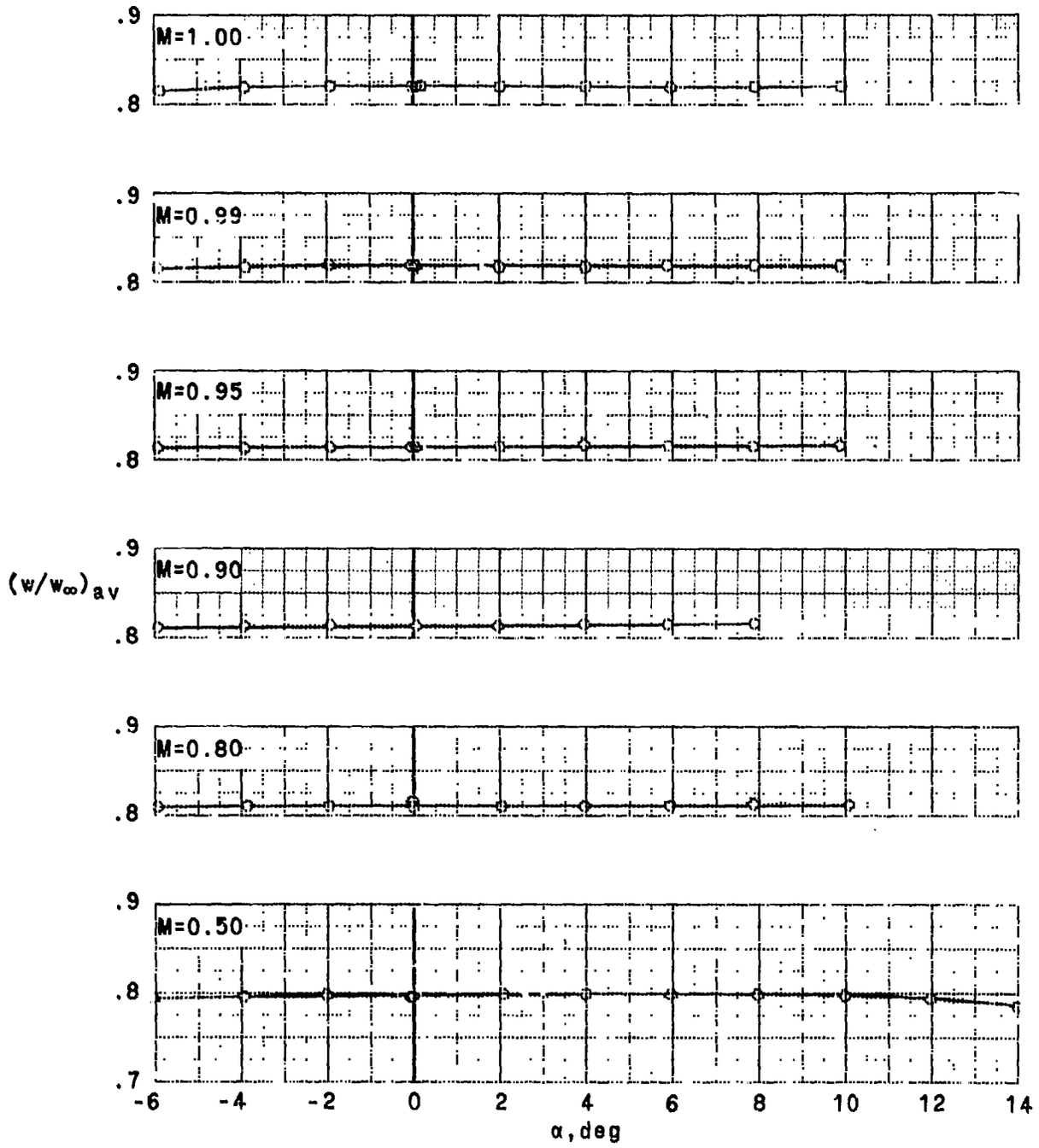

(b) Variation with angle of attack of average mass-flow ratio of ducts as measured in Langley 8-foot transonic pressure tunnel.

Figure 6.- Continued.

ORIGINAL PAGE IS
OF POOR QUALITY

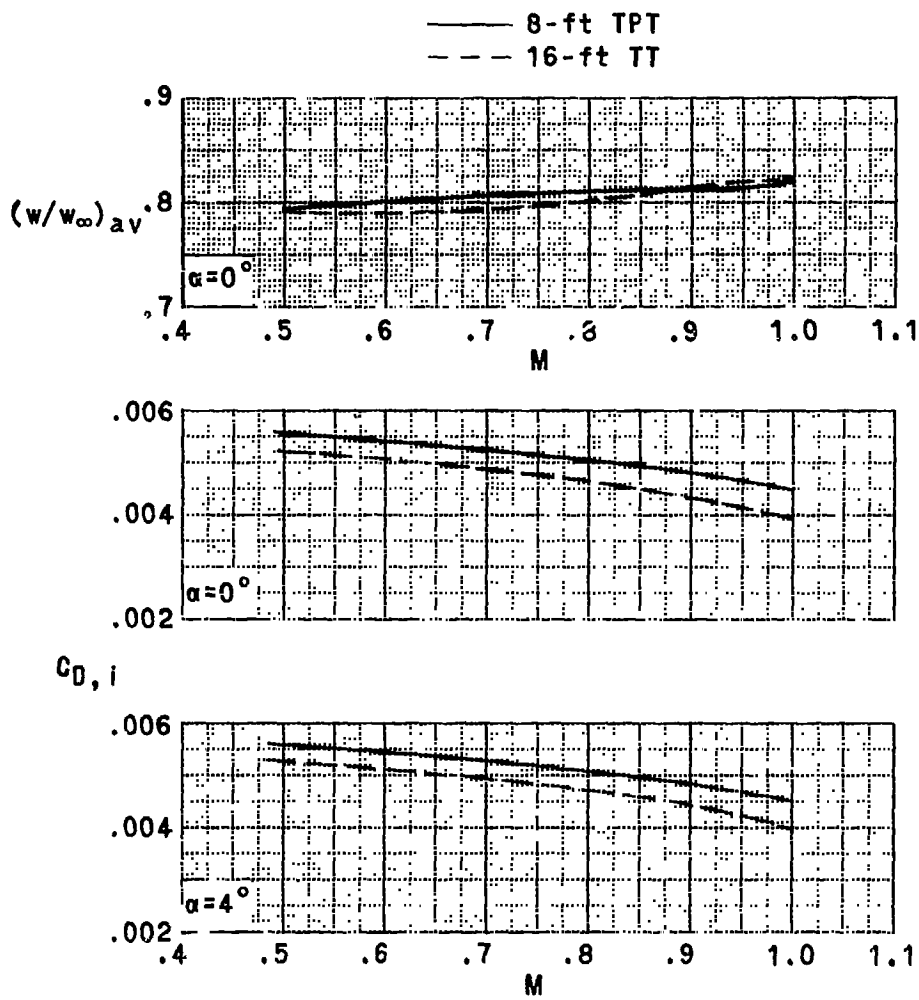

(c) Comparison of internal drag and mass-flow characteristics at selected angles of attack.

Figure 6.- Concluded.

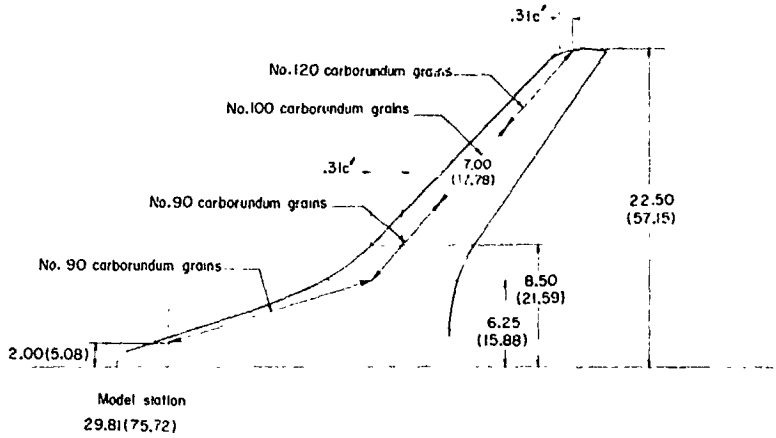

(a) Type I; wing upper surface. M = 0.95 to 1.30.

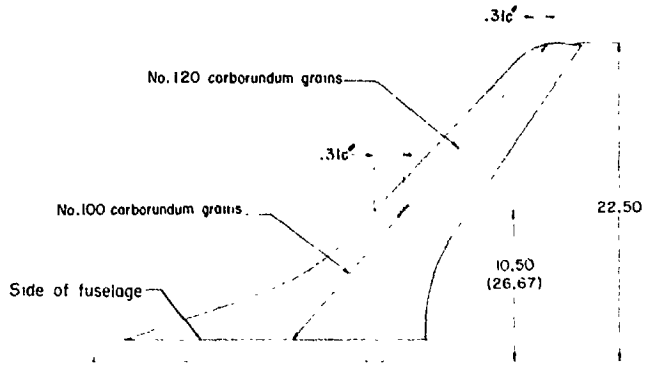

(b) Types I and II; wing lower surface. M = 0.50 to 1.30.

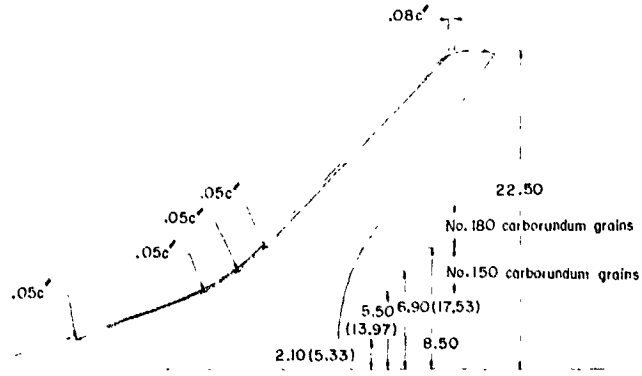

(c) Type II; wing upper surface. M = 050 to 0.90.

Figure 7.- Wing type I and type II boundary-layer transition arrangements. Dimensions are shown in inches and parenthetically in centimeters.

ORIGINAL PAGE IS
OF POOR QUALITY

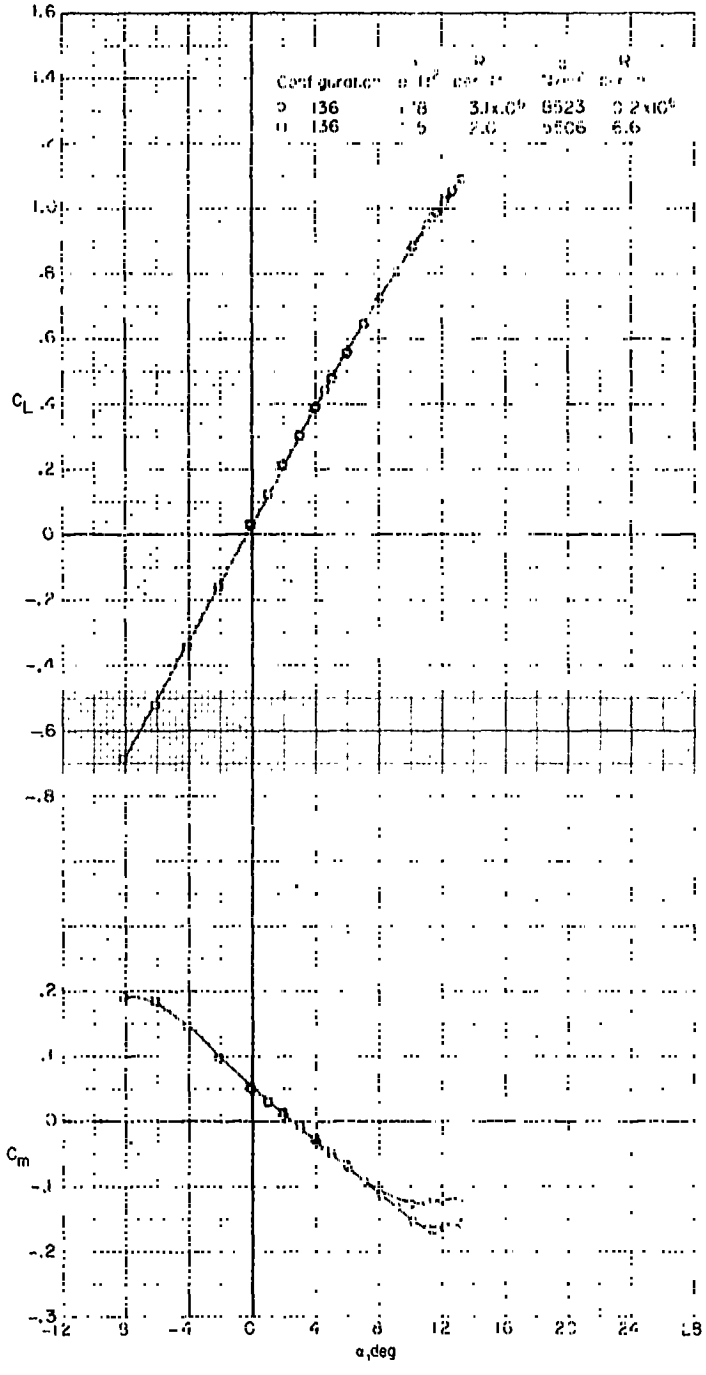

(a) M = 0.25.

Figure 8.- Effect of Reynolds number on longitudinal aerodynamic characteristics. $\beta = 0^{\circ}$ and $\delta_h = -2.5^{\circ}$.

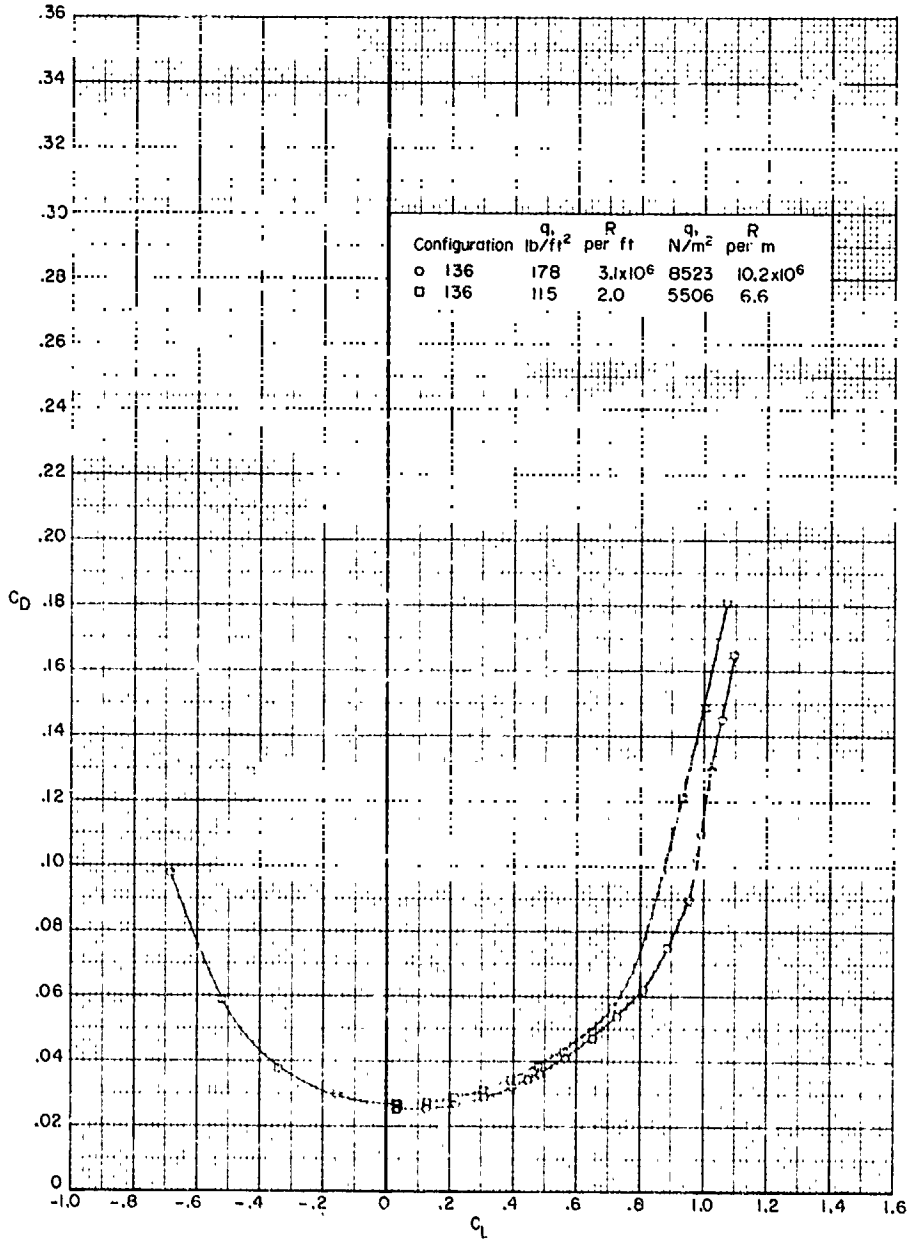

(a) M = 0.25. Concluded.

Figure 8.- Continued.

ORIGINAL PAGE IS
OF POOR QUALITY

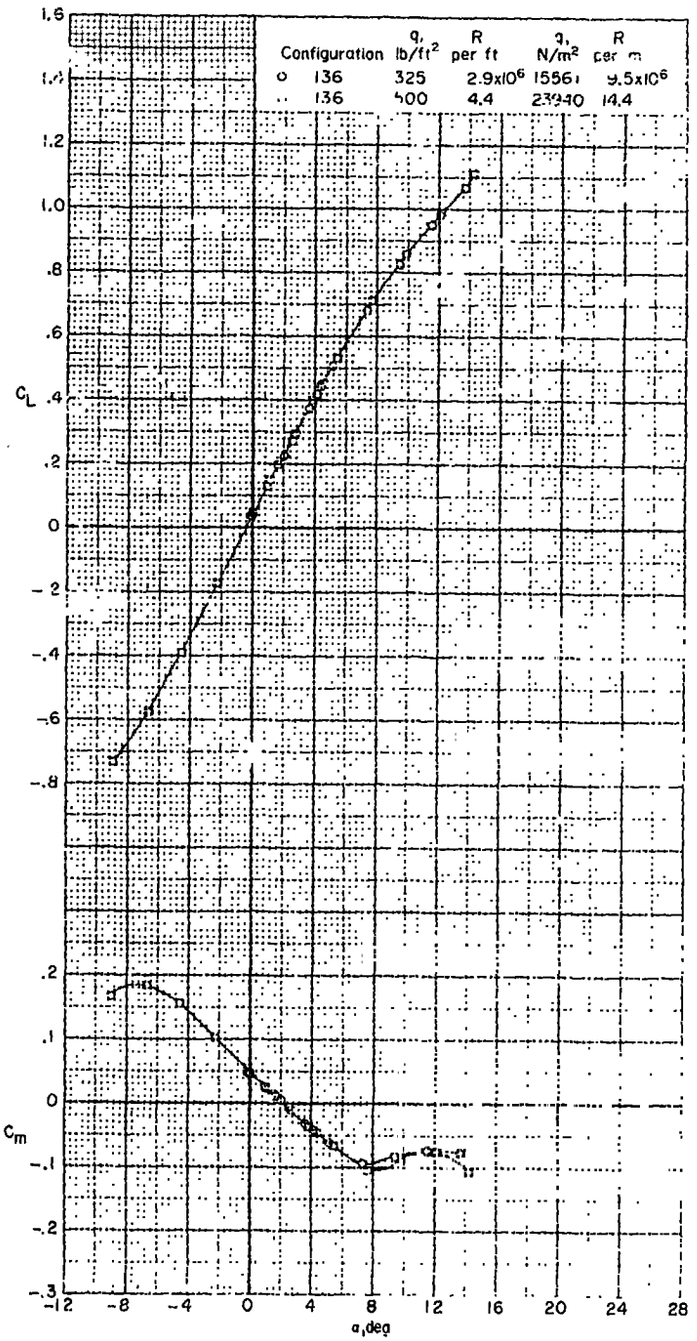

(b) M = 0.50.

Figure 8.- Continued.

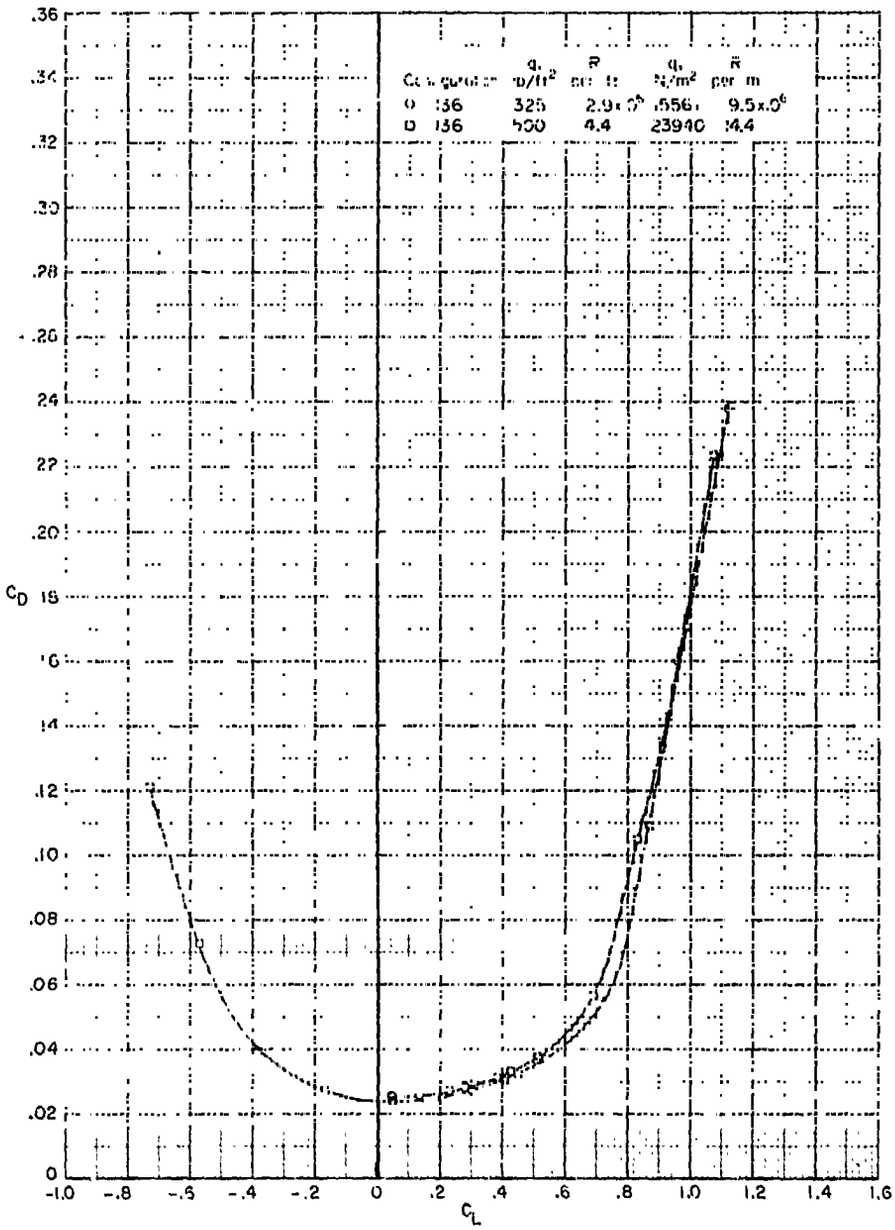

(b) M = 0.50. Concluded.

Figure 8.- Continued.

ORIGINAL PAGE IS
OF POOR QUALITY

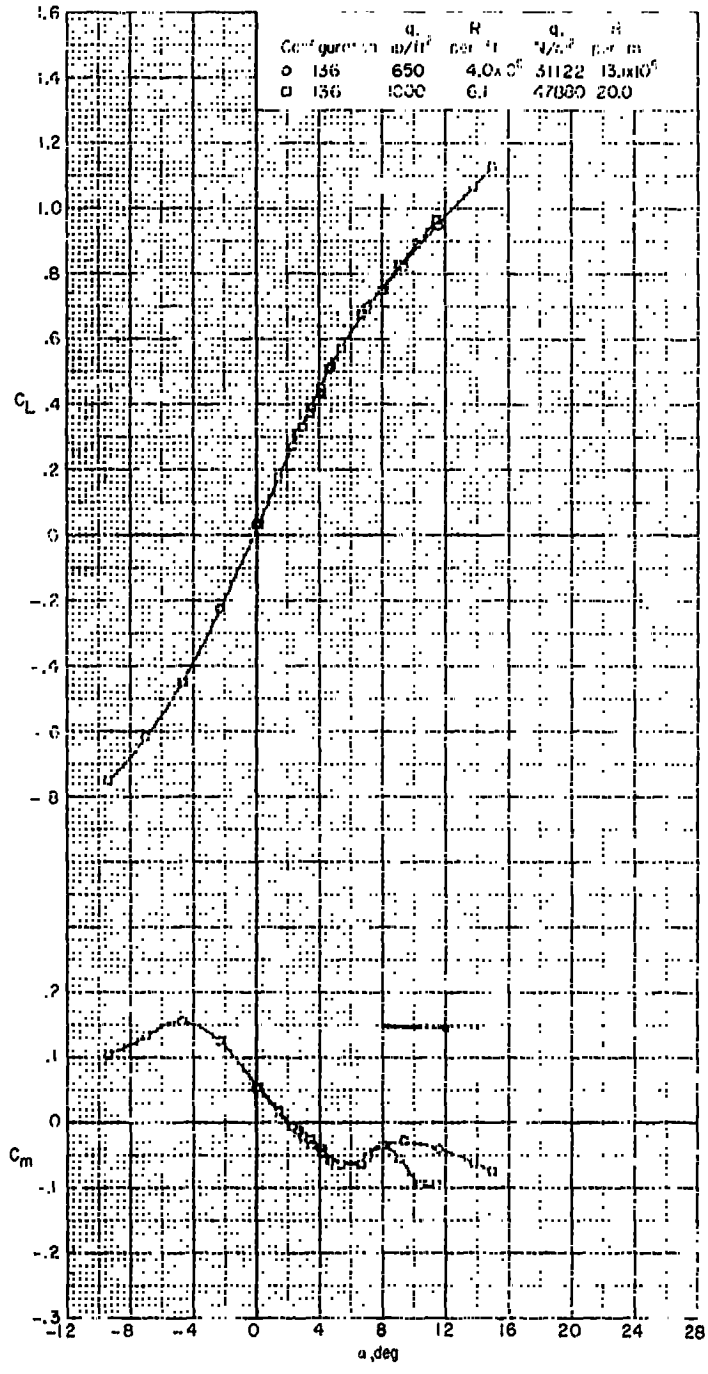

(c) M = 0.80.

Figure 8.- Continued.

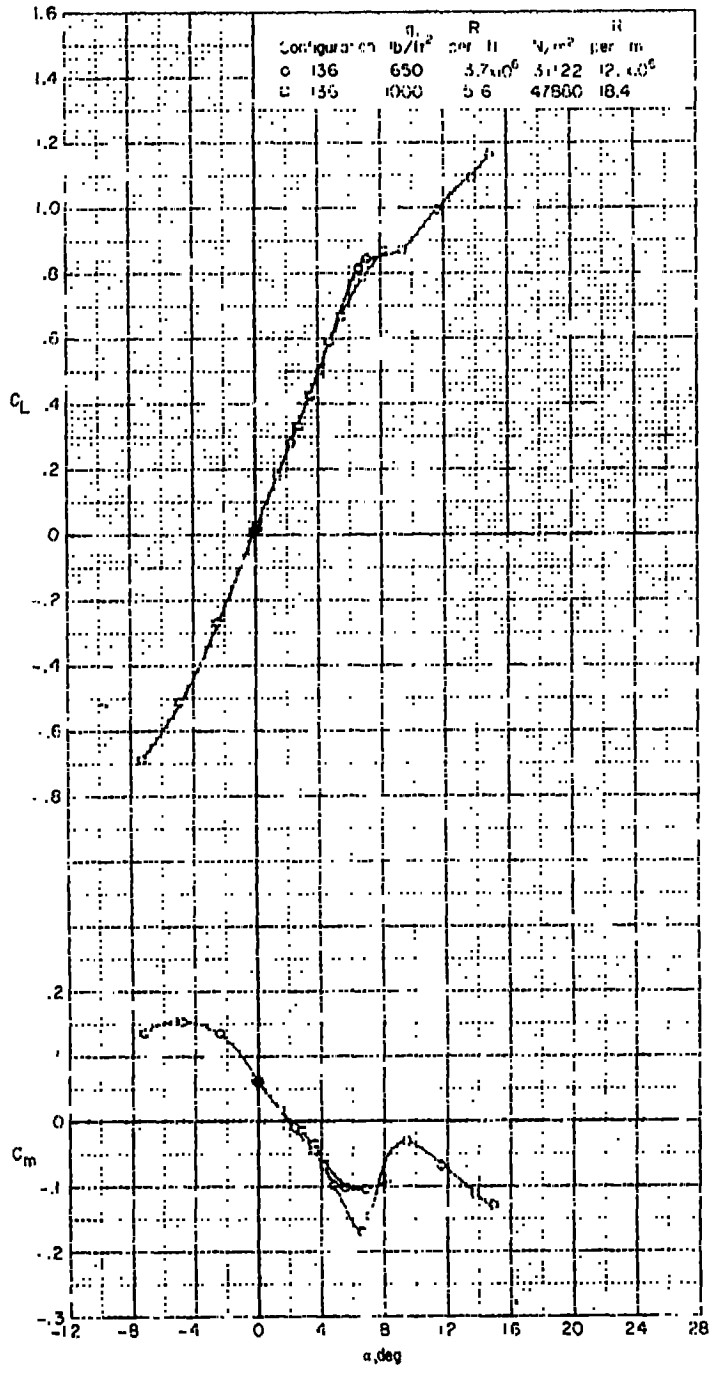

(d) M = 0.90.

Figure 8.- Continued.

ORIGINAL PAGE IS
OF POOR QUALITY

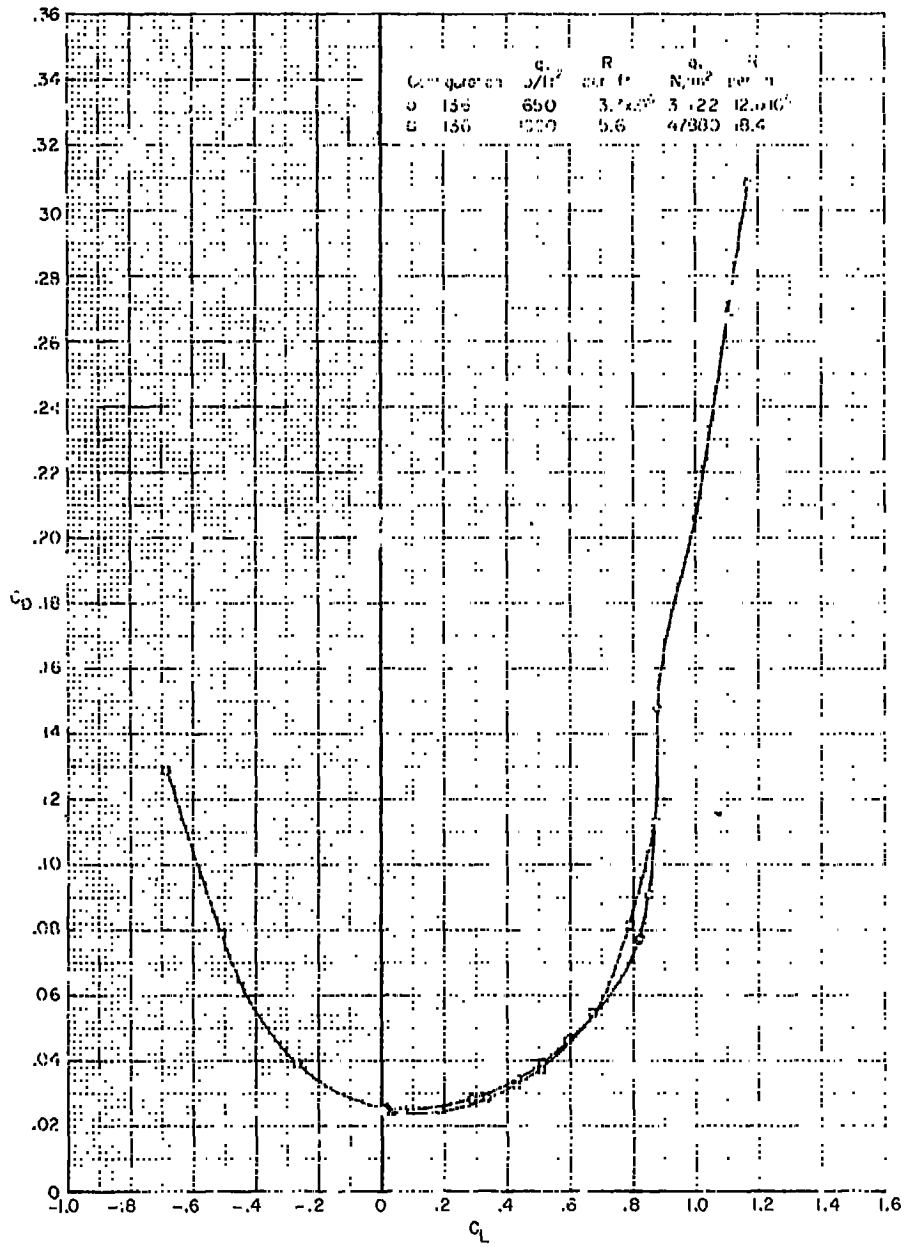

(d) M = 0.90. Concluded.

Figure 8.- Continued.

[redacted]

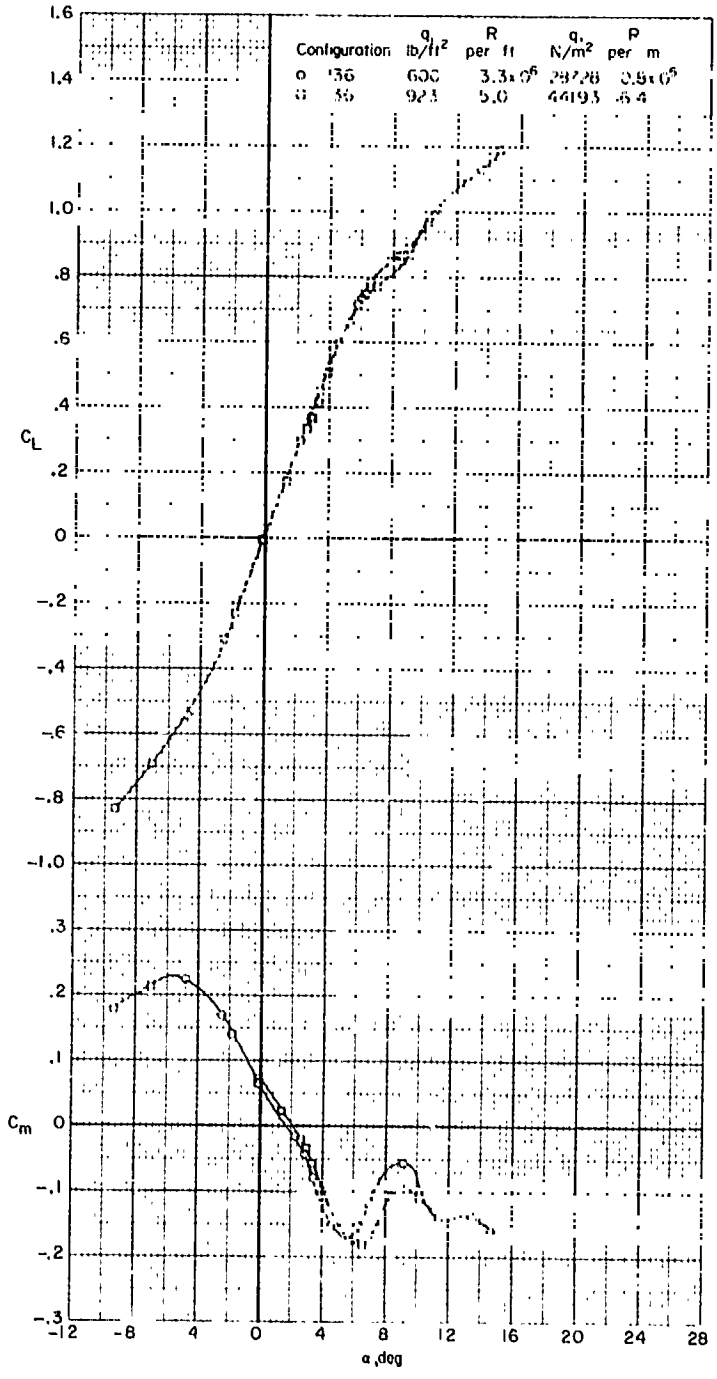

(e) M = 0.95.

Figure 8.- Continued.

ORIGINAL PAGE IS
OF POOR QUALITY

[redacted]

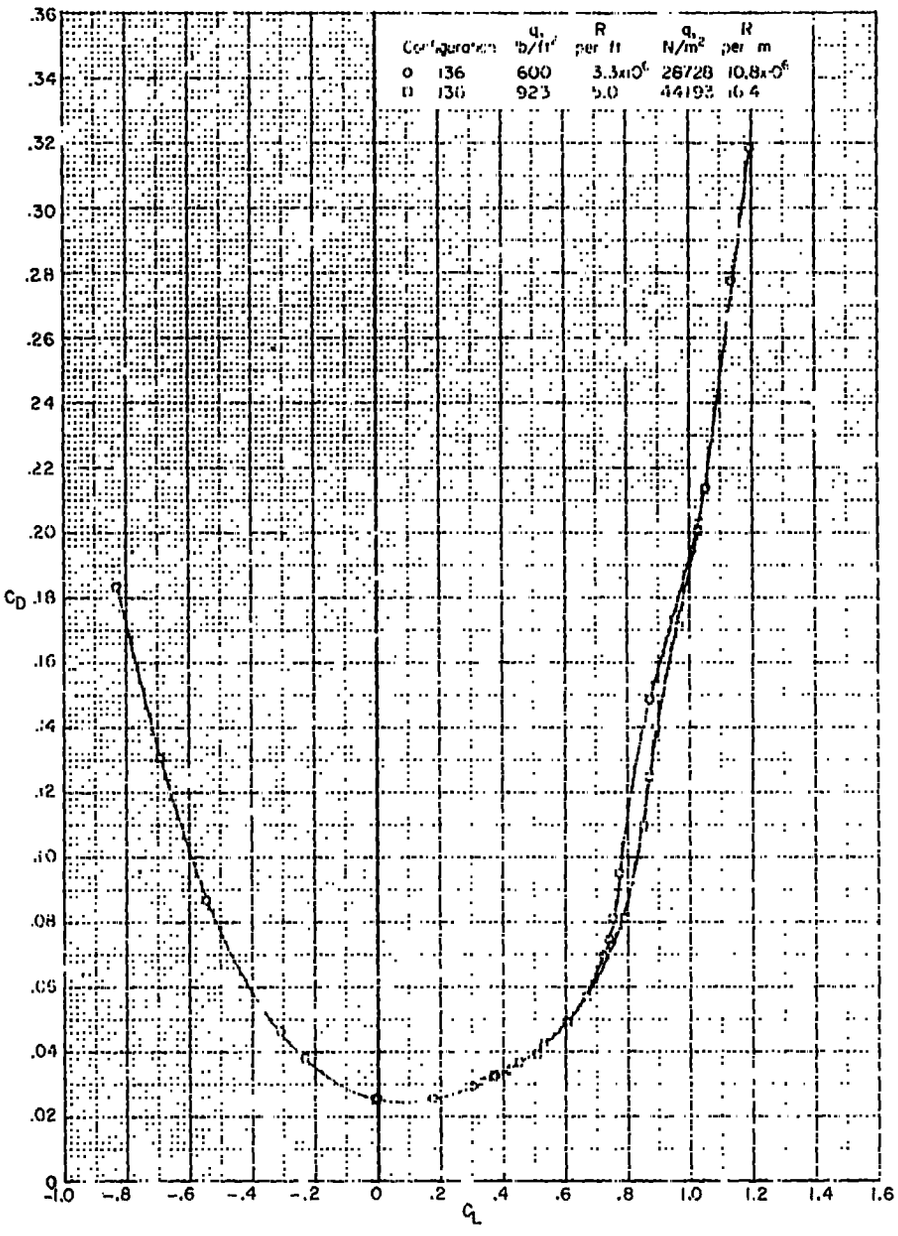

(e) M = 0.95. Concluded.

Figure 8.- Continued.

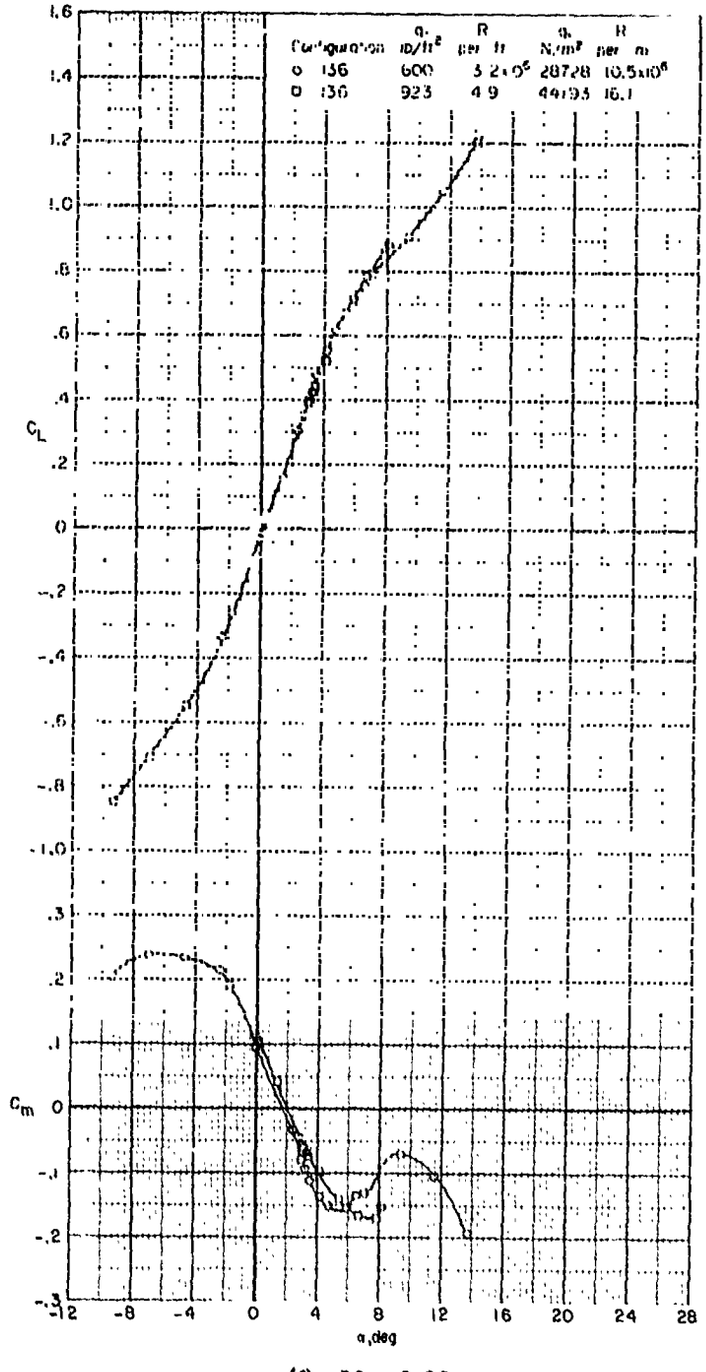

(f) M = 0.99.

Figure 8.- Continued.

ORIGINAL PAGE IS
OF POOR QUALITY

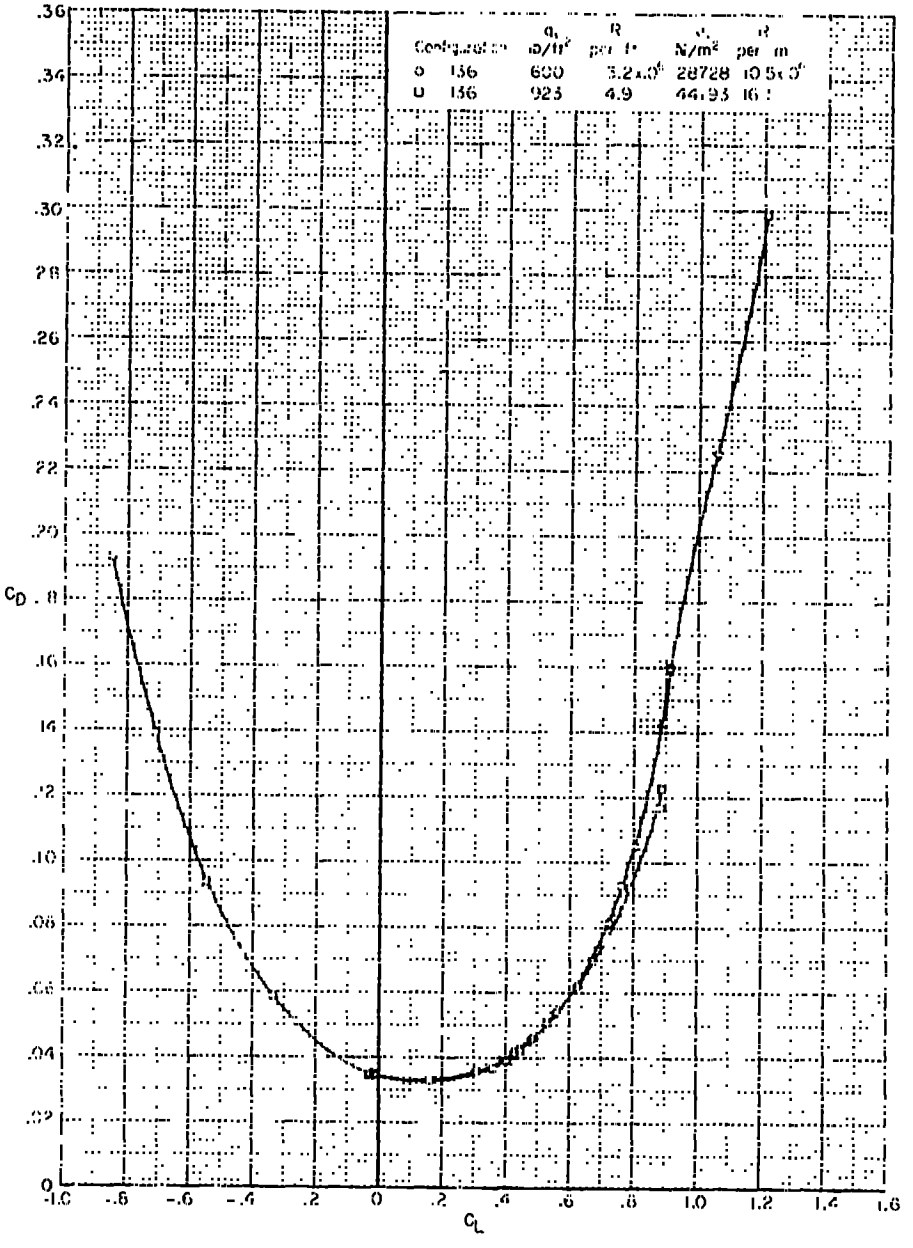

(f) M = 0.99. Concluded.

Figure 8.- Concluded.

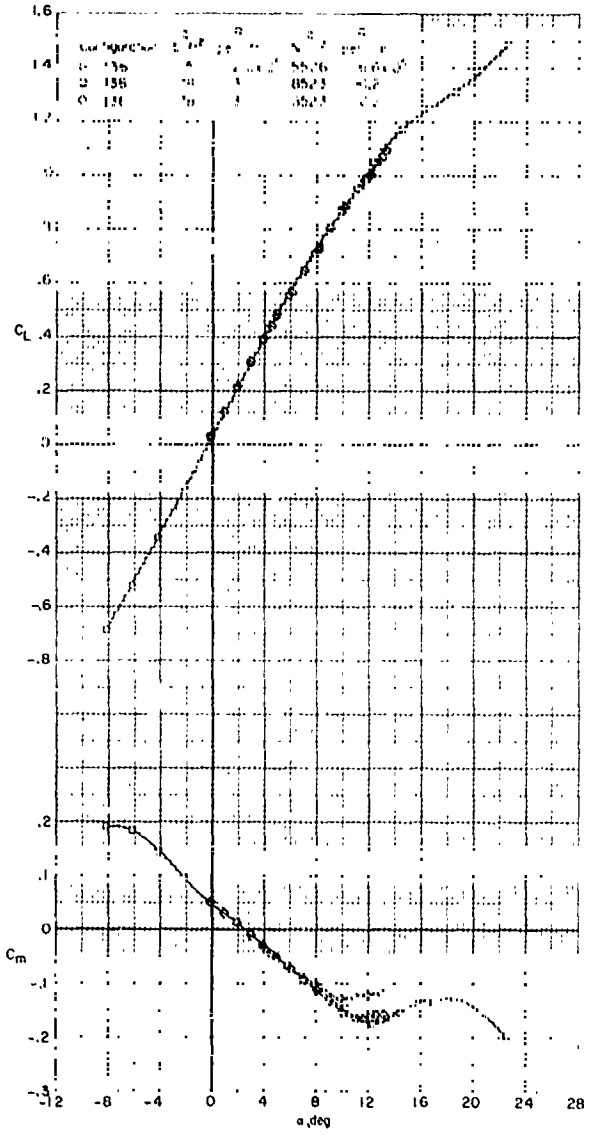

(a) M = 0.25.

Figure 9.- Longitudinal aerodynamic characteristics for an extended angle-of-attack range. $\beta = 0^{\circ}$ and $\delta_h = -2.5^{\circ}$.

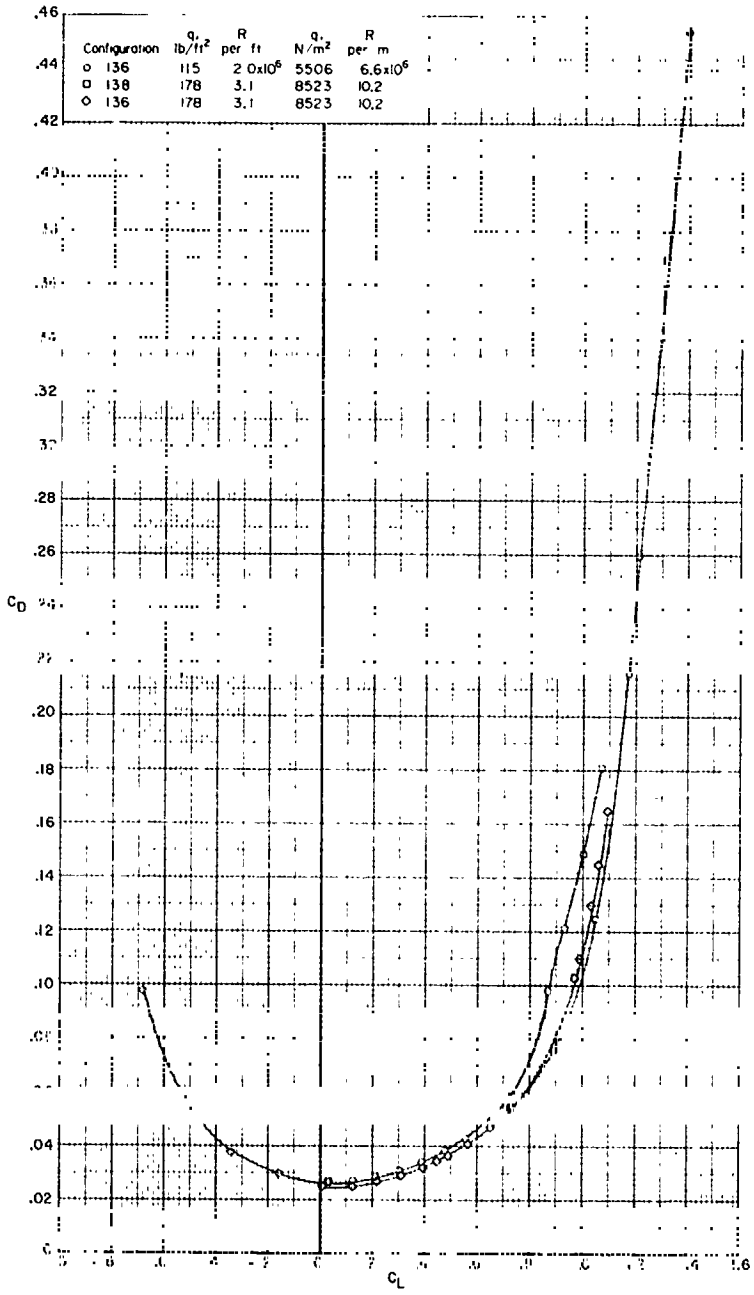

(a) M = 0.25. Concluded.

Figure 9.- Continued.

ORIGINAL PAGE IS
OF POOR QUALITY

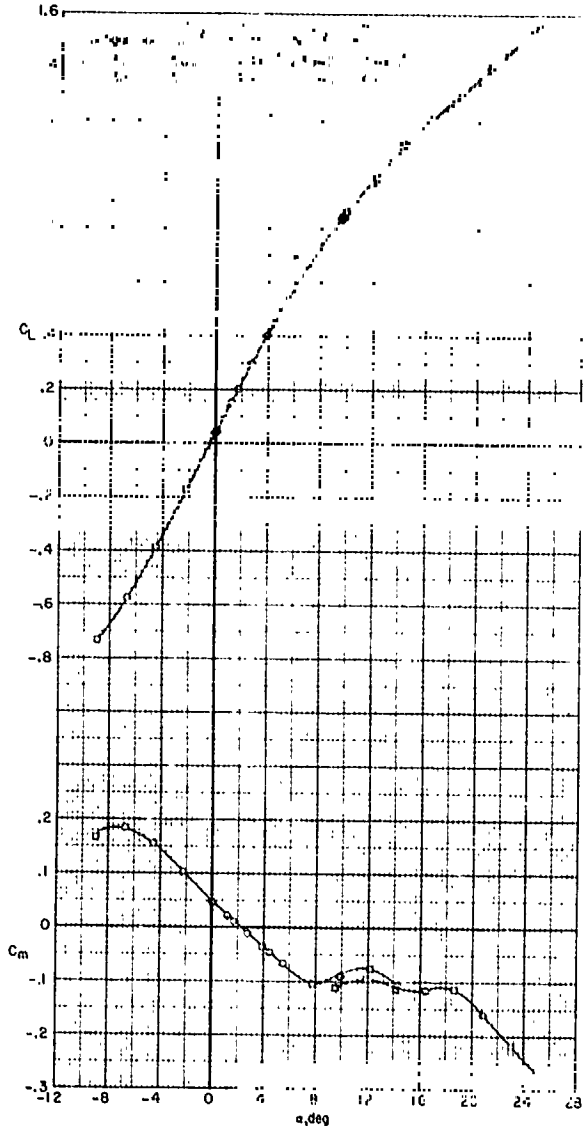

(b) M = 0.50.

Figure 9.- Continued.

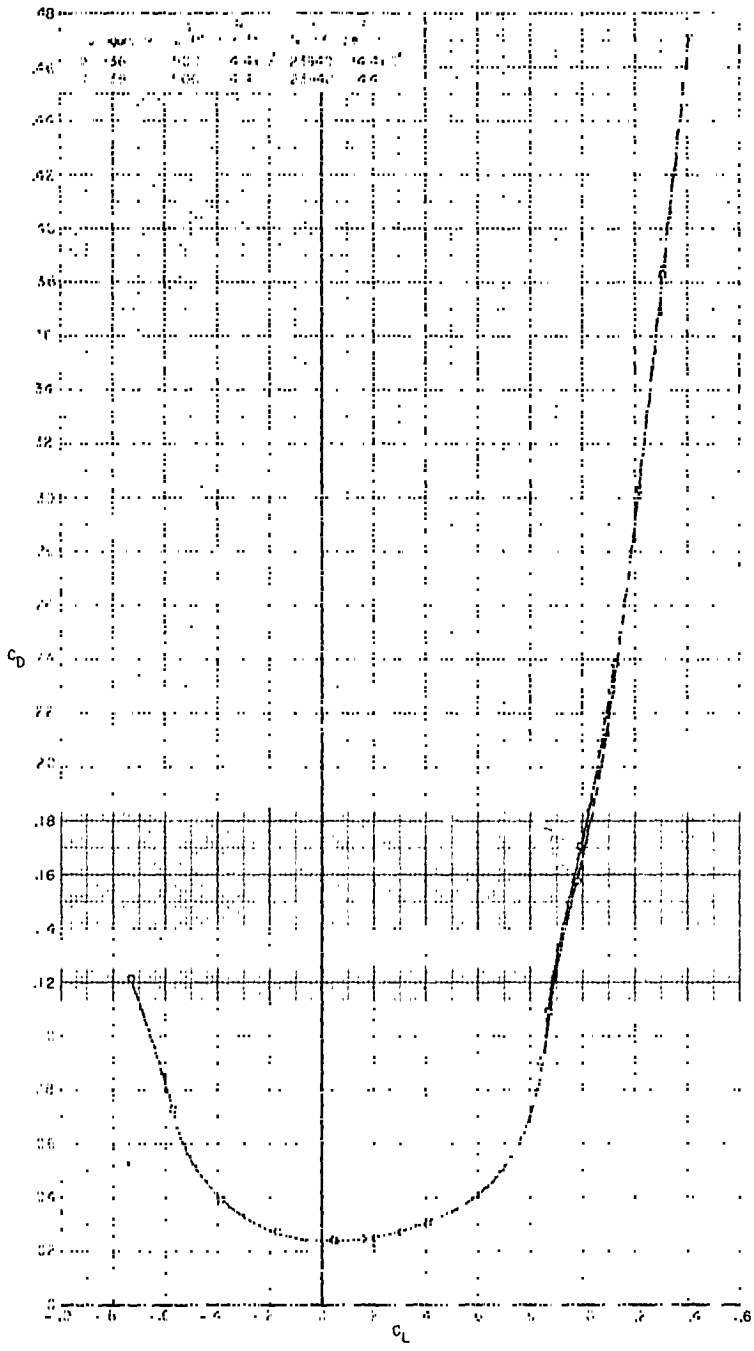

(b) M = 0.50. Concluded.

Figure 9.- Continued.

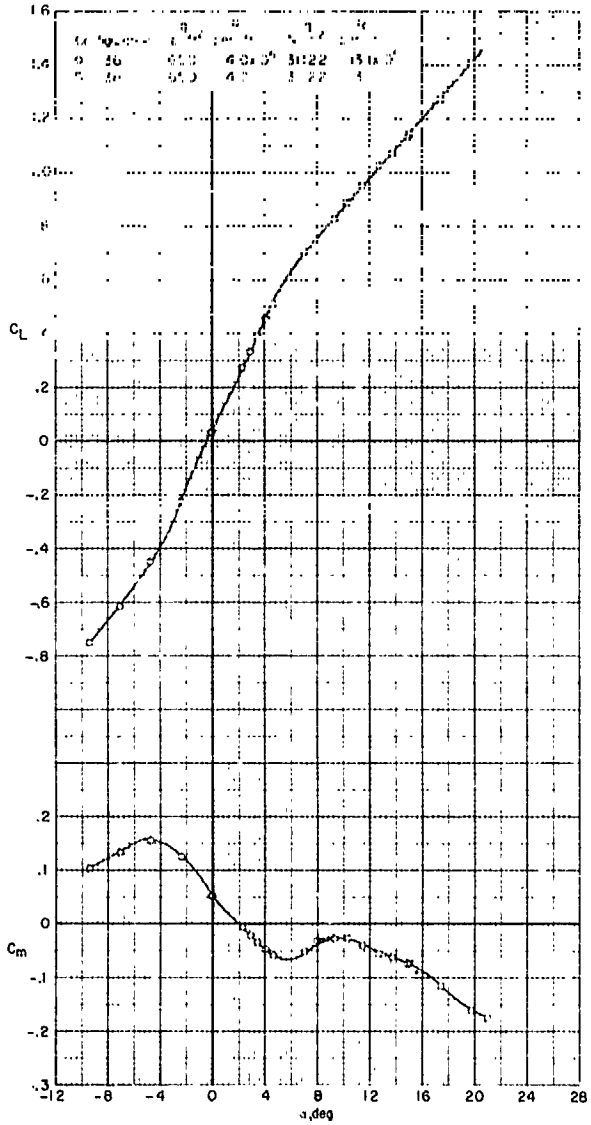

(c) M = 0.80.

Figure 9.- Continued.

ORIGINAL PAGE IS
OF POOR QUALITY

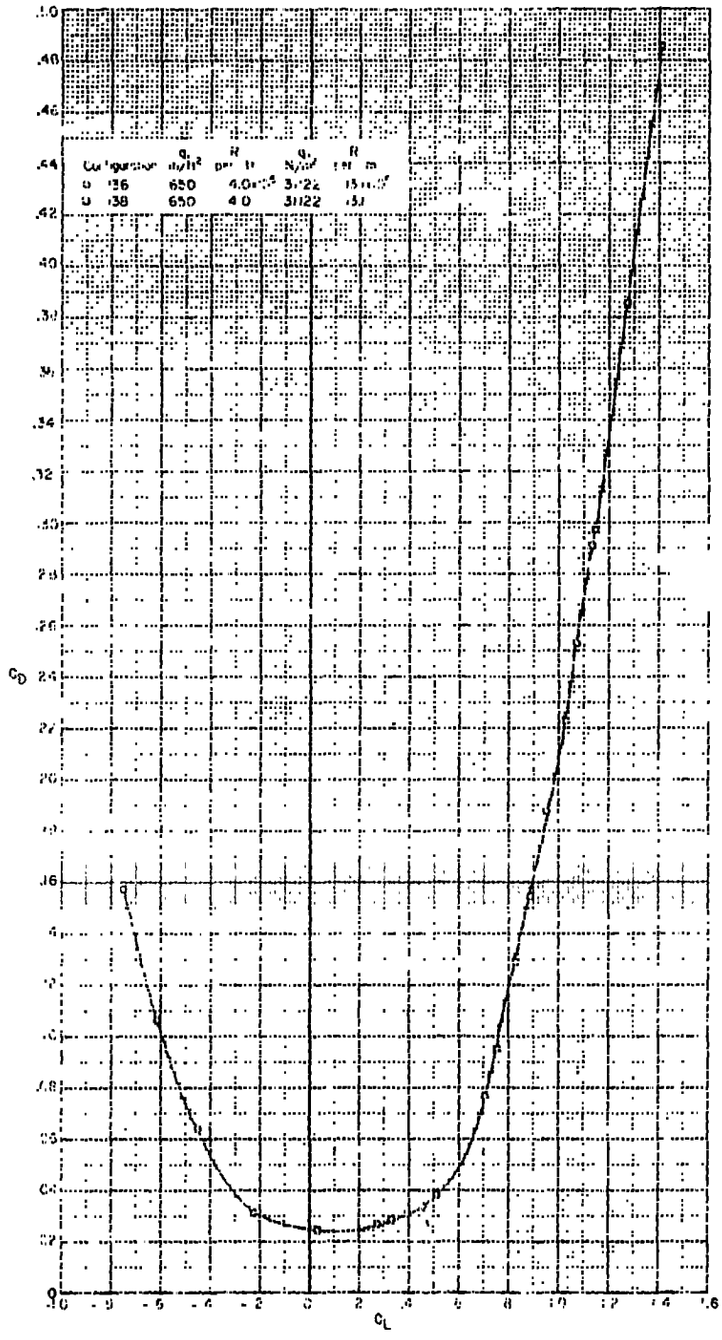

(c) M = 0.80. Concluded.

Figure 9.- Continued.

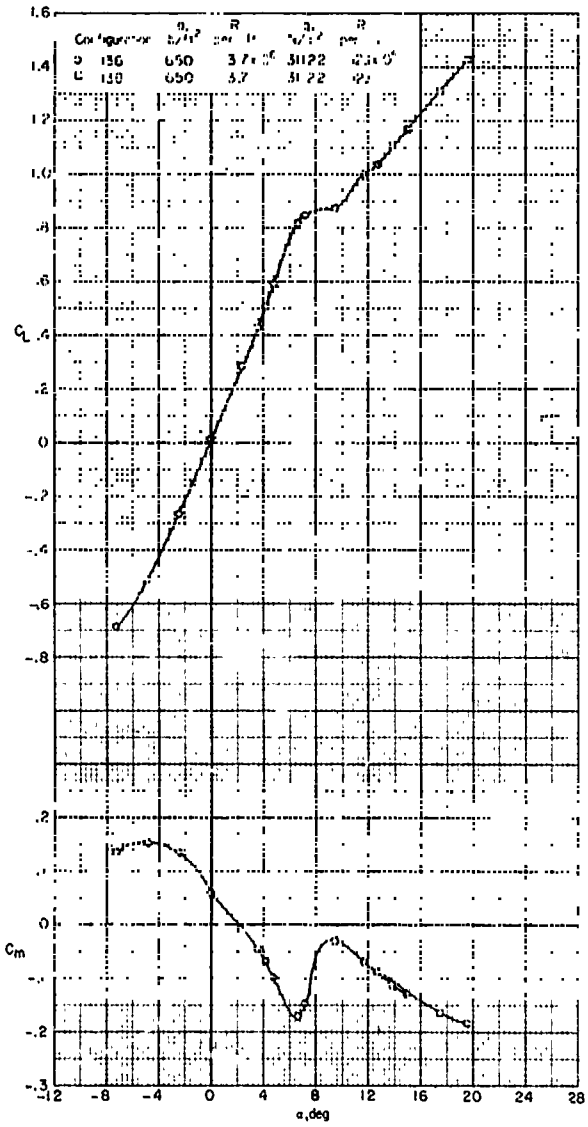

(d) M = 0.90.

Figure 9.- Continued.

ORIGINAL PAGE IS
OF POOR QUALITY

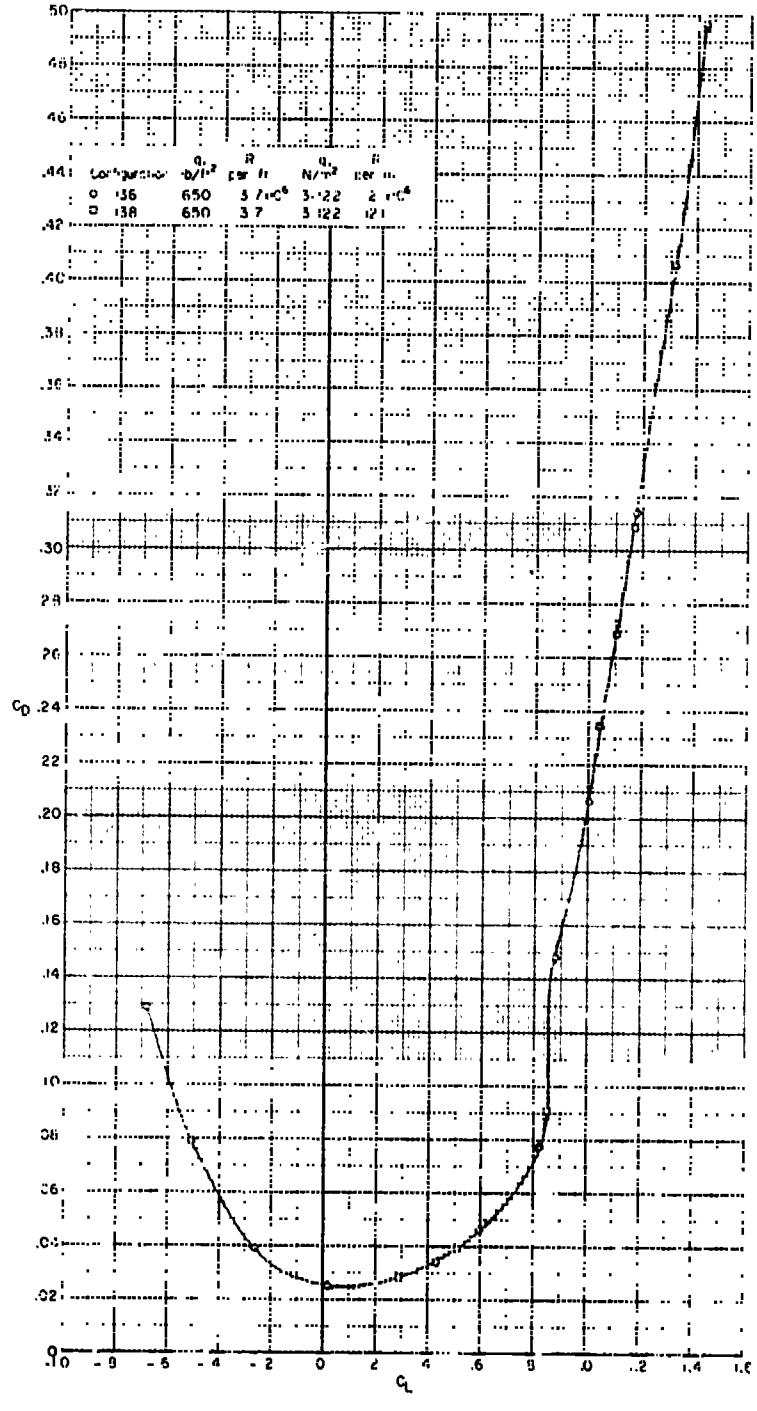

(d) M = 0.90. Concluded.

Figure 9.- Continued.

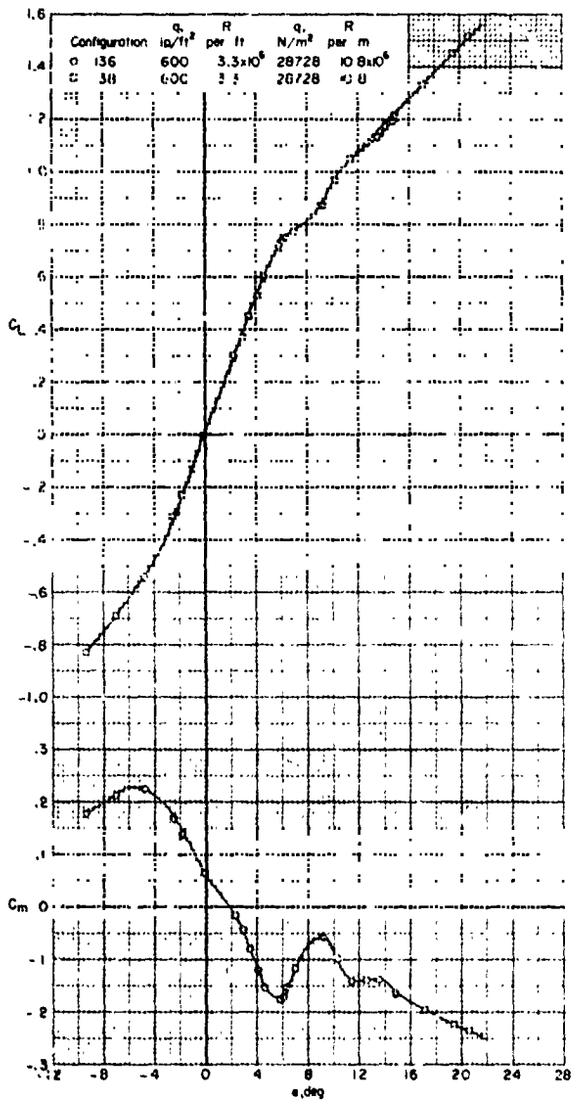

(e) M = 0.95.

Figure 9.- Continued.

ORIGINAL PAGE IS
OF POOR QUALITY

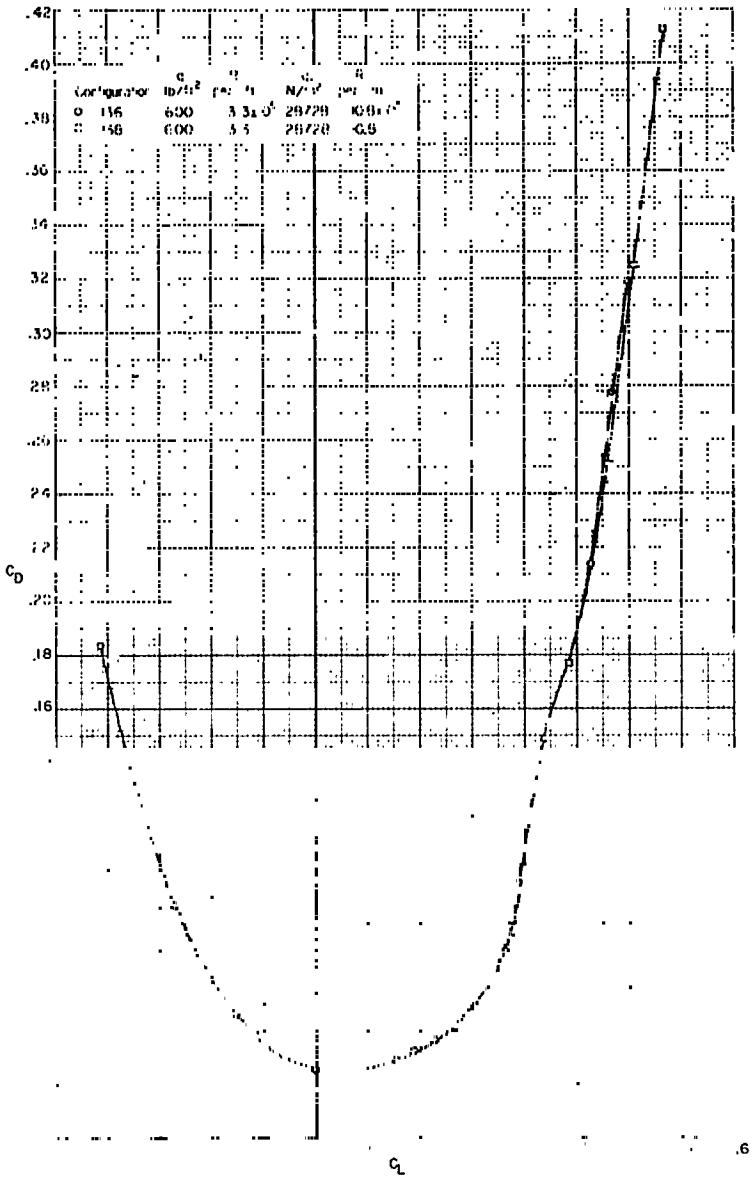

(e) M = 0.95. Concluded.

Figure 9.- Concluded.

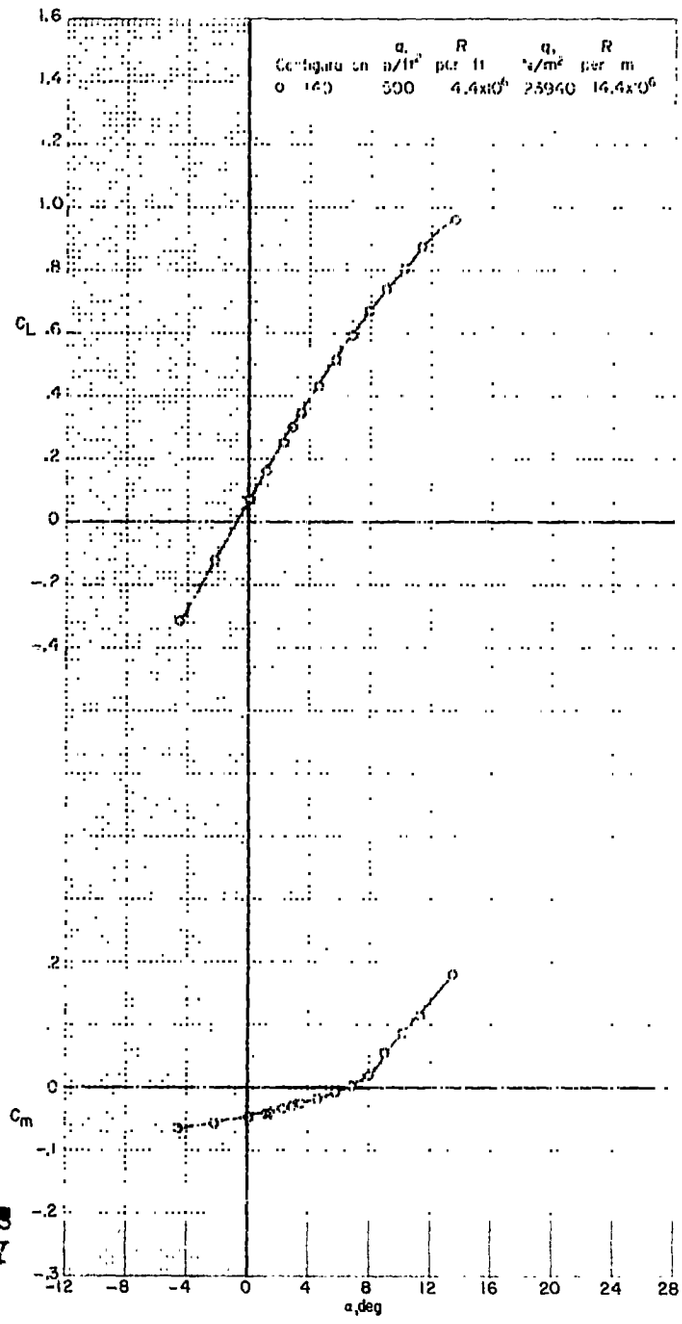

(a) M = 0.50.

Figure 10.- Longitudinal aerodynamic characteristics for configuration 140 with horizontal tail off. $\beta = 0^{\circ}$.

ORIGINAL PAGE IS
OF POOR QUALITY

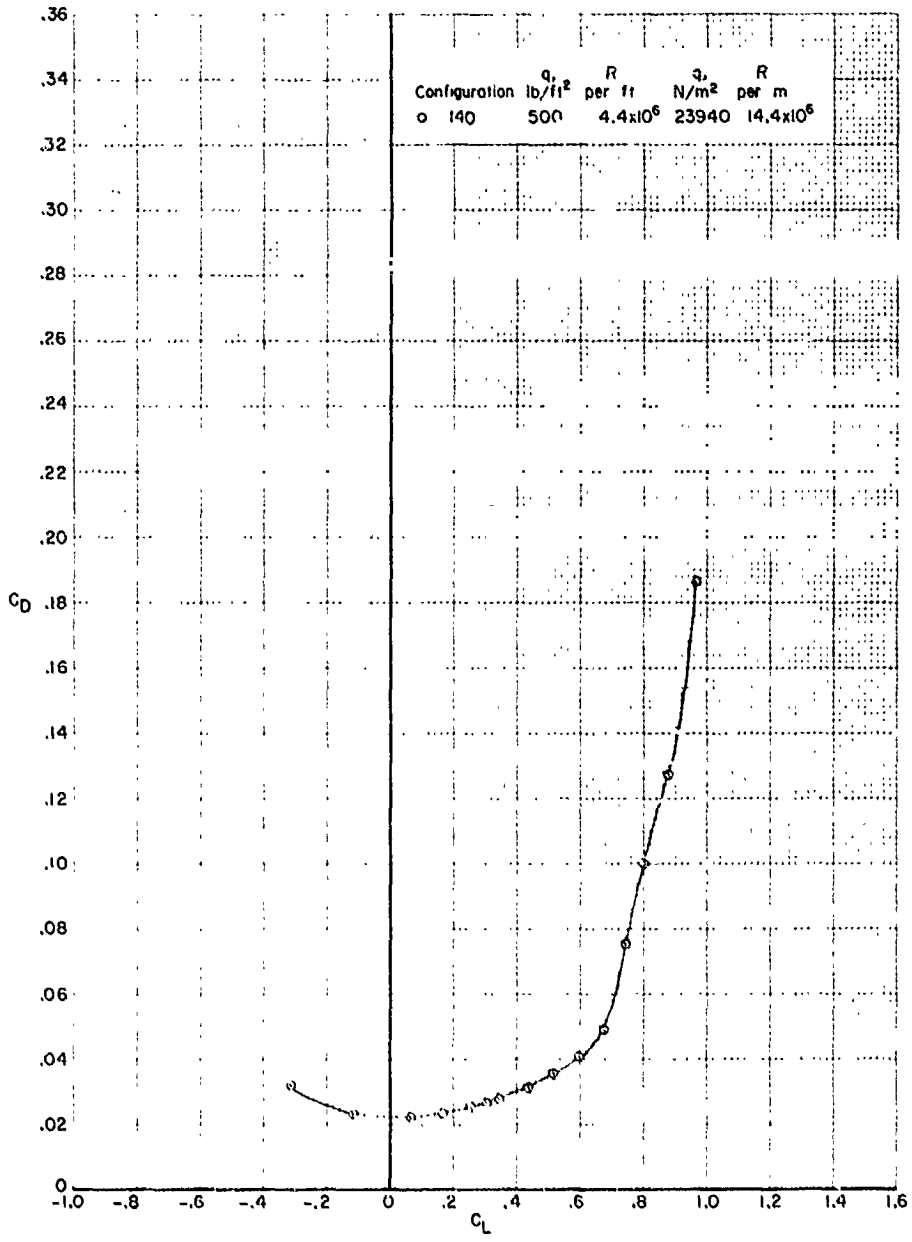

(a) M = 0.50. Concluded.

Figure 10.- Continued.

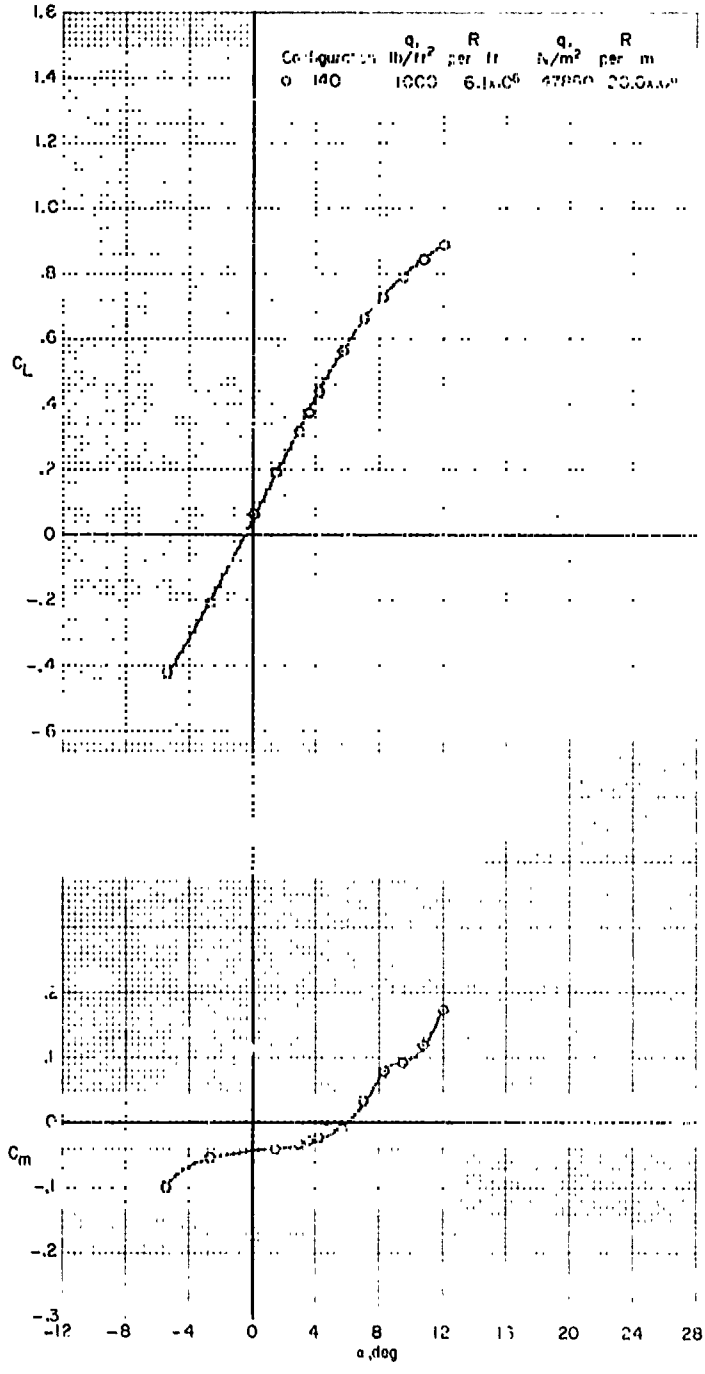

(b) M = 0.80.

Figure 10.- Continued.

ORIGINAL PAGE IS
OF POOR QUALITY

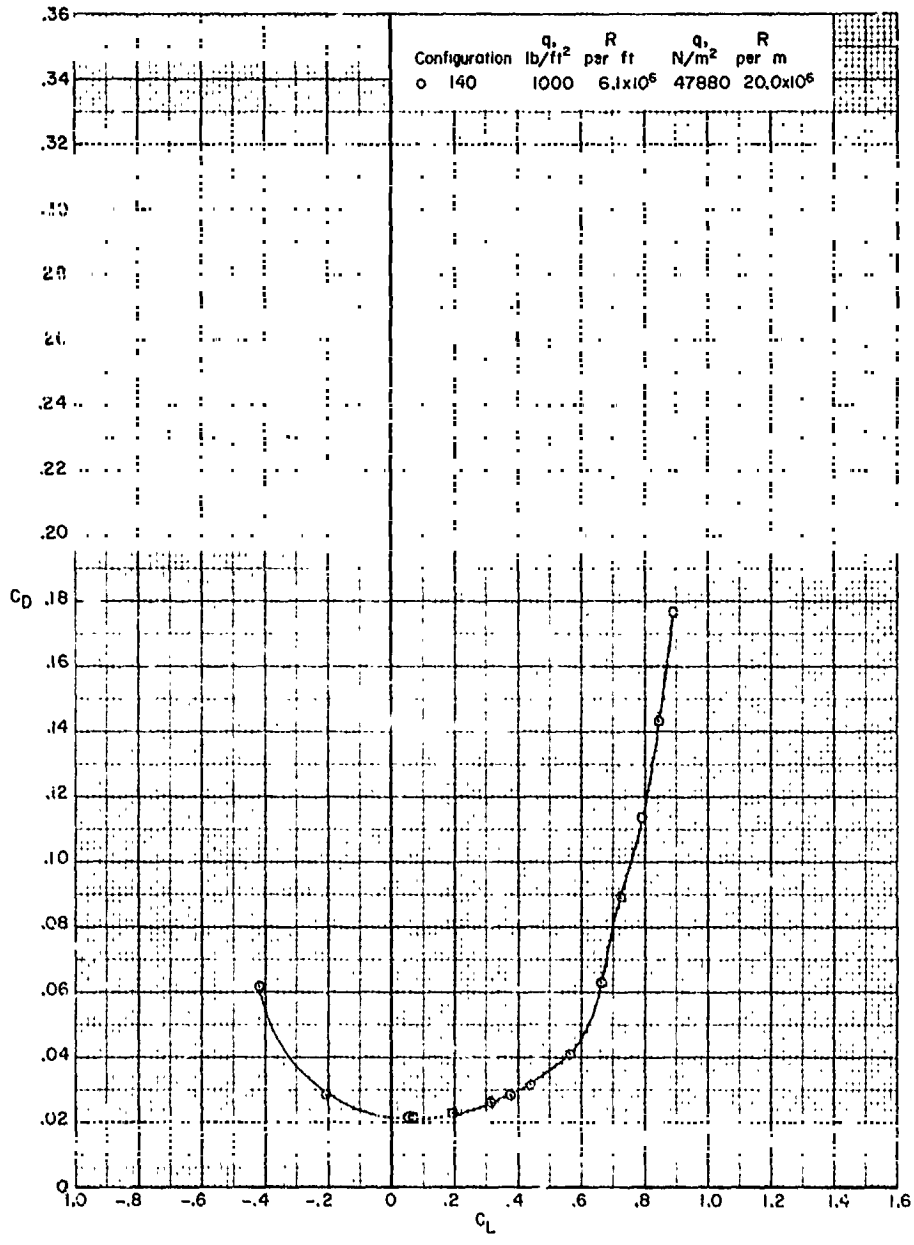

(b) M = 0.80. Concluded.

Figure 10.- Continued.

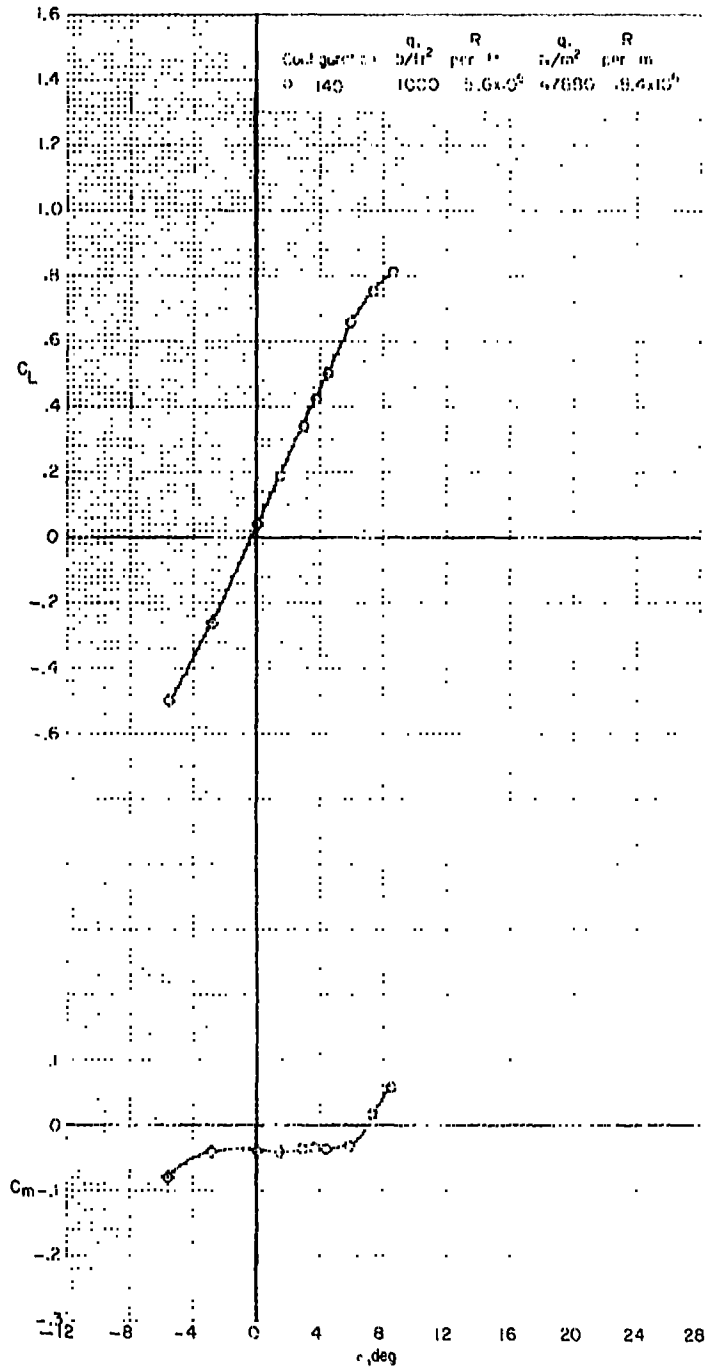

(c) M = 0.90.

Figure 10.- Continued.

ORIGINAL PAGE IS
OF POOR QUALITY

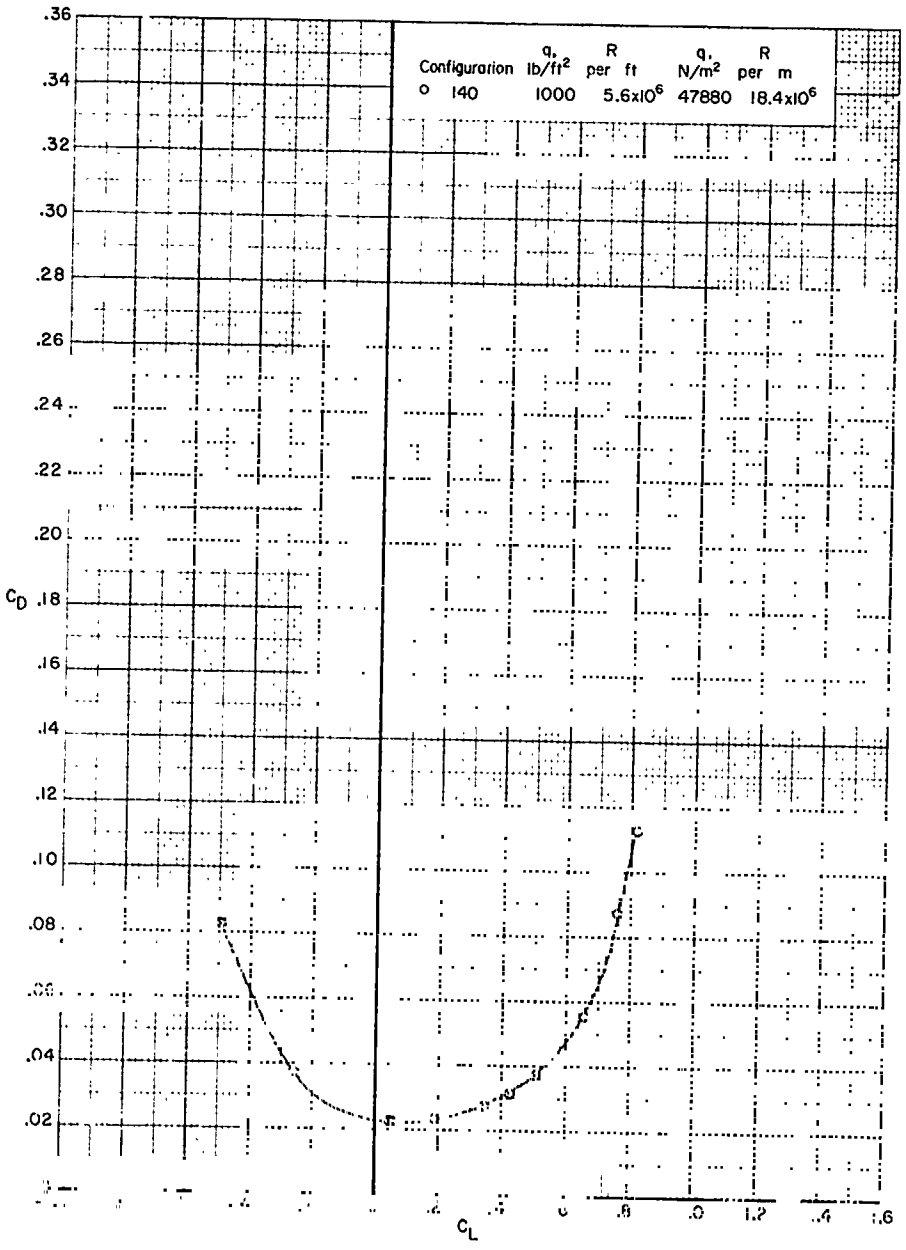

(c) M = 0.90. Concluded.

Figure 10.- Continued.

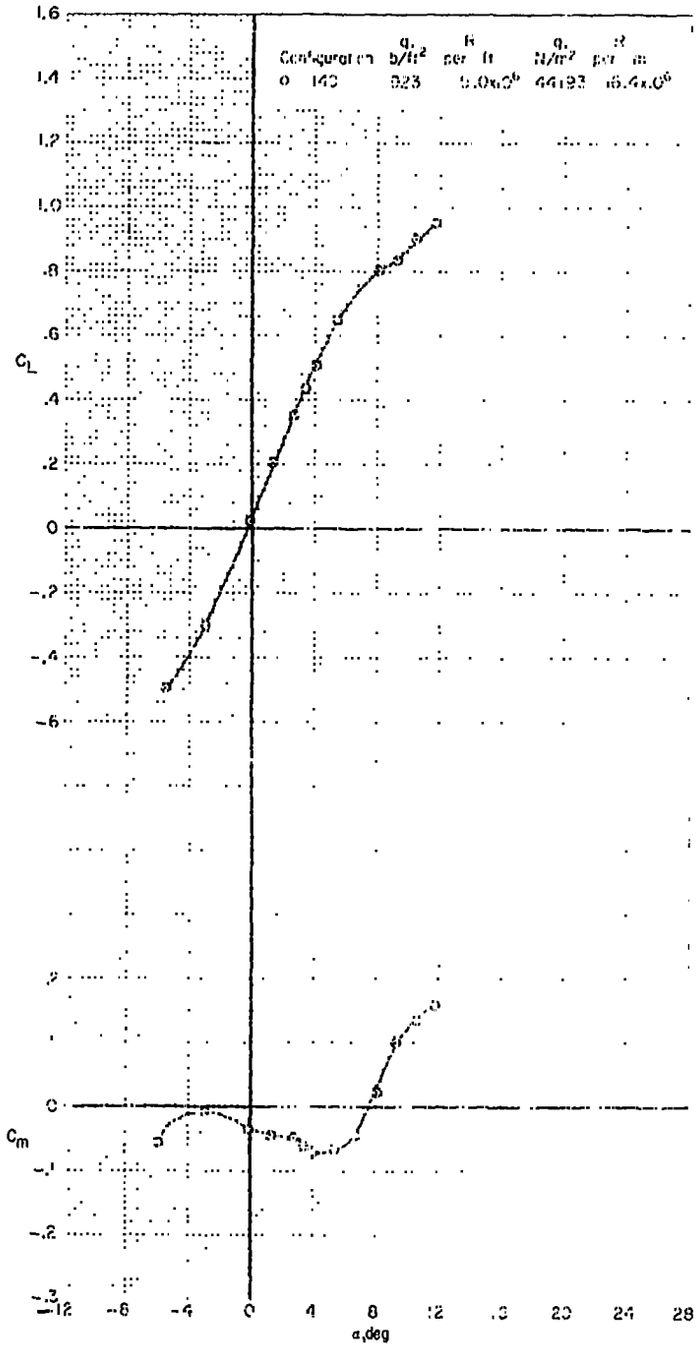

(d) M = 0.95.

Figure 10.- Continued.

[redacted]

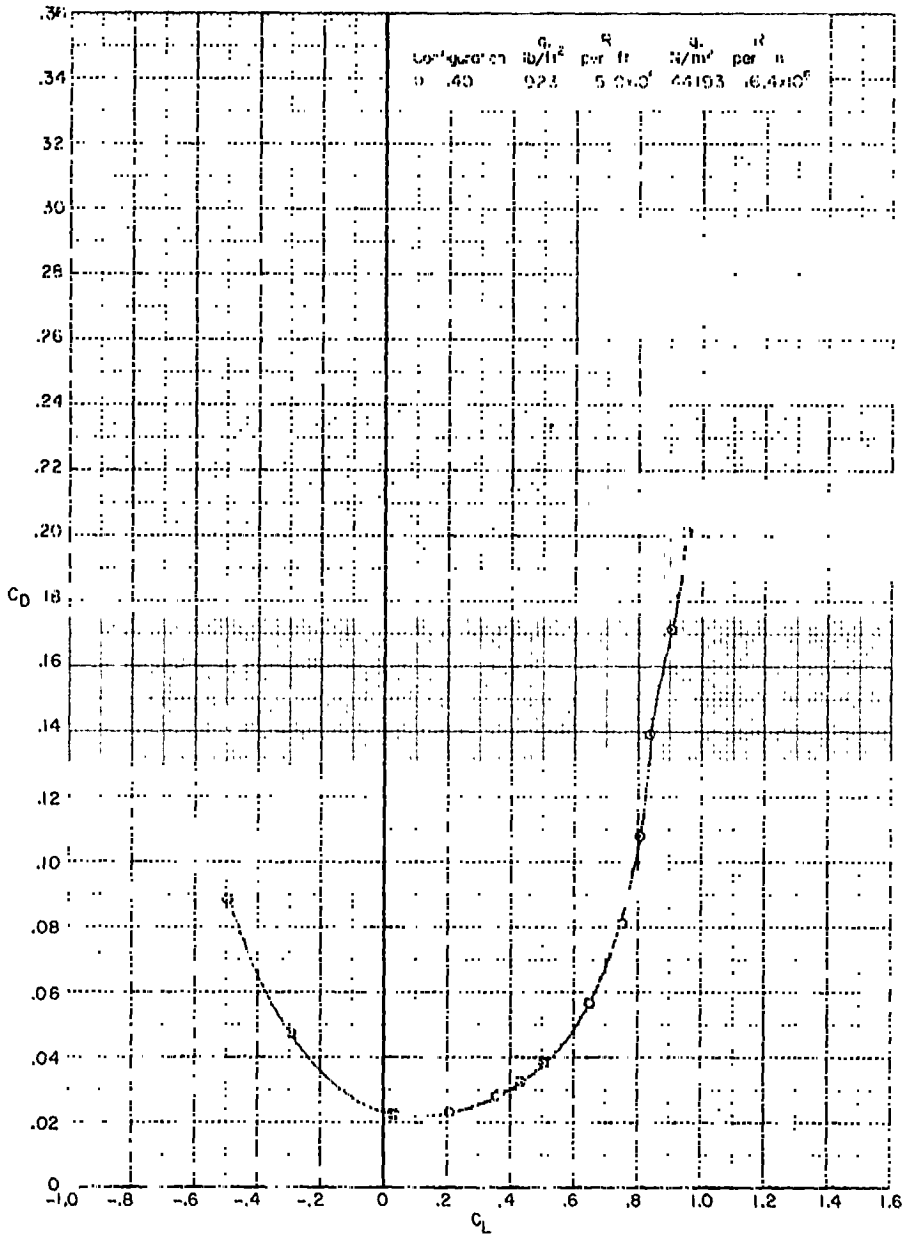

(d) M = 0.95. Concluded.

Figure 10.- Continued.

ORIGINAL PAGE IS
OF POOR QUALITY

[redacted]

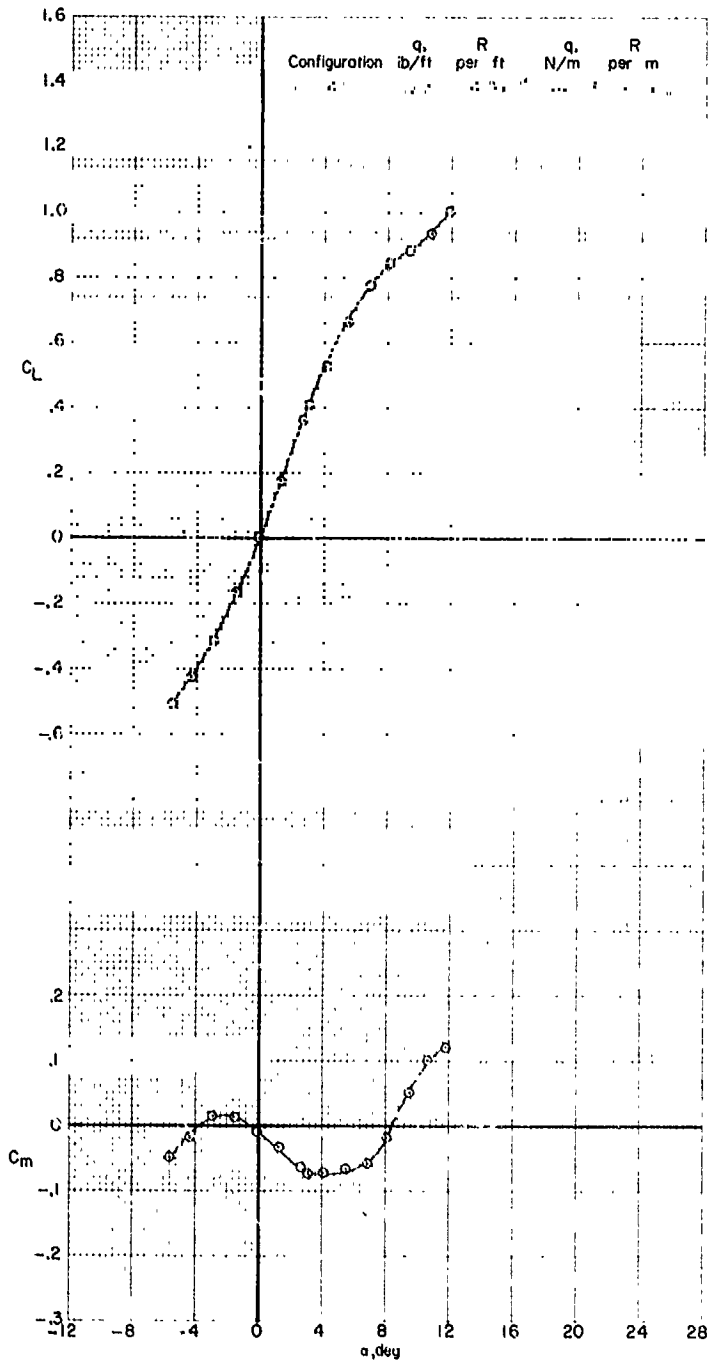

(e) M = 0.99.

Figure 10.- Continued.

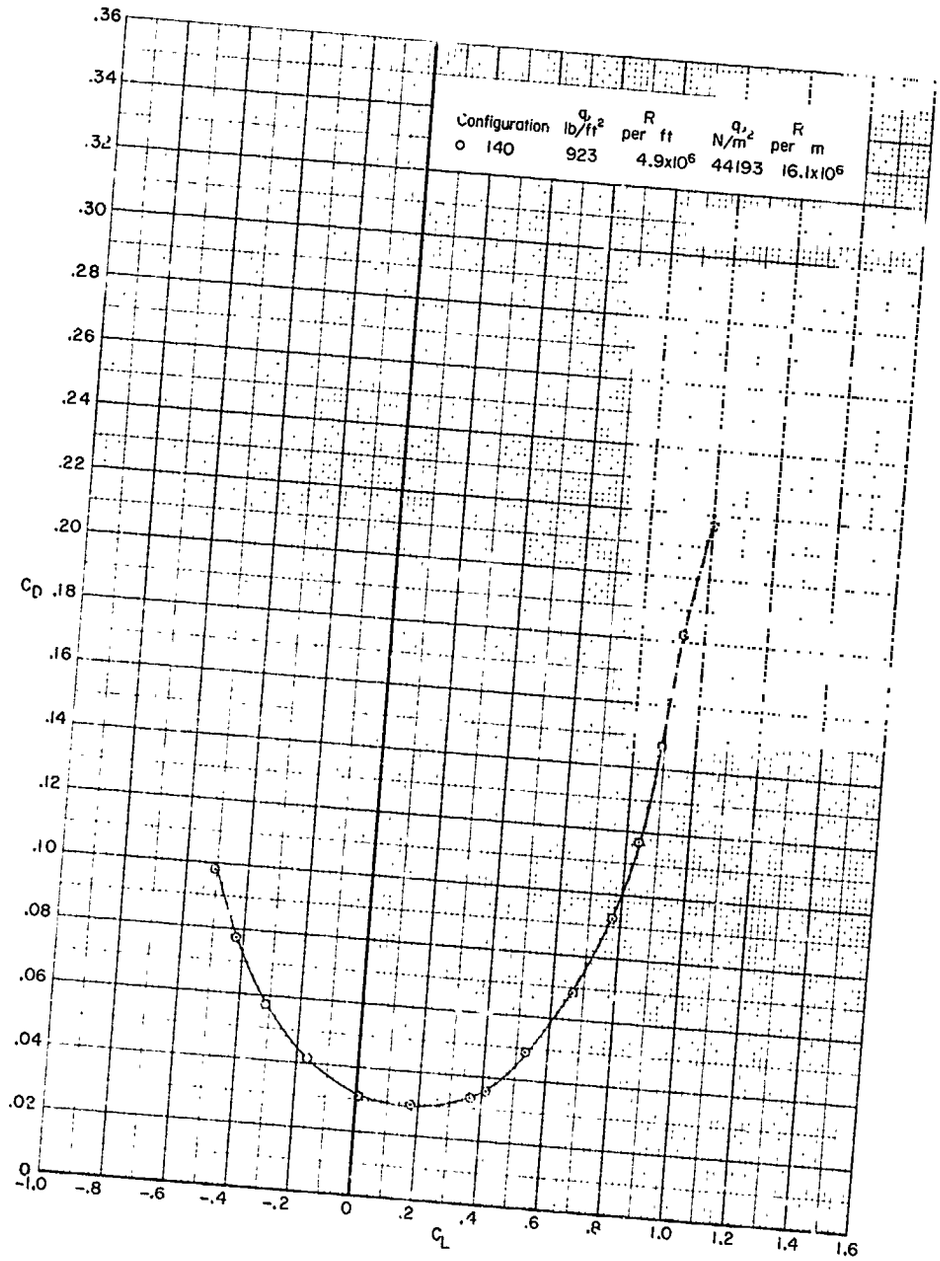

(e) M = 0.99. Concluded.

Figure 10.- Concluded.

ORIGINAL PAGE IS
OF POOR QUALITY

[redacted]

CONFIDENTIAL

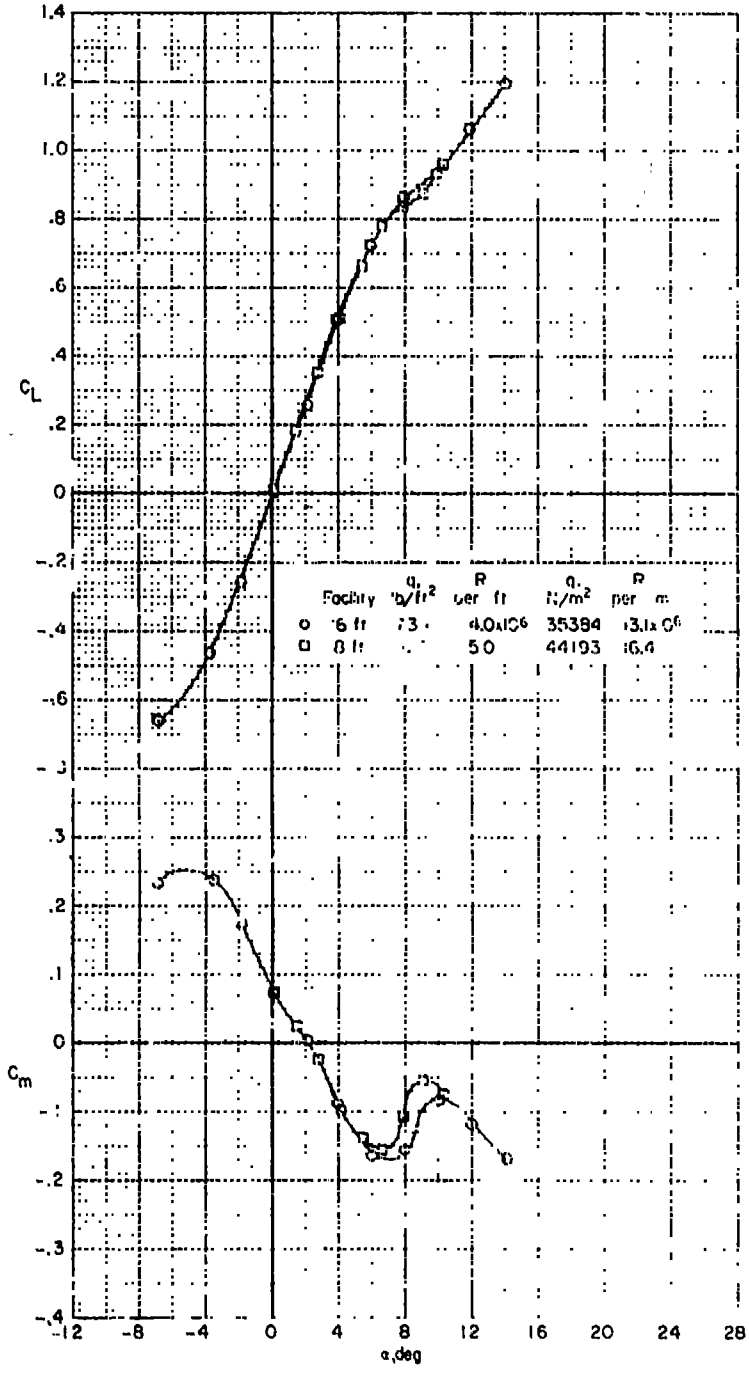

(a) M = 0.95.

Figure 11.- Longitudinal aerodynamic characteristics for configuration 140 obtained in Langley 8-foot transonic pressure tunnel and Langley 16-foot transonic tunnel. $\beta = 0^{\circ}$ and $\delta_h = -2.5^{\circ}$.

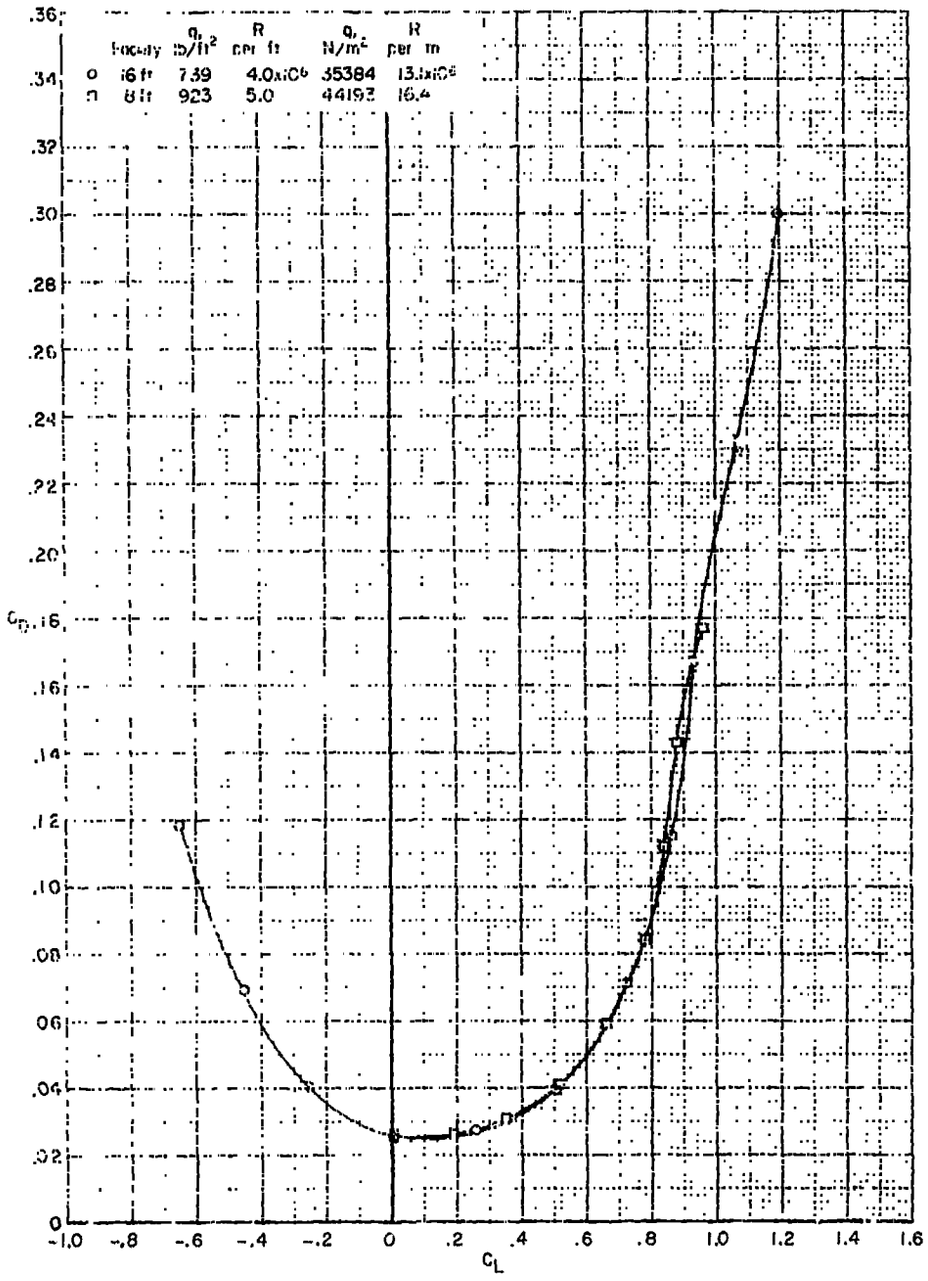

(a) M = 0.95. Concluded.

Figure 11.-- Continued.

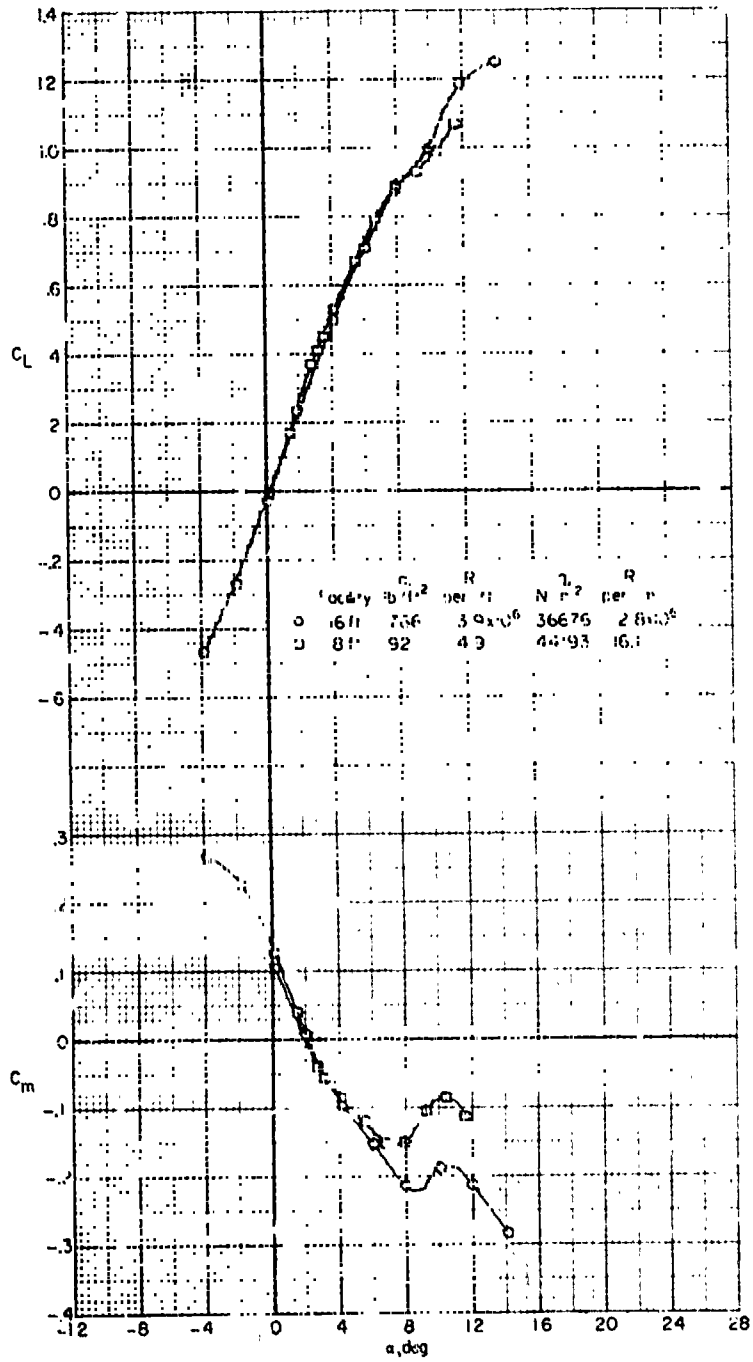

(b) M = 0.99.

Figure 11.- Continued.

ORIGINAL PAGE IS
OF POOR QUALITY

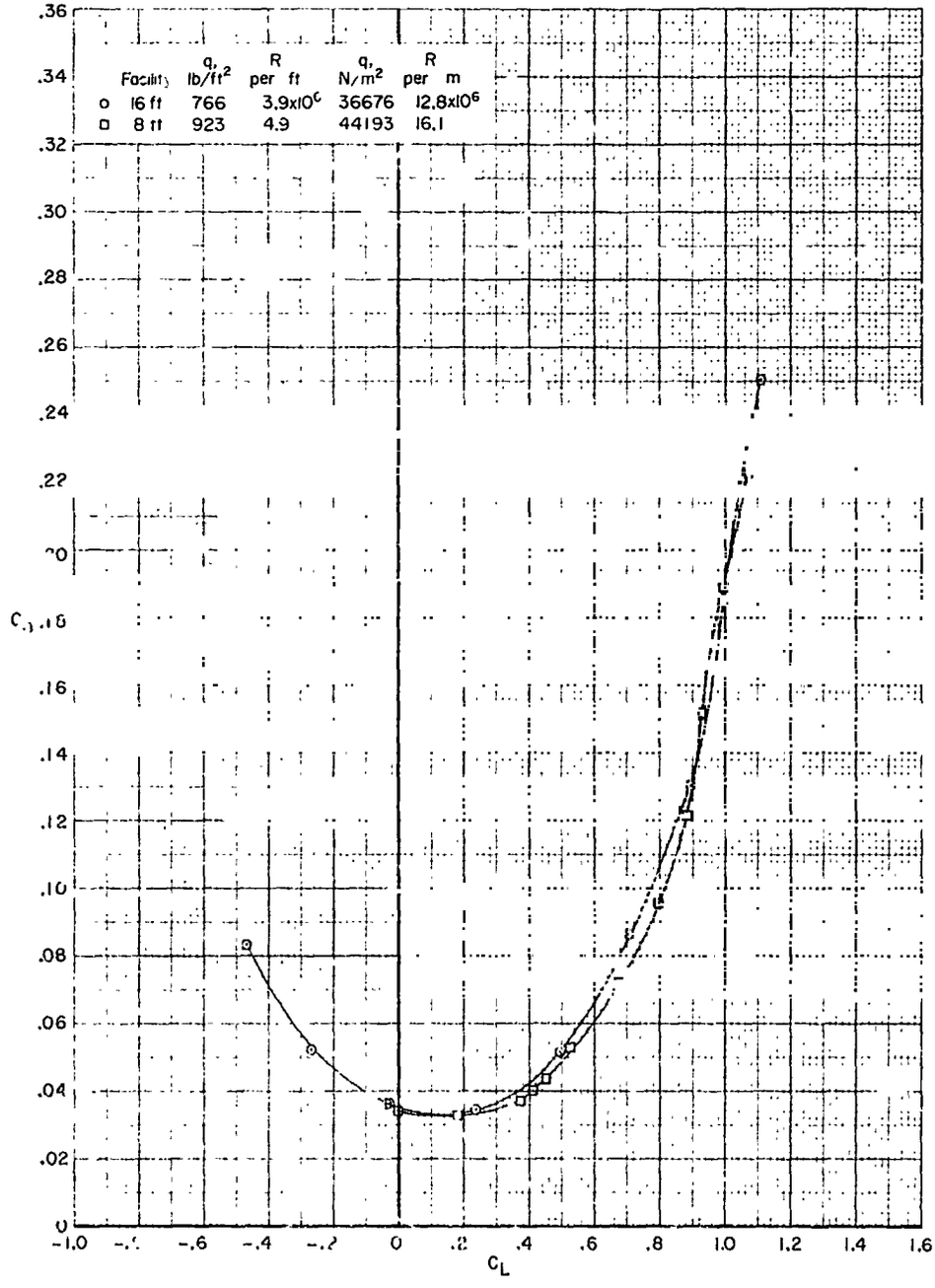

(b) M = 0.93. Concluded.

Figure 11.- Continued.

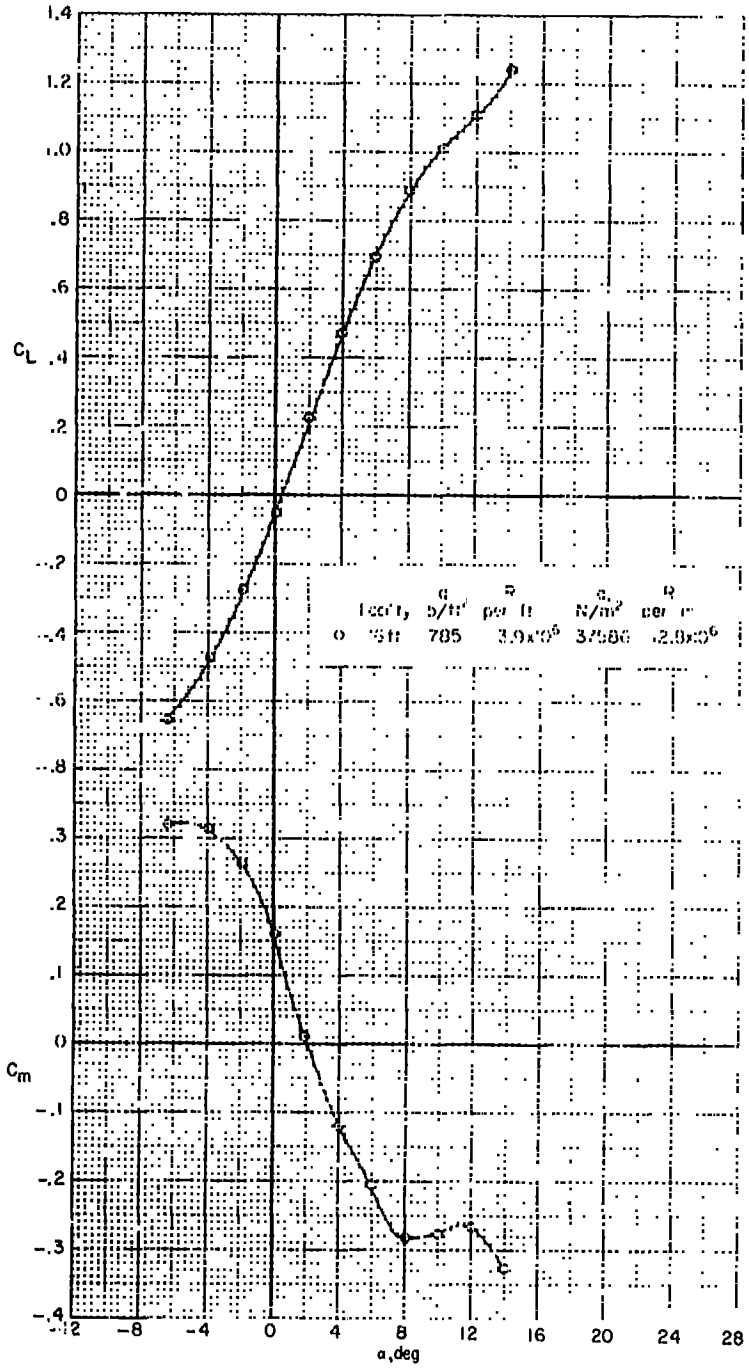

(c) M = 1.02.

Figure 11.- Continued.

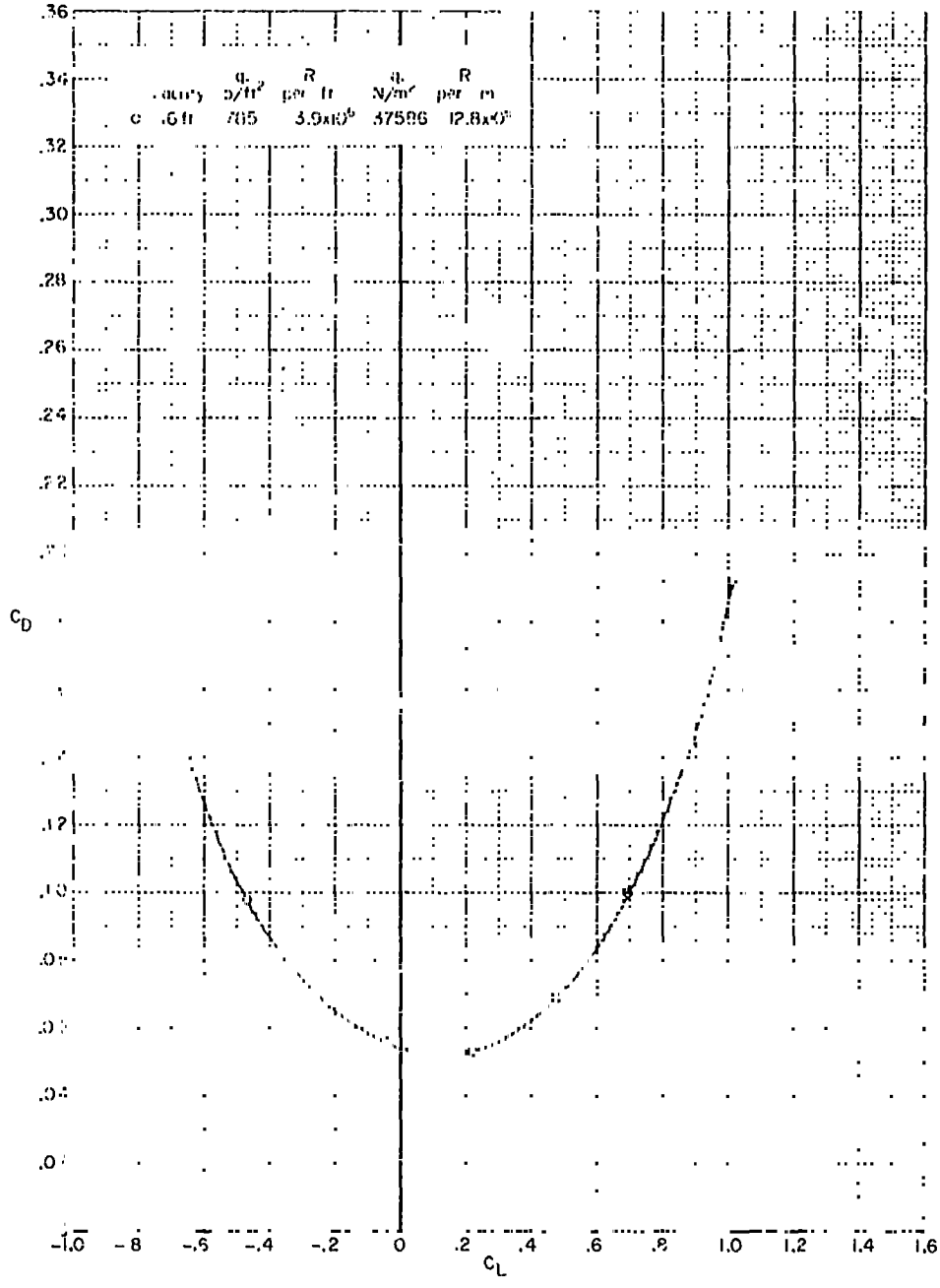

(c) M = 1.02. Concluded.

Figure 11.- Continued.

ORIGINAL PAGE IS
OF POOR QUALITY

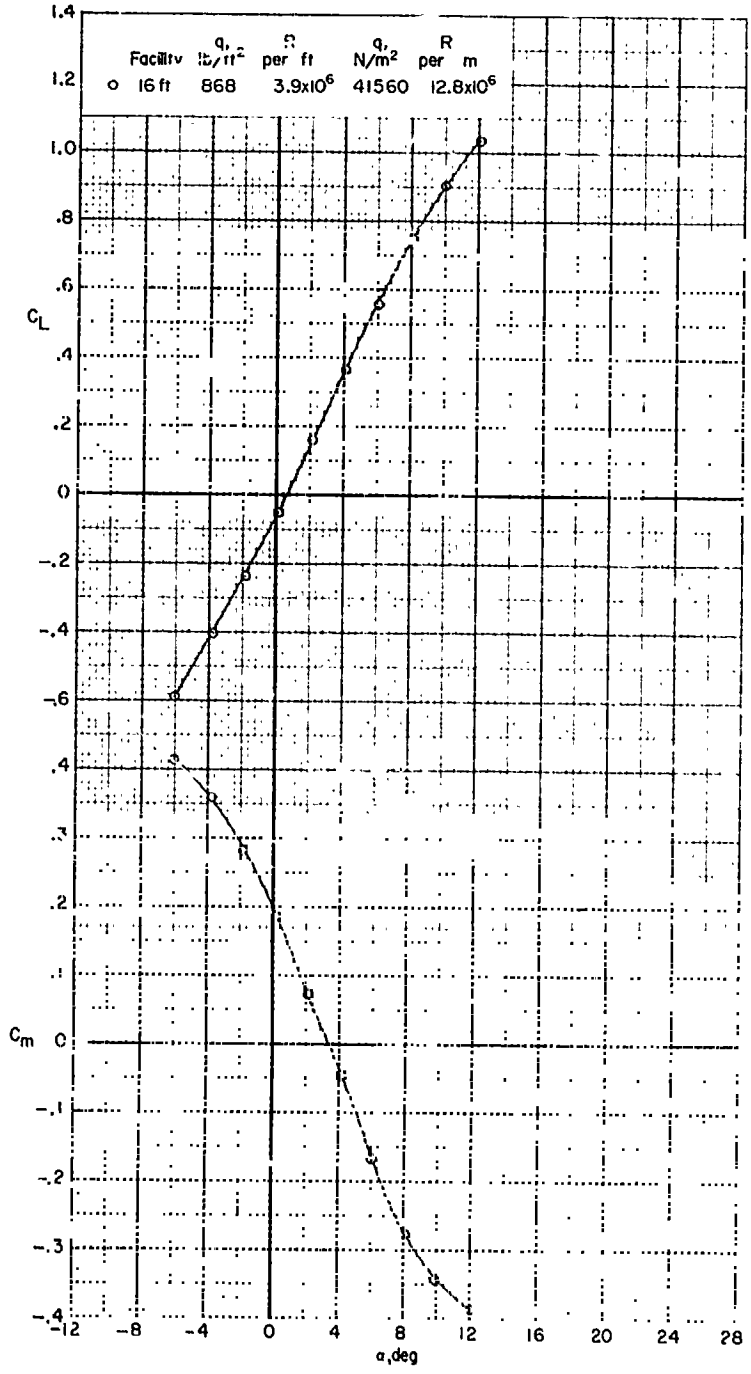

(d) M = 1.20.

Figure 11.- Continued.

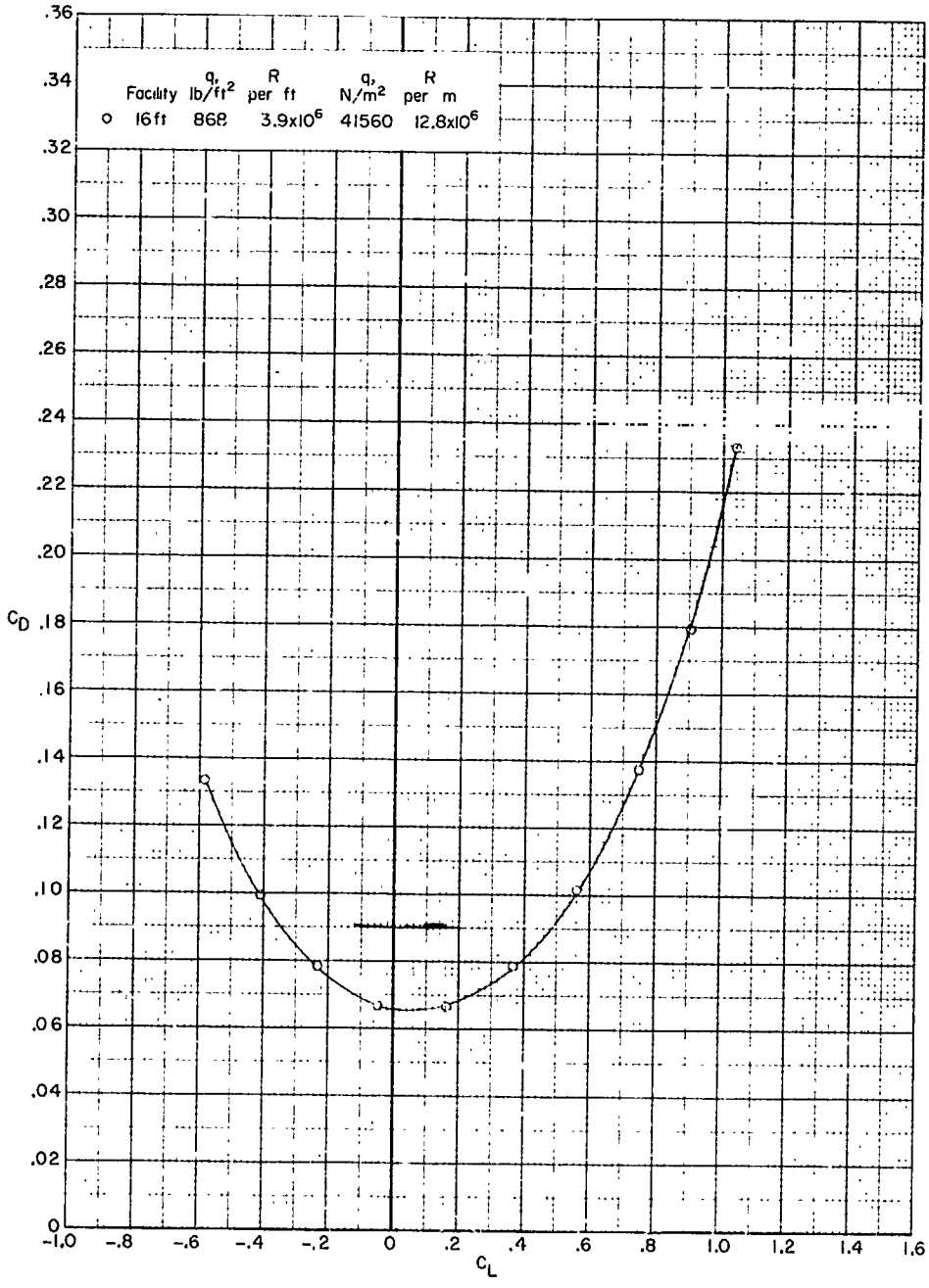

(d) M = 1.20. Concluded.

Figure 11.- Continued.

ORIGINAL PAGE IS
OF POOR QUALITY

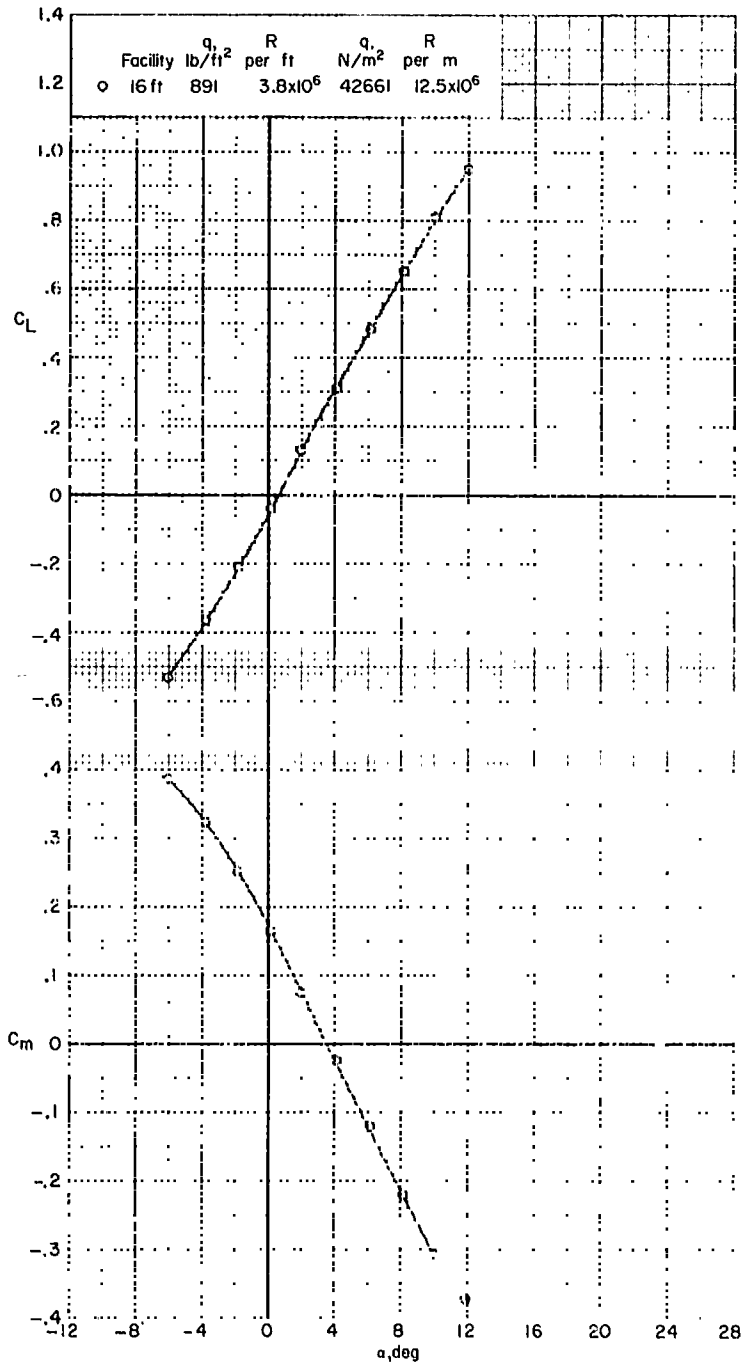

(e) M = 1.30.

Figure 11.- Continued.

[redacted]

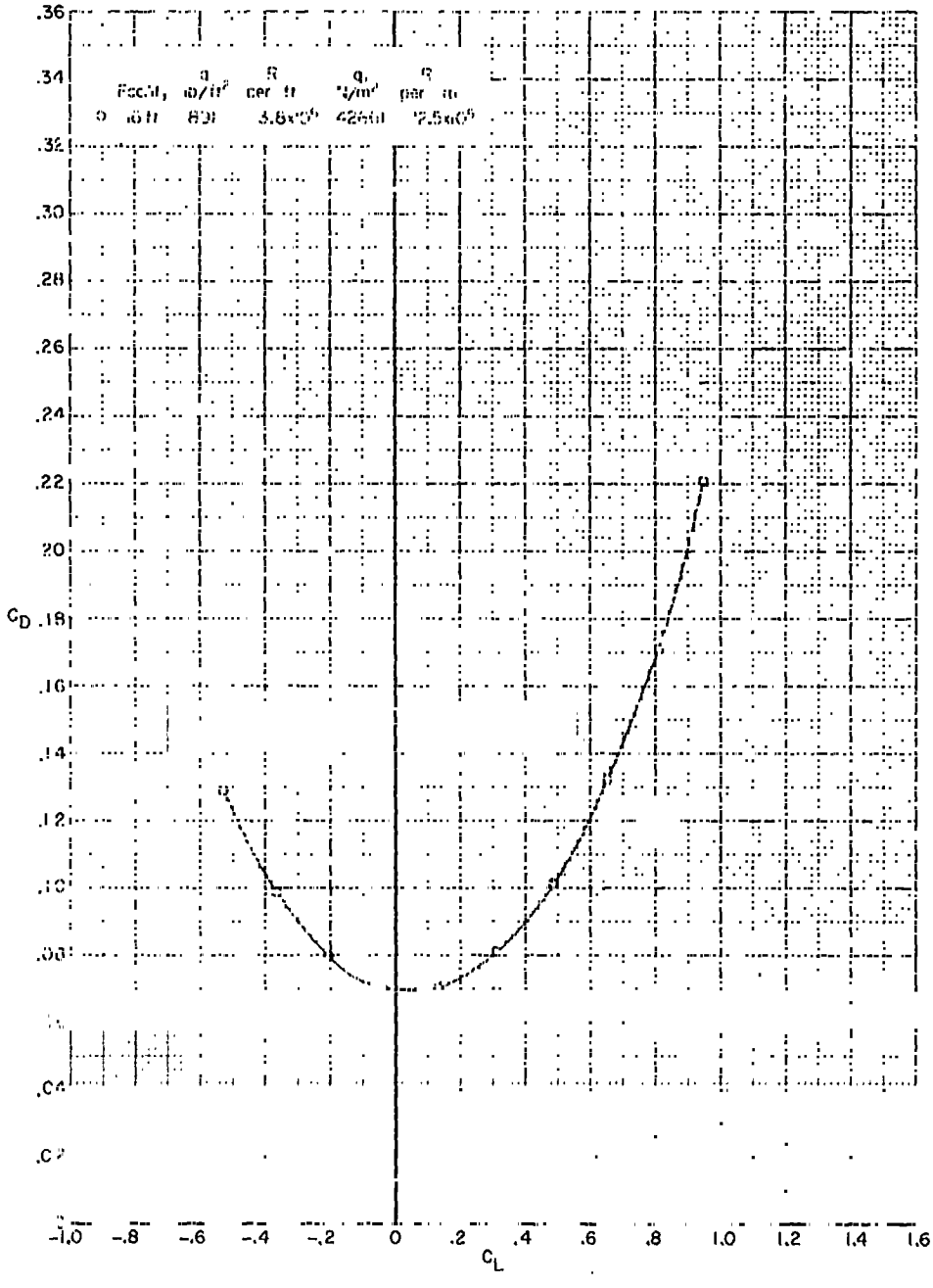

(e) M = 1.30. Concluded.

Figure 11.- Concluded.

ORIGINAL PAGE IS
OF POOR QUALITY

[redacted]

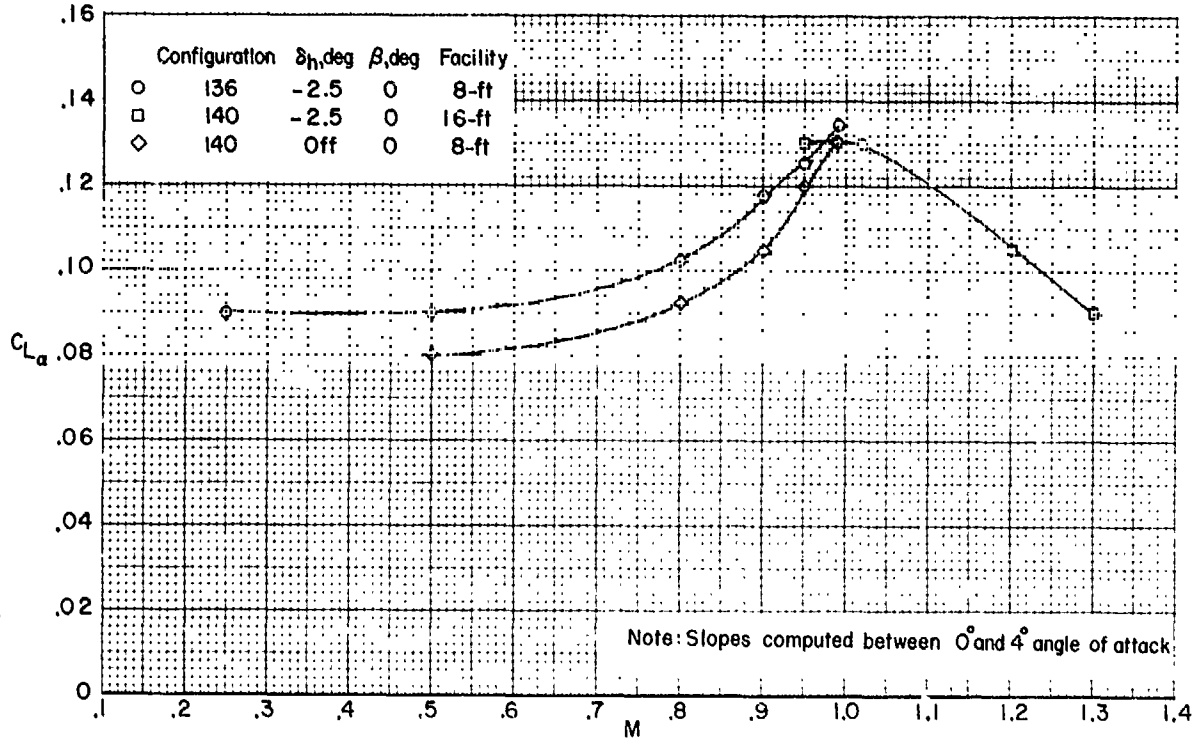

(a) Variation with Mach number of lift-curve slope.

Figure 12.- Variation with Mach number of longitudinal aerodynamic characteristics.

[redacted]

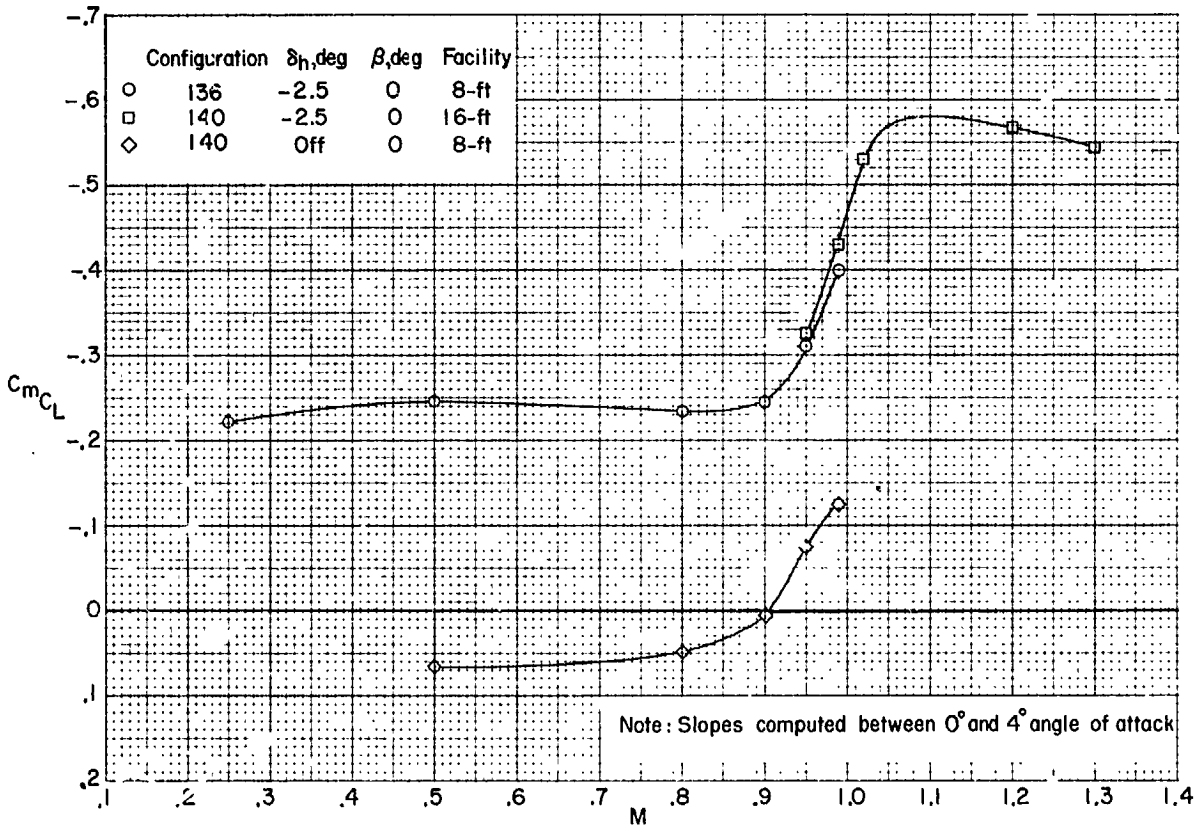

(b) Variation with Mach number of longitudinal stability derivative.

Figure 12.- Continued.

[redacted]

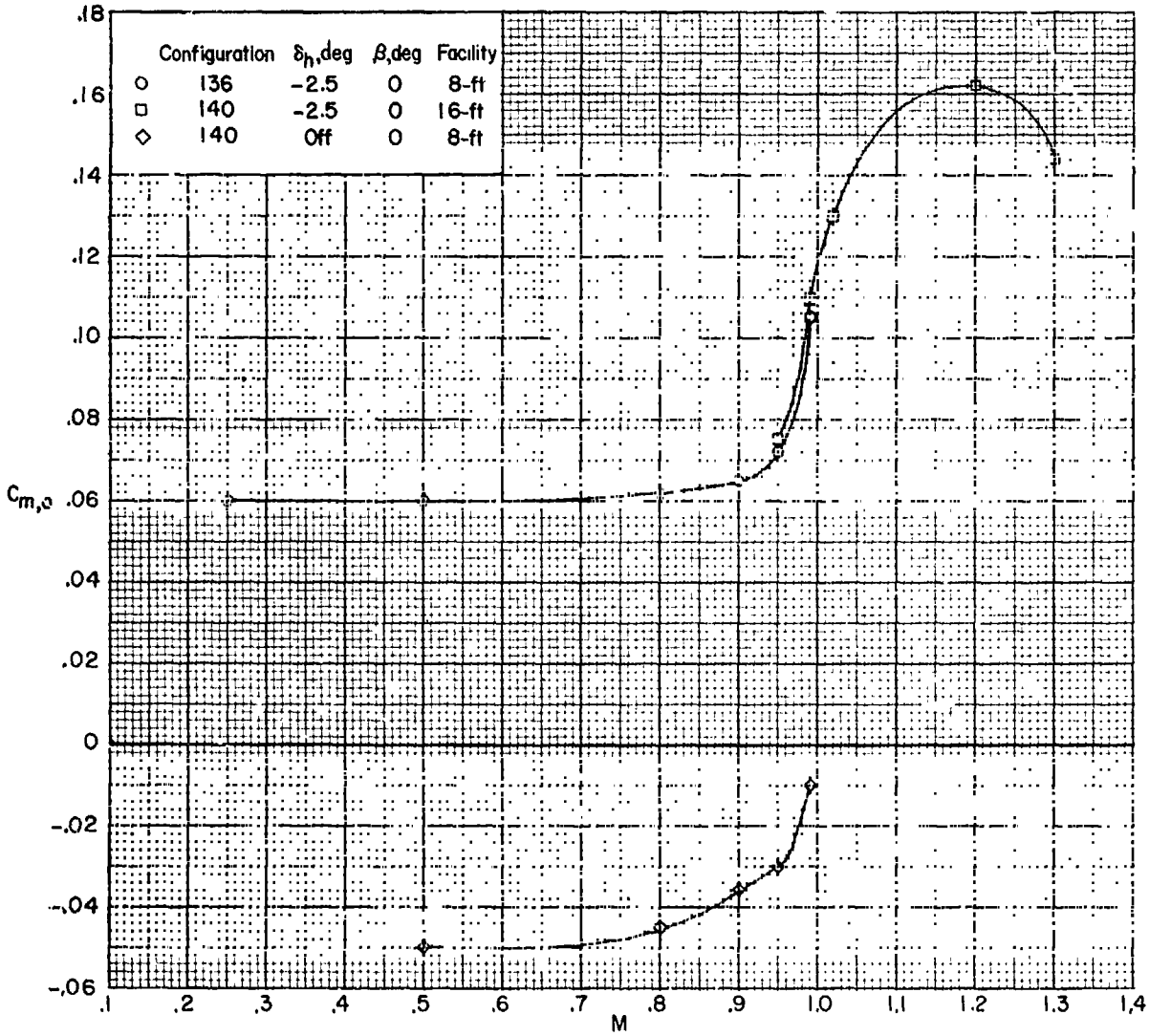

(c) Variation with Mach number of pitching-moment coefficient at zero lift.

Figure 12.- Concluded.

ORIGINAL PAGE IS
OF POOR QUALITY

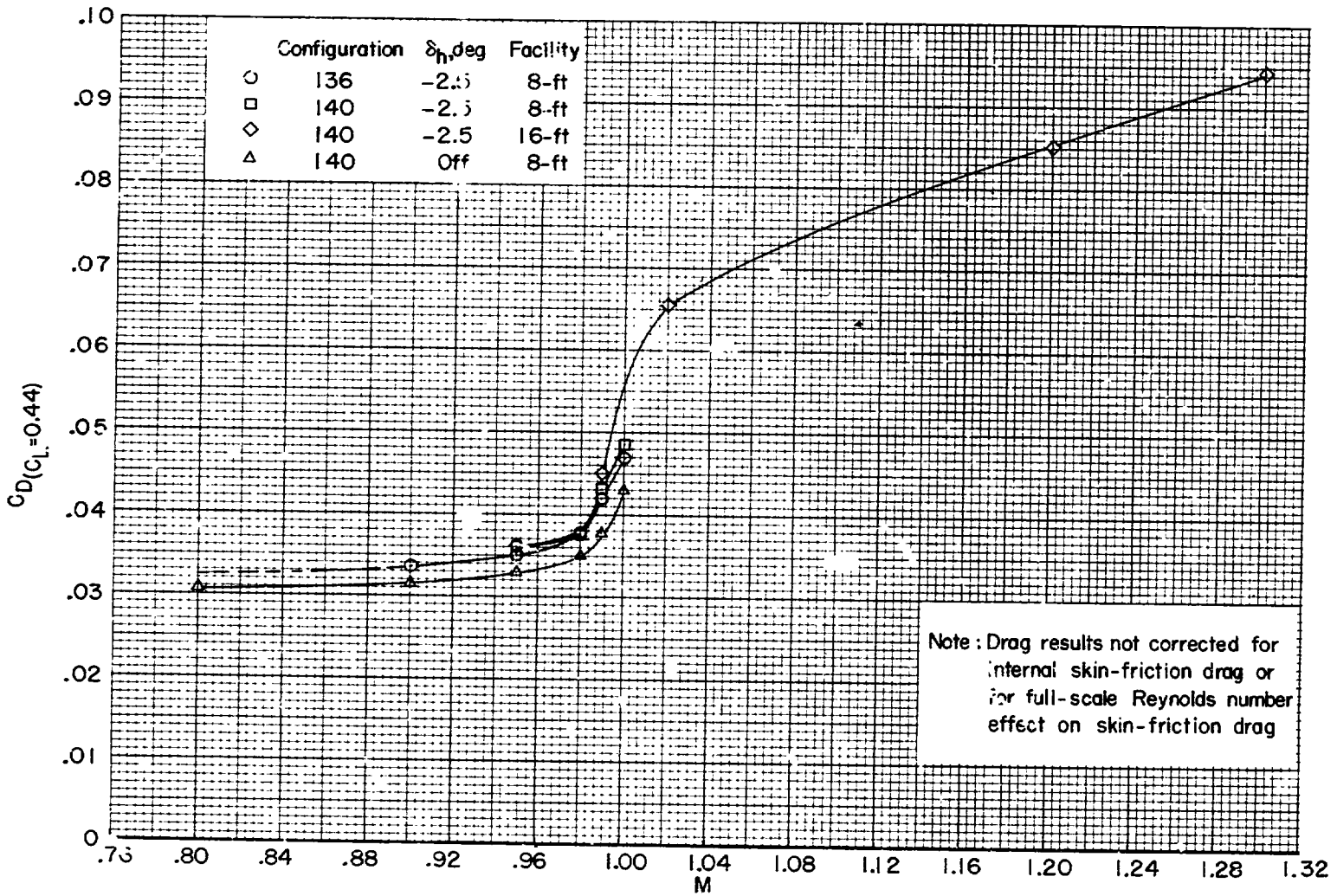

Figure 13.- Variation with Mach number of drag coefficient at a lift coefficient of 0.44. $\beta = 0^{\circ}$.

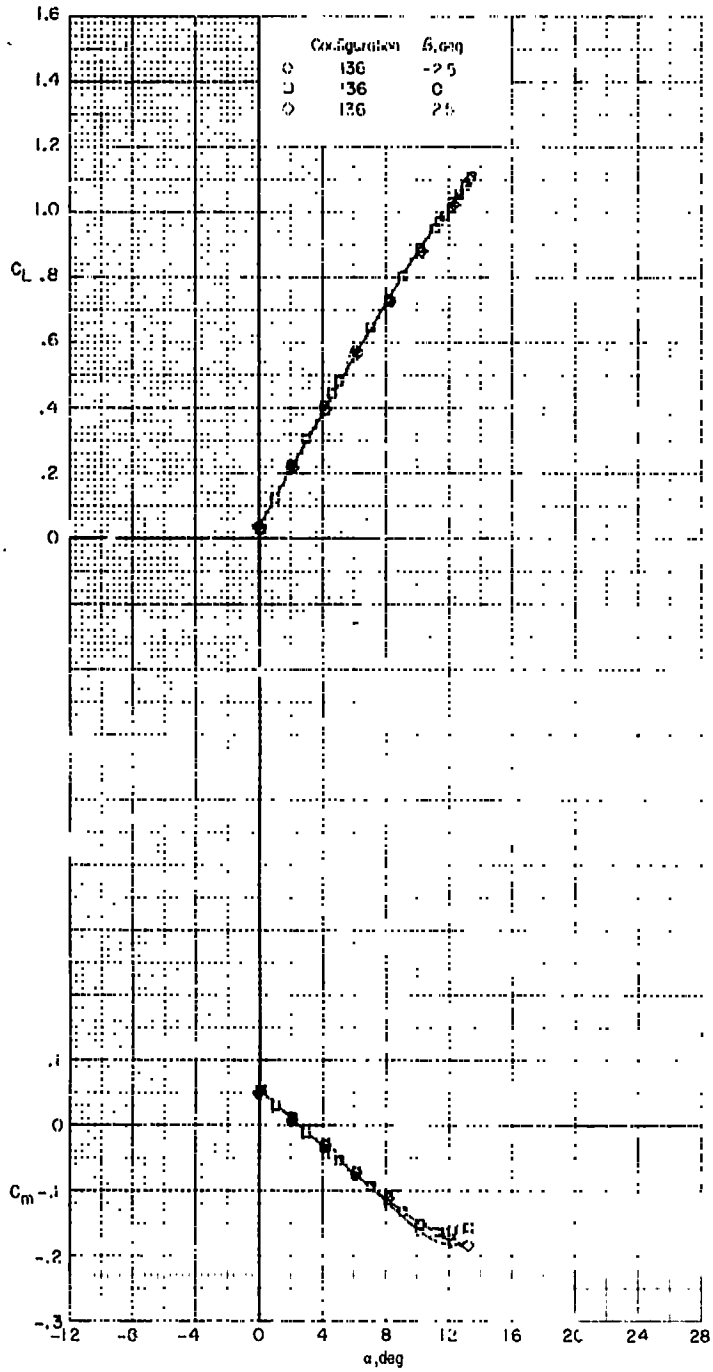

(a) M = 0.25; q = 8523 N/in^2 (178 lb/sq ft); and R/m = 10.2 × 10^6 (R/ft = 3.1 × 10^6).

Figure 14.- Effect of sideslip on longitudinal aerodynamic characteristics. $\delta_h = -2.5^{\circ}$.

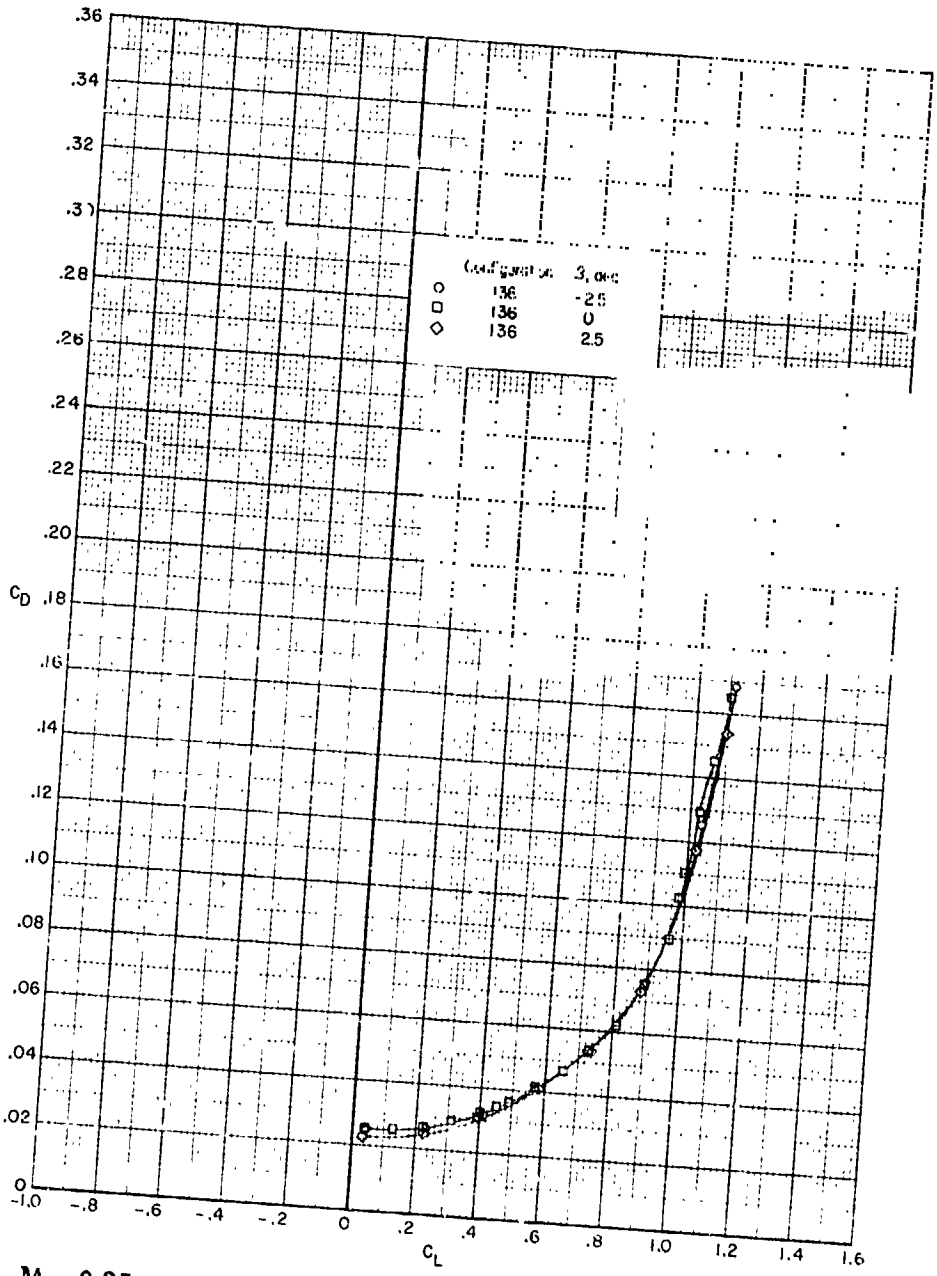

(a) M = 0.25; q = 8523 N/m^2 (178 lb/sq ft); and R/m = 10.2 × 10^6 (R/ft = 3.1 × 10^6). Concluded.

Figure 14.- Continued.

ORIGINAL PAGE IS OF POOR QUALITY

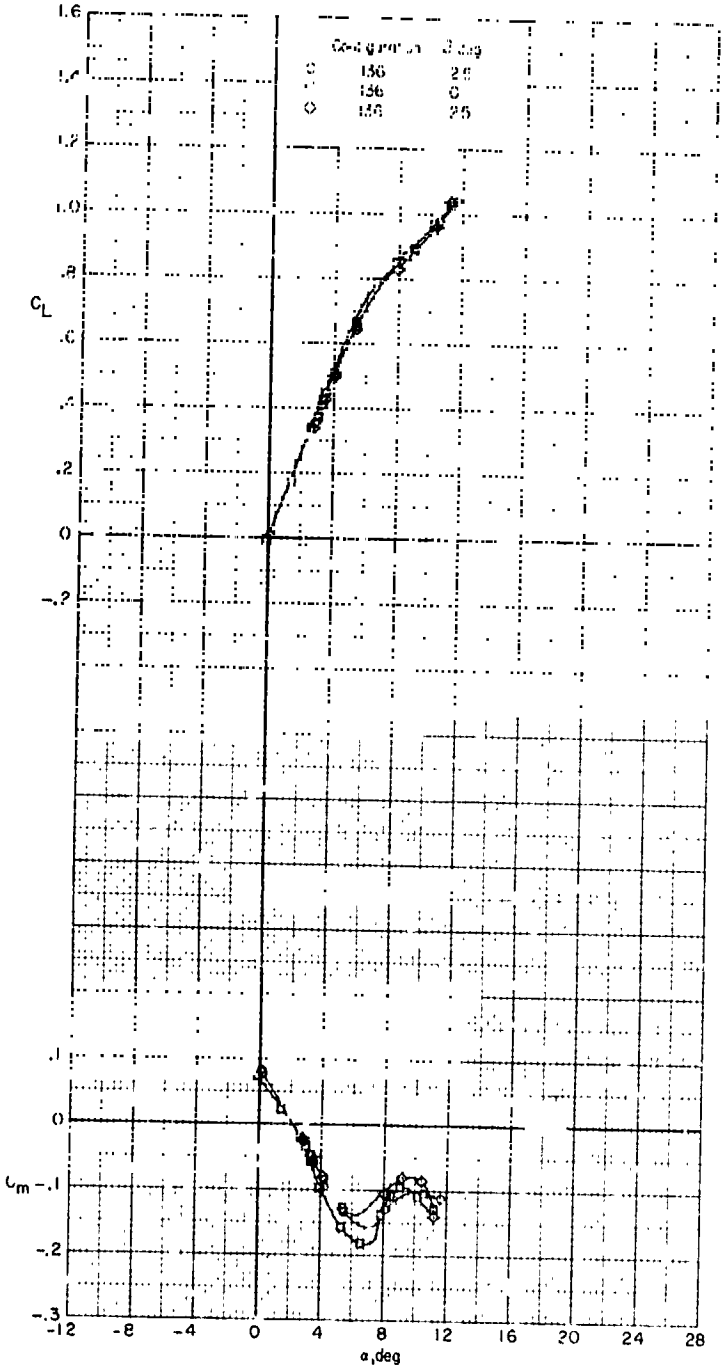

(b) M = 0.95; q = 44 193 N/m^2 (923 lb/sq ft); and R/m = 16.4 × 10^6 (R/ft = 5.0 × 10^6).

Figure 14.- Continued.

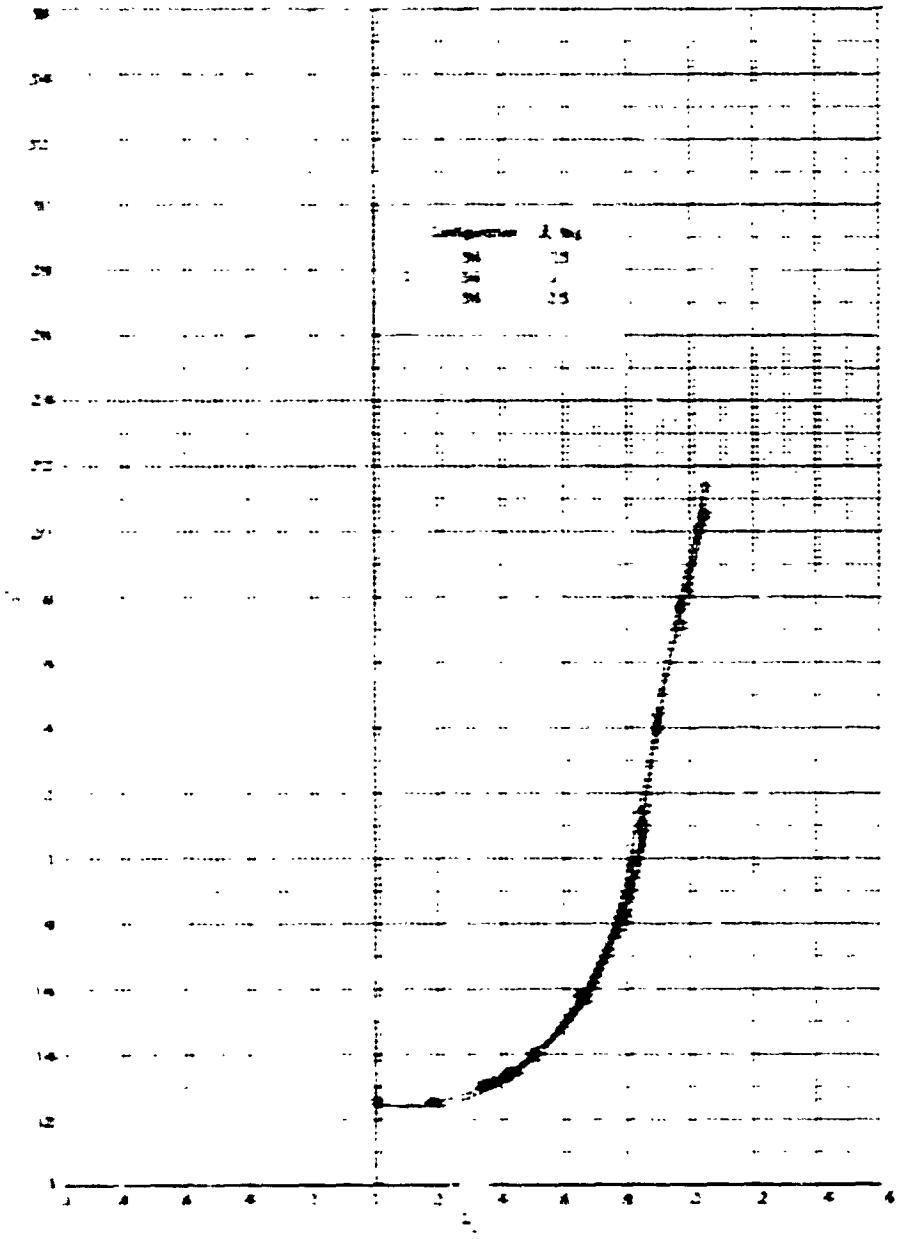

(b) M = 1.55; q = 44 150 N/m^2 (923 lb/sq ft); and R/m = 16.4 × 10^6 (R/ft = 5.0 × 10^6). Concluded.

Figure 14.- Continued.

ORIGINAL PAGE IS
OF POOR QUALITY

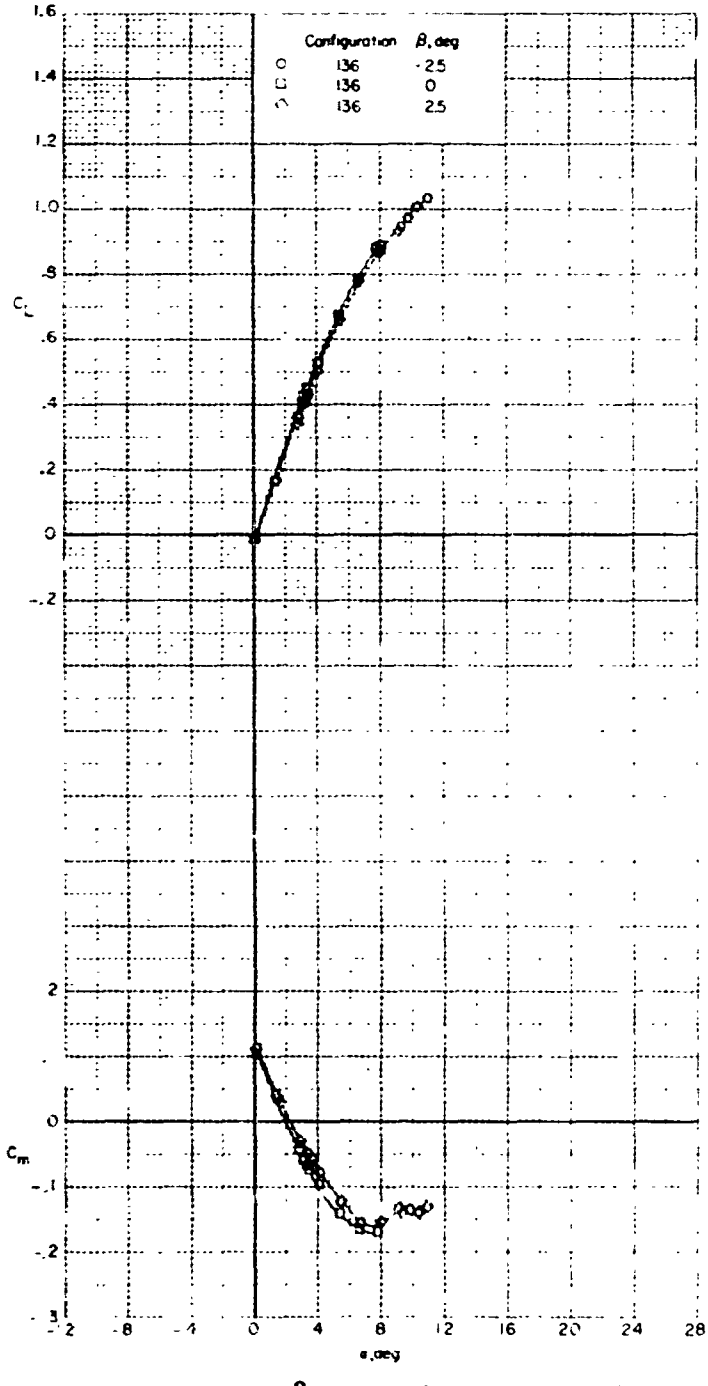

(c) M = 0.99; q = 44 193 N/m^2 (923 lb/sq ft); and R/m = 16.1 × 10^6 (R/ft = 4.9 × 10^6).

Figure 14.- Continued.

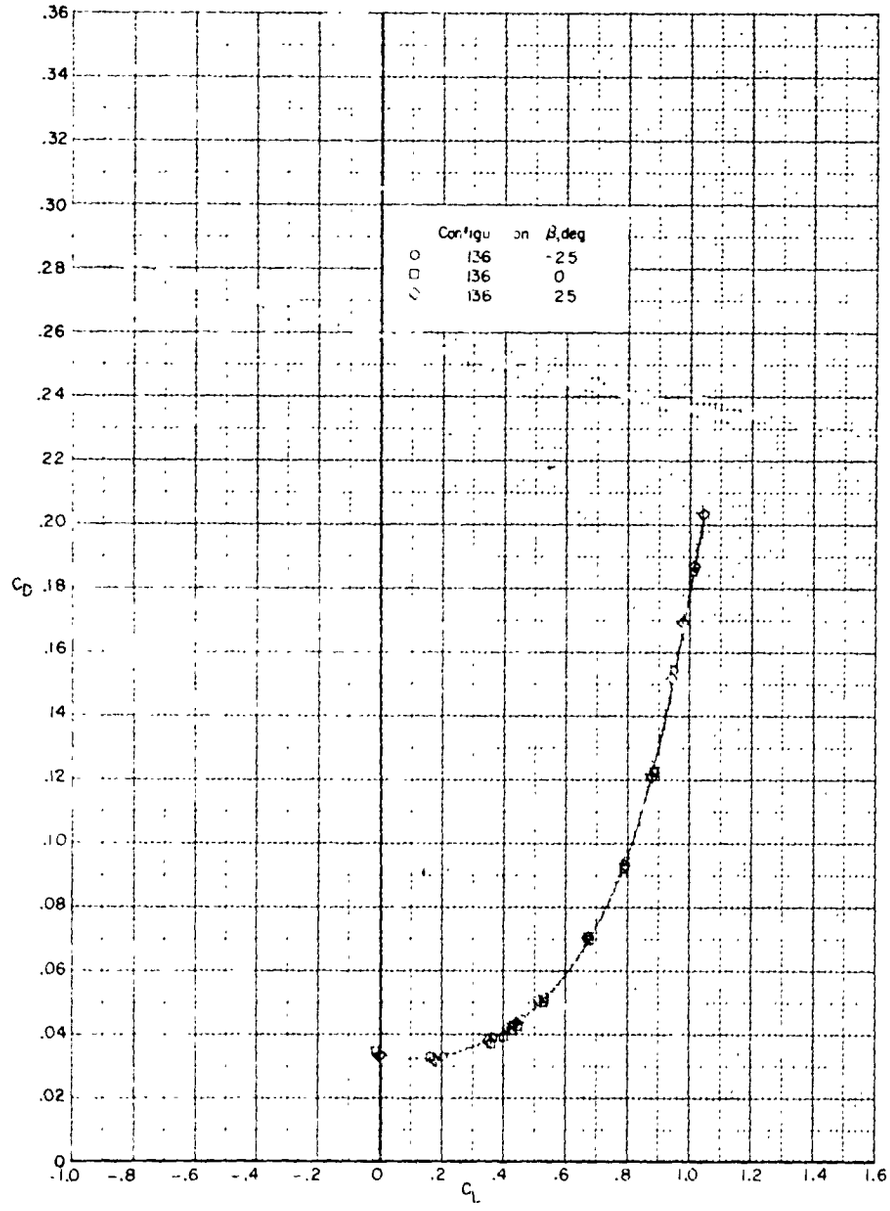

(c) M = 0.99; q = 44 193 N/m^2 (923 lb/sq ft); and R/m = 16.1 × 10^6 (R/ft = 4.9 × 10^6). Concluded.

Figure 14.- Concluded.

ORIGINAL PAGE IS
OF POOR QUALITY

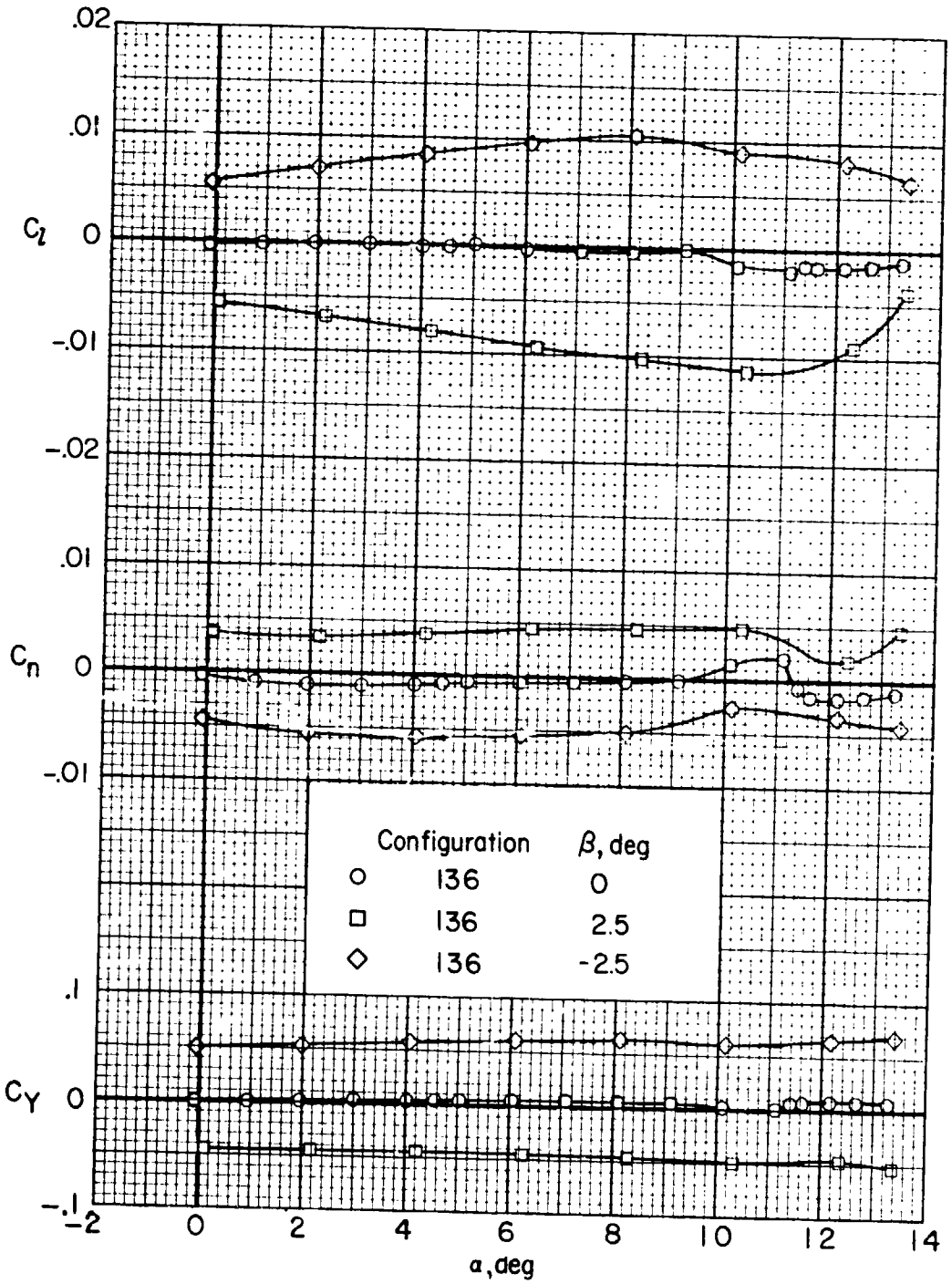

(a) M = 0.25; q = 8523 N/m^2 (178 lb/sq ft); and R/m = 10.2 × 10^6 (R/ft = 3.1 × 10^6).

Figure 15.- Effect of sideslip on lateral-directional aerodynamic coefficients. $\delta_h = -2.5^o$.

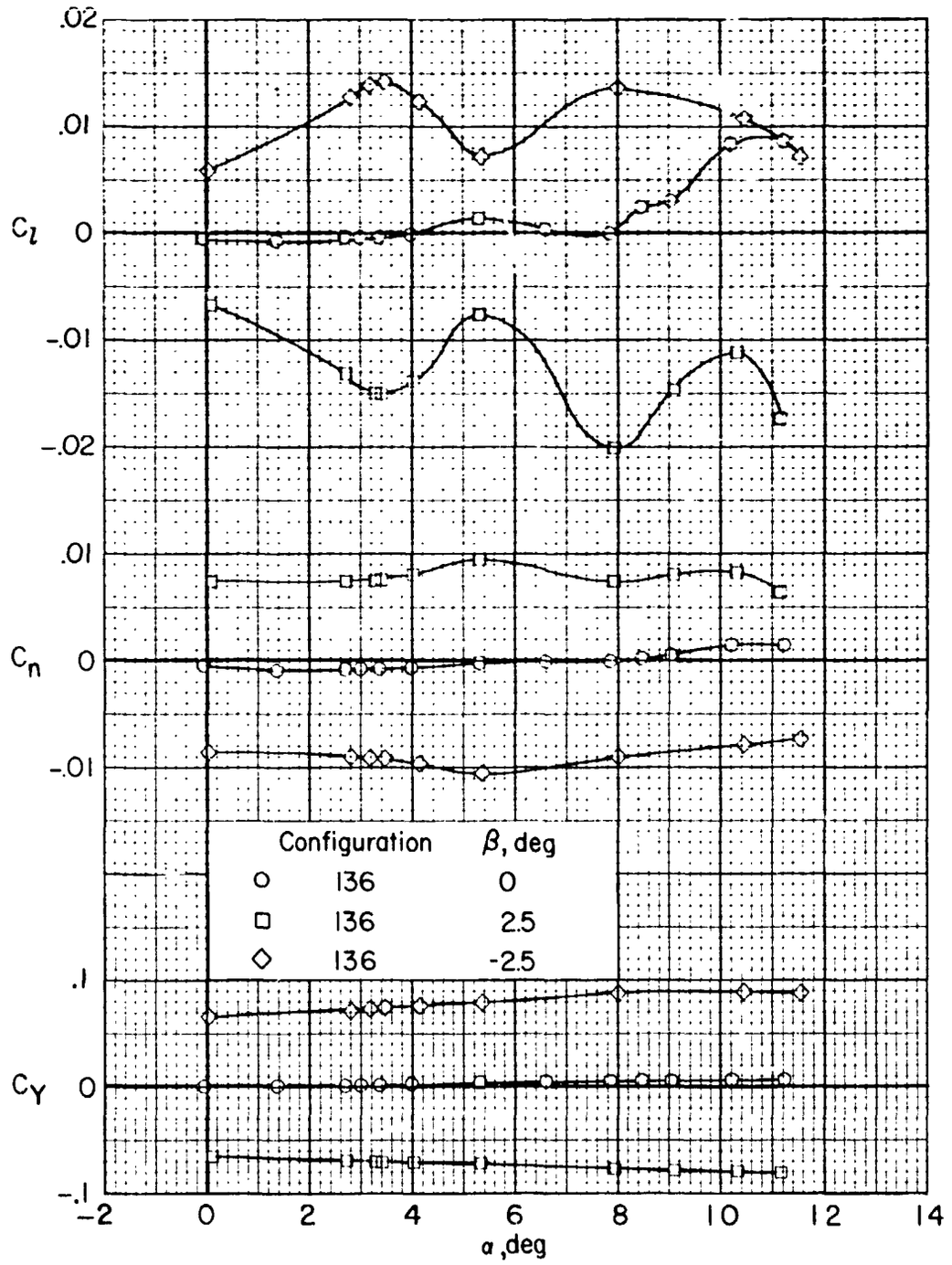

(b) M = 0.95; q = 44 193 N/m^2 (923 lb/sq ft); and R/m = 16.4 × 10^6 (R/ft = 5.0 × 10^6).

Figure 15.- Continued.

ORIGINAL PAGE IS
OF POOR QUALITY

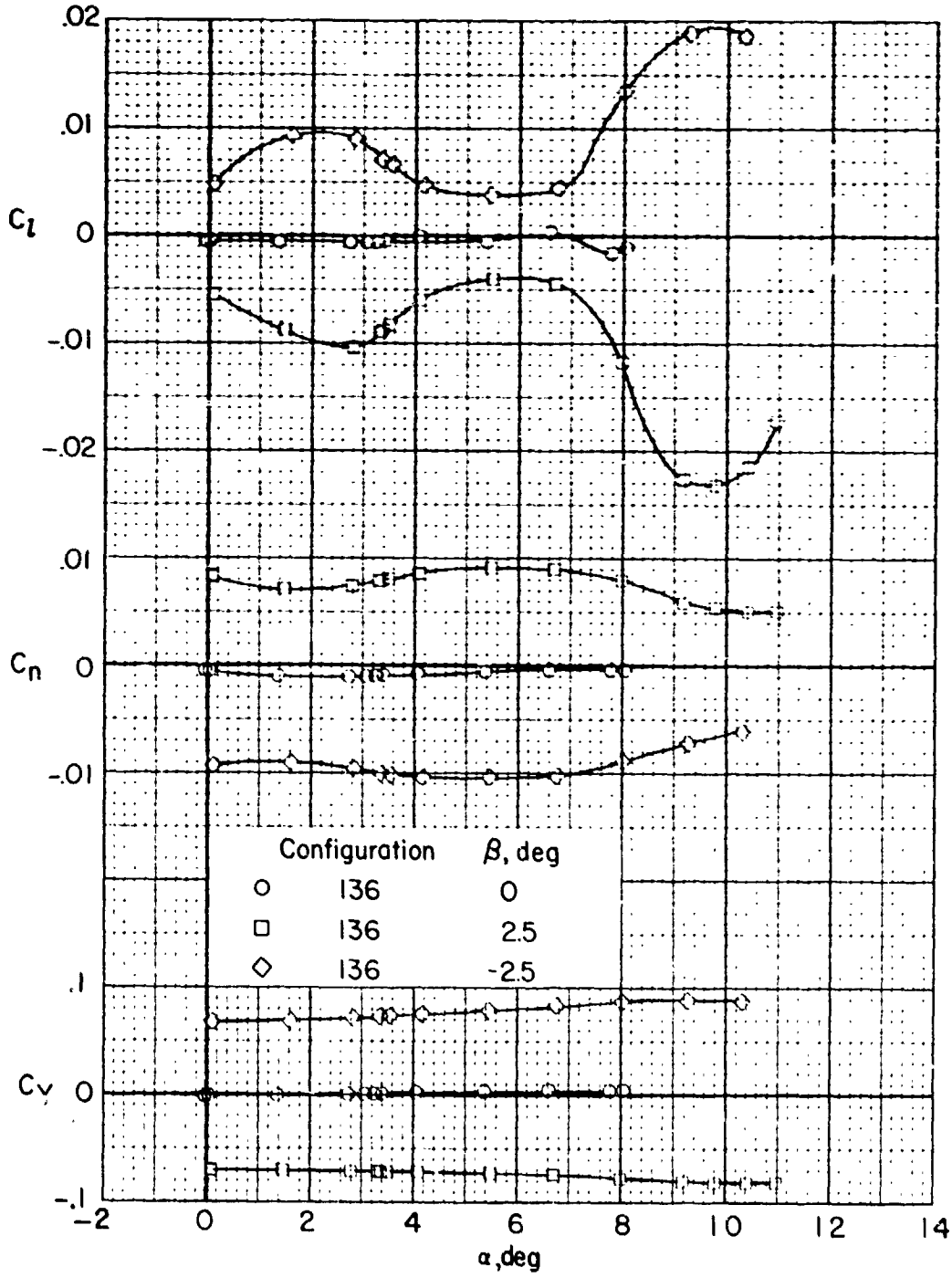

(c) M = 0.99; q = 44 193 N/m^2 (923 lb/sq ft); and R/m = 16.1 × 10^6 (R/ft = 4.9 × 10^6).

Figure 15.- Concluded.

ORIGINAL PAGE IS
OF POOR QUALITY

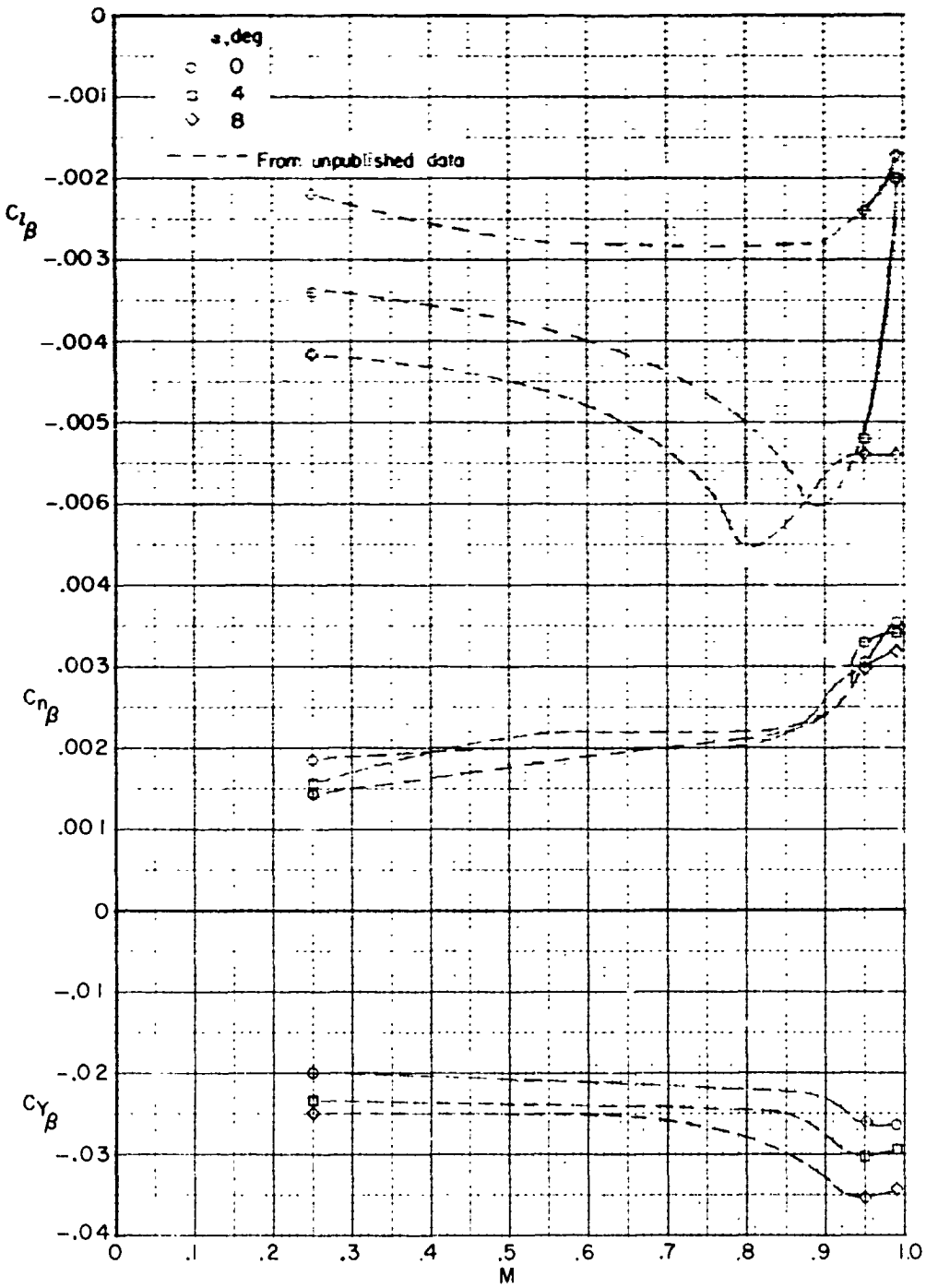

Figure 16.- Variation with Mach number of lateral-directional aerodynamic stability derivatives. $\delta_h = -2.5^{\circ}$.

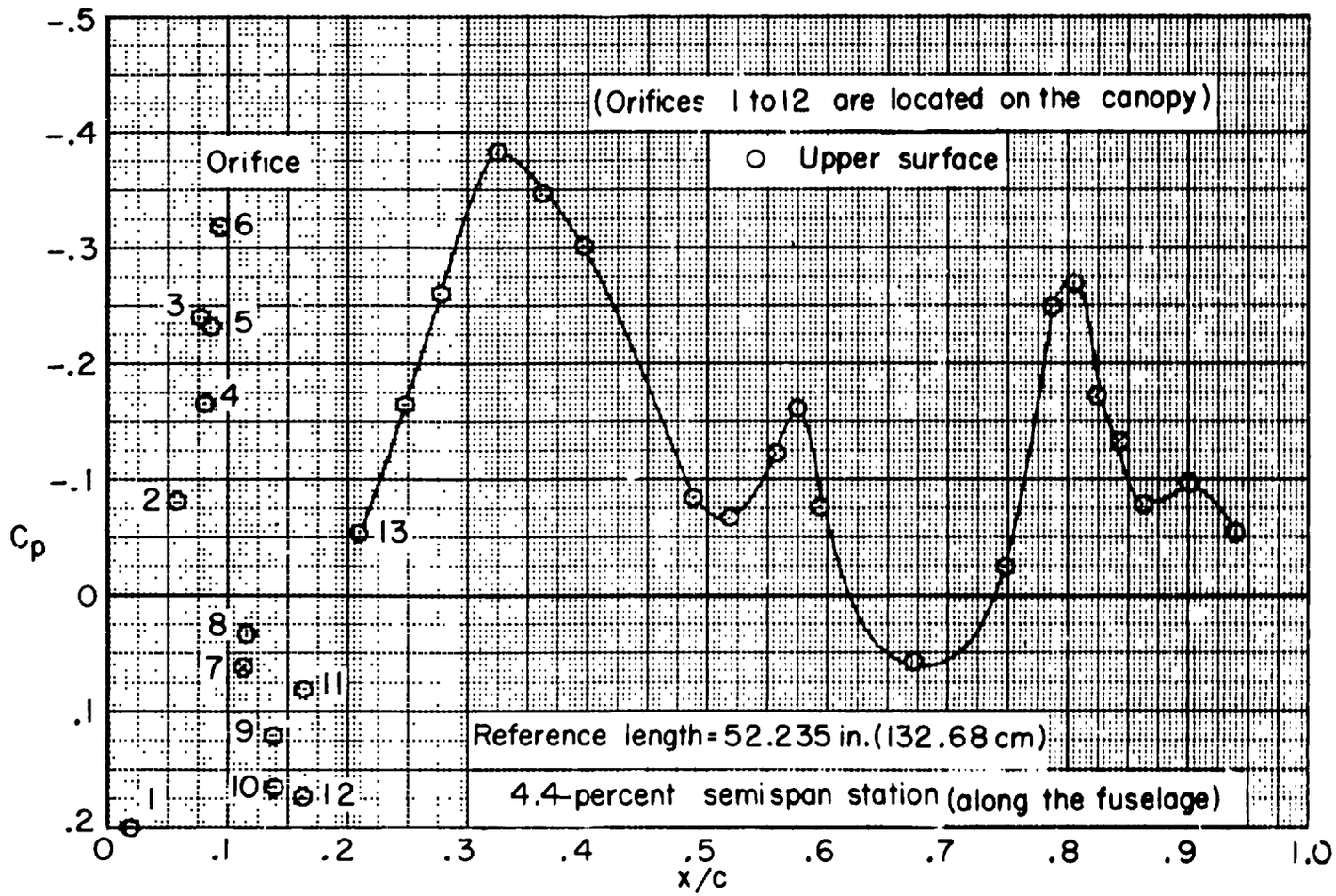

Figure 17.- Streamwise-chord pressure distributions. Configuration 140; $M = 0.99$; $C_L = 0.443$; $q = 44\ 193\ N/m^2$ (923 lb/sq ft); and $R/m = 16.1 \times 10^6$ ($R/ft = 4.9 \times 10^6$). Note that c is defined for basic wing in inches and centimeters.

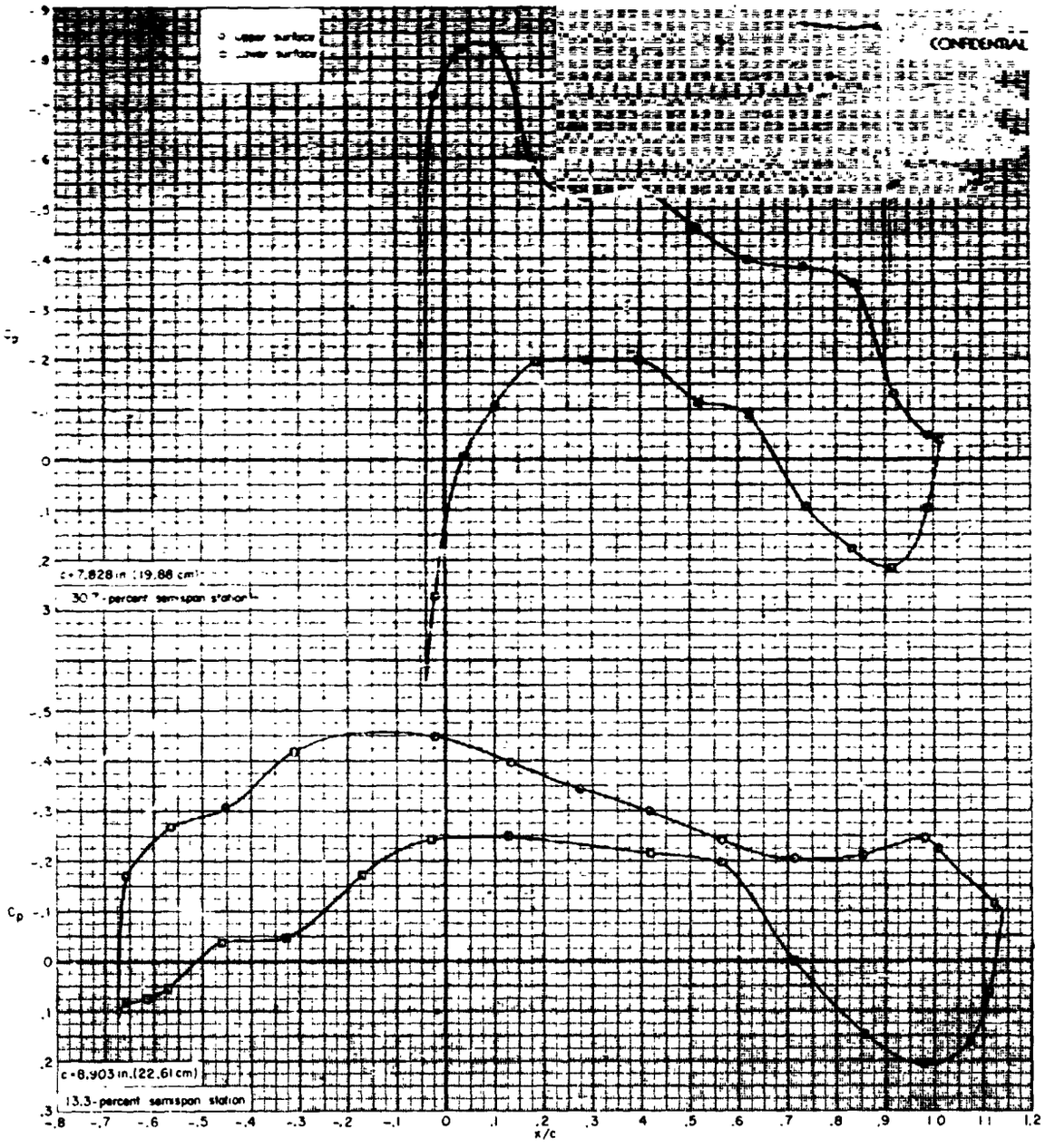

Figure 17.- Continued.

ORIGINAL PAGE IS
OF POOR QUALITY

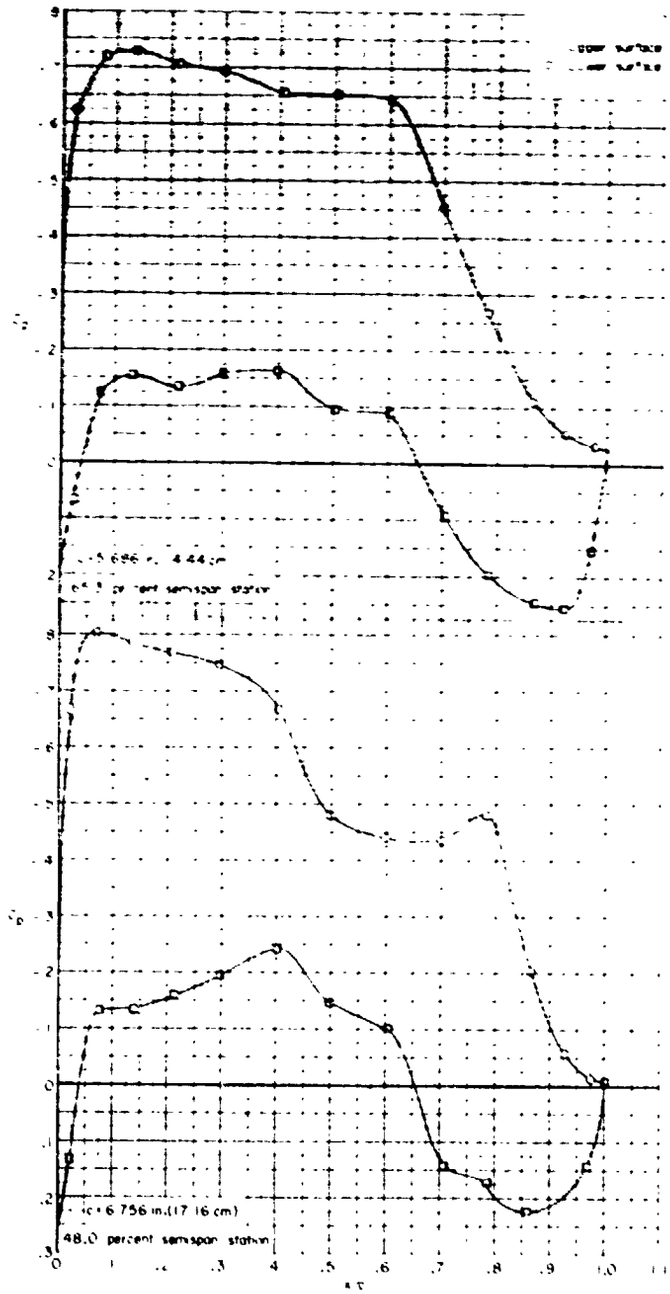

Figure 17.- Continued.

ORIGINAL PAGE IS
OF POOR QUALITY

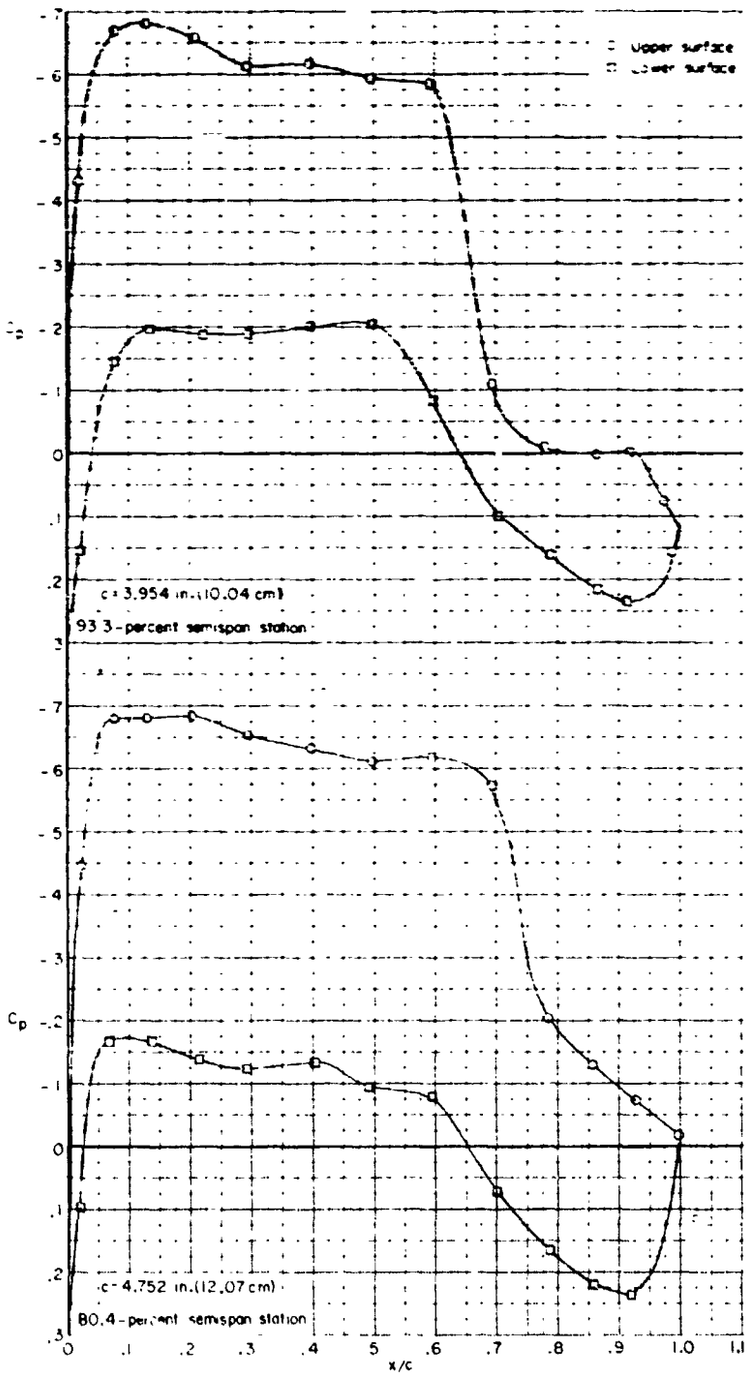

Figure 17.- Concluded.

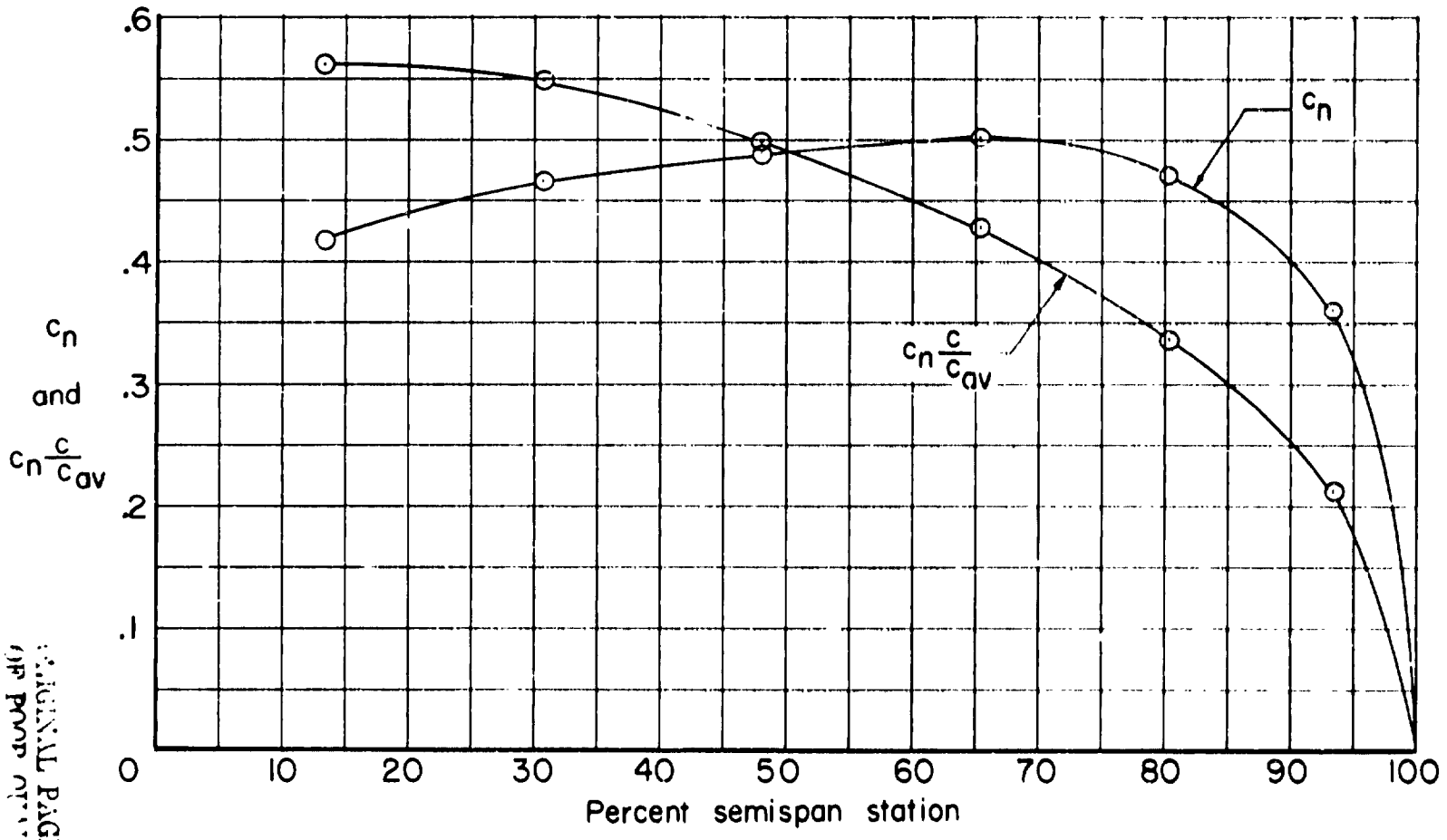

Figure 18.- Semispan aerodynamic load distribution. Configuration 140; $M = 0.99$; $C_L = 0.443$; $q = 44\ 193\ N/m^2$ (923 lb/ft^2); and $R/m = 16.1 \times 10^6$ ($R/ft = 4.9 \times 10^6$).

ORIGINAL PAGE IS
OF POOR QUALITY

NASA-Langley, 1972 — 1 L-7979

CONFIDENTIAL